GEOLOGICAL AND STRUCTURAL INTERPRETATION OF PART OF THE BUEM FORMATION, GHANA, USING AEROGEOPHYSICAL DATA

By

Kenny Mensah Graham
(BSc Mathematic and Statistics)

A Thesis Submitted to the Department of Physics,

Kwame Nkrumah University of Science and Technology, Kumsai

in partial fulfillment of the requirements for the degree

of

MASTER OF SCIENCE (GEOPHYSICS)

College of Science

Supervisor: Dr. Kwasi Preko

April, 2013

Declaration

I hereby declare that this submission is my own work towards the award of MSc Geophysics degree and that, to the best of my knowledge, it contains no material previously published by another person or material which has been accepted for the award of any other degree of the University, except where due acknowledgement has been made in the text.

....	....	....
Student's Name	Signature	Date

Certified by:

....	....	....
Supervisor's Name	Signature	Date

Certified by:

....	....	....
Head of Dept.'s Name	Signature	Date

Abstract

Airborne magnetic and radiometric datasets were processed to interpret the geology of part of the Buem formation and estimate the depth to basement of magnetic source in the area. The study was aimed at mapping lithology, delineating structural lineaments and their trends as well as estimating the depth to magnetic source bodies of the area. The data processing steps involved enhancement filters such as reduction to the pole, analytic signal and first vertical derivative, Tilt angle derivative and these helped delineate geological structures and lithology within the Buem formation. The radiometric datasets displaying the geochemical information on potassium, thorium and uranium concentrations within the study area proved valuable in delineating the Buem shales, sandstones, basalts and part of the Voltaian sediments that underlie the Buem formation. Lineament analysis using the rose diagram showed that the area is dominated by north-south (NS) and east-west (EW) trending lineaments. Depths to the magnetic source bodies were estimated using Werner deconvolution method, indicating two depth source models. The depth of the magnetic body produced from the dike model ranged from 101.15 m to 1866.34 m and that of the contact model ranged from 100.36 m to 983.709 m.

Table of Content

List of Figures

List of Tables

List of Symbols and Acronyms

eU	Equivalent Uranium
eTh	Equivalent Thorium
K	Potassium
RTP	Reduction to the pole
RMI	Residual magnetic intensity
TDR	Tilt angle derivative
1VD	First vertical derivative
DEM	Digital elevation map
UP	Upward continuation
κ	Magnetic susceptibility
WGS84	World Geodetic System 1984
UTM	Universal Transverse Mercator

Acknowledgments

My first and foremost appreciation goes to the Almighty God for His unending strength, mercies and grace towards me throughout the duration of this work. I sincerely thank my supervisor Dr. Kwasi Preko for his motivation, encouragement, criticism and fatherly love he showed me. I am highly indebted to my co-supervisor Mr. D. D. Wemegah for the advice, motivation and the training he gave me on the GIS and the other geophysical softwares. This work would not have been possible without the supports of Mr. Attah (Ghana Geological Survey Department) who gave me the Oasis Montaj (Geosoft) training and some advice. I am also grateful to the administration of Geological Survey Department, Accra, for granting the dataset and allowing me to use their library for this work. I also thank all the staff and MSc students of Physics Department for their immense support. Finally to my family and all my love ones God bless you all.

CHAPTER ONE

1 INTRODUCTION

Airborne geophysics is a powerful technique available to the Earth scientists for investigating very large areas rapidly. The broad view of the Earth that the airborne geophysics perspective provides has been well recognized since the early days of balloon photography and military reconnaissance (Dobrin and Savit, 1988). Compared with ground-based methods, the advantages of these methods are that very large areas and difficult terrain can be surveyed remotely in short periods of time thus making it very cost effective. There are many airborne geophysical methods (e.g. gravity, radiometry, magnetic, electromagnetic) whose operations are based on different physical principles, techniques and physical properties (e.g. density, magnetic susceptibility, electrical, conductivity, radioactive) of the Earth which can be employed for the provision of solutions for various geological problems and structural mapping of an area. These physical properties and formation of different rock types driven by different physical and chemical compositions of the Earth vary from one area to another (Roy, 1966). Depending on the dominant physical properties of the different rock types, the appropriate geophysical methods have the potential to aid identification of the geology as well as mapping geological structures likely to have developed in a particular area (Afenya, 1982).

Aeromagnetic survey is a common type of geophysical survey carried out using a magnetometer aboard or towed behind an aircraft allowing much larger areas of the Earth's surface to be covered quickly. The resulting magnetic map shows the spatial distribution and relative abundance of magnetic minerals (most commonly magnetite) in the upper levels of the crust. The magnetic map allows a visualization of the geology and geological structures of the upper crust of the Earth. This is particularly helpful where bedrock is obscured by surface sand, soil or water. The apparent variation in the intensity of the magnetic value (high, ridges and valleys) observed on the interpreted data are referred to as magnetic anomalies for which a mathematical modelling can be used to infer the shape, depth and properties of the rock bodies responsible for these anomalies (Koulomzine et al., 1970).

Airborne radiometric data on the other hand is normally collected over large areas using an aircraft mounted scanner with the data collected digitally. The scanner measures the amount of potassium (K), thorium (Th) and uranium (U) radiation emitted from the ground within certain parts of the electromagnetic spectrum. These three radioisotopes are naturally found in most rock types. When the rock weathers, the relative proportions of the potassium, thorium and uranium are reflected in the soils (Shi and Butt 2004).Many times, there is a good correlation between patterns in the radiometric data and un-weathered rocks (Gunn et al. 1997b). In 1961, Fugro Airborne Surveys estimated that 90 % of gamma rays are sourced from the top 30 – 45 cm of the soil. The amount and proportion of K, Th and U which is emitted from the surface can be useful in mapping soil properties and regolith (Gunn et al., 1997b).

1.1 Literature Review

Airborne geophysical surveys have been carried out in Ghana since 1952 (Kesse, 1985). However, it was only within these few decades that airborne geophysical dataset was established as a powerful tool in geological mapping (Reeves et al., 1997). On regional scale, airborne geophysical data have often been used to identify several features, such as: limits of geologic provinces, fold belts, sedimentary basin and tectonic and structural detail of shear zones and overprinted structural trends (Direen et al., 2001).

In 2012, Cardero Ghana contracted Geotech Airborne Limited to conduct a 3,000 km line of V-TEM, Magnetic, and Radiometric airborne geophysical survey to define the extent of banded iron formation and outline and interpret the geological setting of the Shiene area within the Buem Formation (PGEO, 2012). Delor, et al., (2009) used aeromagnetic dataset to map structures such as fault, linearment, folds and share zones in the Nkwanta area of Ghana. Delor, et al., (2009) also used airborne radiometric dataset to map lithology from the ternary image of Potassium, Uranium and Thorium and also used the Potasium grid to map out weathered zones. Various geophyiscal surveys have also been conducted in various parts of the country mainly for the exploration of precious mineral mainly gold by some mining comapies and the Geological Survey of Ghana. Some were also carried out for the purpose of of scientific research.

In 1997, a high-resolution airborne geophysical survey over the Lake Bosumtwi impact structure, Ghana, was carried out by the Geological Survey of Finland in collaboration with the University of Vienna, Austria, and the Geological Survey Department of Ghana. The magnetic data yielded a new model of the structure by showing several magnetic rims and by providing hints for the existence of a central uplift. The gamma radiation data turned out to be surprisingly valuable and clearly pinpoint two ring features (Pesonen, et al., 2003).

Most of the airborne geophysical exploration works being carried out by mining companies in Ghana are located along the well-known 'Ashanti belt', which hosts the major economic deposit of the gold.

A complementary interpretation of magnetic data together with gravity, gamma-ray or seismic dataset has shown to be very useful in geological and structural mapping (Chandler, 1990; Gunn, 1997a). Asadi and Hale (1999) used the analytical signal of total magnetic intensities to delineate intermediate composition magmatic rocks in the Takab area of Iran. Chandler (1990) used the second vertical derivative enhanced-aeromagnetic data together with gravity data to interpret the geology of the poorly exposed central part of the Duluth Complex. Isolated outcrops and the well mapped surrounding areas were used as geological controls. Gunn et al. (1997a) reported that correlation with seismic reflection data has shown that geological structures mapped by magnetic data in sedimentary rocks in northern Australia are indeed present. Experience from Finland also show high degree of correlations between results from aeromagnetic data and bedrock structure (Airo, 2005). Kesse (1985) reported that results from the 1960 magnetic survey by Hunting Survey Limited across the Ashanti belt were quite satisfactory. Geological interpretation based mostly on the magnetic maps proved successful in differentiating lithologies, faults and fracture zones.

Silva et al., (2003) concentrated on processing and enhancing of airborne geophysical data for accurate positioning of geological boundaries. The rationale was that in exploration, we should not be looking for geophysical anomalies, but the responses related to mineralization, lithology, and structure that may have economic importance. Silva et al., (2003) also showed that aeromagnetic survey can be used to identify magnetic greenstone units; important structures related to mineralization and allowed a better understanding of structural geophysical pattern. The radiometric data is an excellent tool for mapping and tracing individual lithological units in areas of less geological outcrop. The most important host rocks or mineralized domains show high conductivity response illustrating the utility of the airborne EM data as a tool to improve the geological mapping (Silva et al., 2003).

The interpretation of the aeromagnetic survey over the Faiyum area, Western Desert, Egypt was carried out by El-awady et al., (1984). Qualitative as well as quantitative interpretations of the aeromagnetic data were carried out to obtain more information about the crystalline basement structure and the local structure in the sedimentary section. The analysis of the constructed magnetic maps which include the total intensity map, the vertical map, the regional map, the residual map, the second vertical derivative map and the downward continuation maps serve as basis for revealing the structural pattern of the basement complex, and the shallower structures.

Galbraith and Saunders (1983) having analysed large amounts of airborne gamma ray spectral data collected by the United States National Uranium Resource Evaluation Program established that lithological unit can be classified according to the relationship between Th and K. They have also shown that a classification based on a plot of $\log_{10}$Th versus K can subdivide igneous rocks into conventional groupings. Gamma-ray data from Lady Loretta in Australia were useful as a means of defining lithological changes within formation which provided insight into regional variations in sediment maturity, provenance and carbonaceous content (Duffett, 1998). Guillemont (1987), applying gamma-ray spectrometry in Gabon, showed that it is possible to collect consistent data in an equatorial environment, although such areas are characterised by dense vegetative cover, substantial humidity and superficial alteration. He observed that the ternary colour synthesis of K-U-Th concentration is a powerful tool for discriminating lithologies. In Malawi, a ternary map compilation of spectrometric data in conjunction with an interpretation of the accompanying magnetic data have provided the basis for the revision of existing geological maps (Misener, 1987).

Billings (1998) and Wilford et al. (1997) reviewed the application of airborne gamma ray spectrometry for regolith and soil mapping (since the interpretation of aerial photography and satellite imagery has been the traditional means for the rapid mapping of soil types over large areas) and found that the airborne gamma ray spectrometry interpretation is a powerful means for regolith and soil mapping. Hardy (2004) on the other hand showed that radiometric data are useful in identifying soil characteristics to the level of Australian Soil Classification order and useful in delineating broad lithological units when used with a geology map. Hardy (2004) also showed that the potassium and thorium data sets are useful in delineating differences in the age of alluvium and broad difference in lithology such as acid to basic igneous rock. Jones, (1990) performed a filed and geochemical investigation of the Buem volcanic and its associate sedimentary rocks and showed the various lithological unit and how they dip. Osae et al., (2006) also investigated the Buem sandstone and determined their provenance and tectonic setting.

1.2 Problem Definition

Many airborne geophysical surveys have been conducted in Ghana including airborne magnetic, gravity, electromagnetic and radiometric to identify the various geological features over the country. The study area and its environs have been surveyed and studied by several geoscientists, particularly for the surface geological mapping and geochemical studies (Jones, 1990). The subsurface geological mapping has less been performed in the study by integrating geological records and geophysical data. Irrespective of this, only a little attempt has been made so far to understand the detailed relationship between structural features observed on the ground and those extending into the subsurface.

This project is aimed at re-processing aeromagnetic and radiometric data to study major surface and subsurface structures, and their relationship with surface structural features in the study area. A new interpretation (detailed geological map) would be generated showing magnetic units and structures, and the model of subsurface structures present in the area of study. Attempt would be made to estimate the depth to basement of the magnetic body.

1.3 The study area

1.3.1 Background

The study area is located mainly within the Jasikan District which is one of the old districts in the Volta Region of the Republic of Ghana. It covers five (5) other districts in the Volta region namely Hohoe, Kadjebi, Kpandu, Krachi and Biakoye (Fig. 1.1). The area is situated about 260 km north-east of Accra, the capital of Ghana and 135 km from Ho, the regional capital of Volta Region. It is one of the major agricultural production areas in the Volta Region of Ghana. The area covers most of Buem Traditional Area. Agriculture is the main source of employment and income generation venture for the majority of the inhabitant in the area. Majority of the local population are farmers with some involved GBG V VC VC VC VC in fishing, commerce and other works (Dickson & Benneh, 1985). The perennial and annual water bodies in the area do support much fishery activities, however big potentials exist for aquaculture in the area. The area is connected to the national grid, with available infrastructure, financial institutions, health and educational facilities. The road network in the area is relatively good (first and second class roads). There are also lot of feeder roads that link some key farming communities which are in deplorable state (Dickson & Benneh, 1985). The population of the area is just over 66,000 (Ghana Statistical Service, 2012).

1.3.2 Location and Accessibility

The study area is located in the mid-east portion of the Volta Region of Ghana and the area can be located between latitudes 7º 0' 18.0" N and 7º 40' 33.6" N longitudes 0º 8' 45.6" E and 0º 30' 3.6" E. It is bounded on the North-East by Kadjebi and North-West by Krachi District, on the west is the river Volta, Hohoe District to the South- East, and Kpando District to the South-West. The area has a total land surface area of 2386.02 Km^2 (Fig. 1.1)

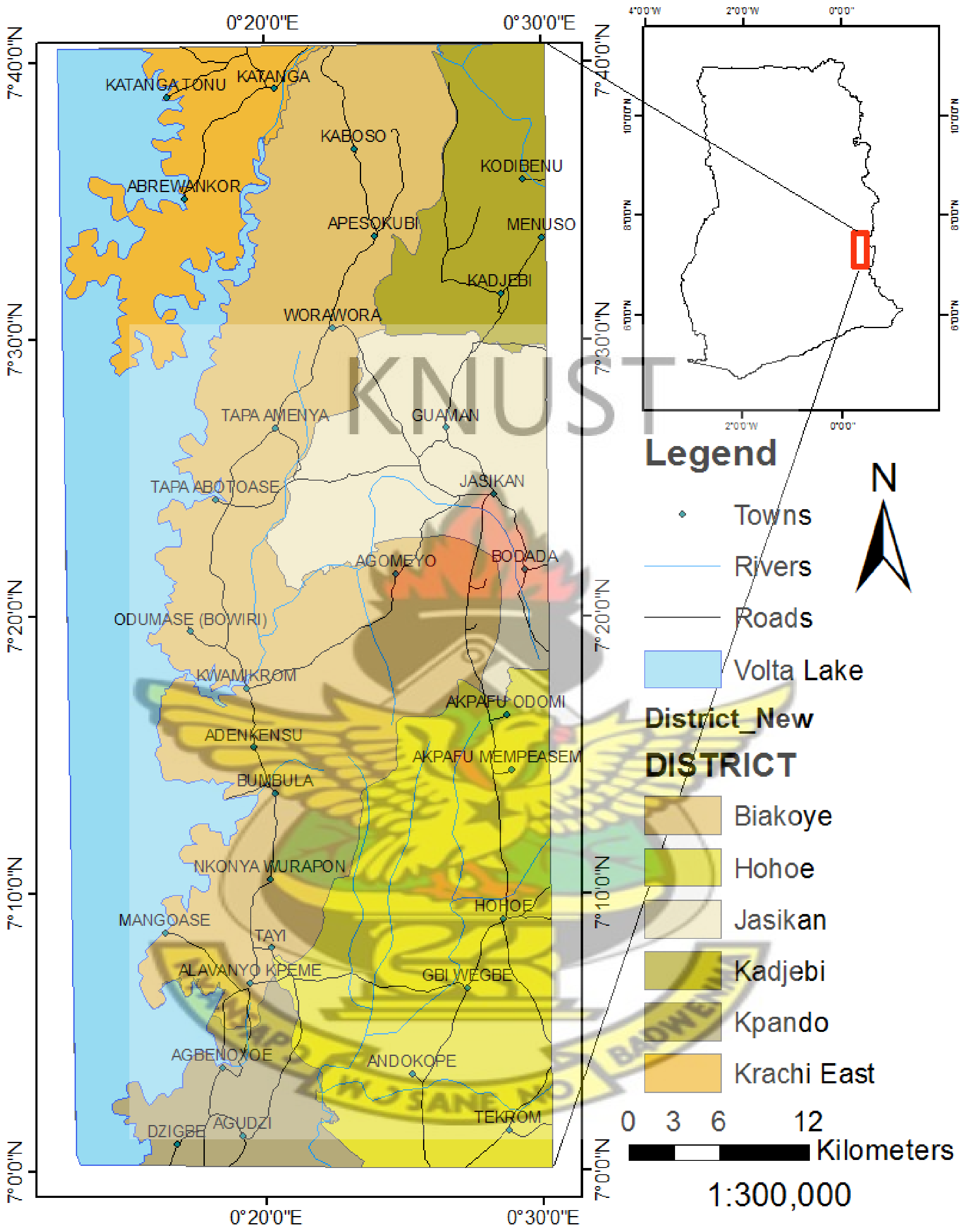

Figure 1.1 Location map of the Study area

1.3.3 Climate

The area falls within the wet equatorial agro-climatic zone. The area experiences an alternating wet and dry season each year. It experiences a double maxima rainfall regime. The major rainy season occurs between May and July with the peak occurring in June while the minor one occurs between September and October with the peak occurring in October (Dickson & Benneh, 1985). The mean annual rainfall generally varies between 1250 mm and 1750 mm. The dry season is mostly between December and February. The mean maximum temperature is 32ºc usually recorded in March whiles the mean minimum temperature is 24 ºc usually recorded in August (Dickson & Benneh, 1985).

1.3.4 Vegetation

The vegetation is generally depicted by moist deciduous forest. Due to the relatively high rainfall experienced annually in the eastern parts, the vegetation is thicker and more luxuriant. The forests are made up of different species of trees typical of the semi deciduous forest. The western part of the district is also characterized by the mixed savannah dotted with tree vegetation. Bamboo and other wet species are also found, especially along the banks of the streams and rivers. The vegetation supports wildlife and major animals found are monkeys, antelopes, bush pigs, pangolins grass-cutter, and reptiles. The area is endowed with the Odomi River Forest Reserve which covers about 18.45 km^2 of land. The area is also noted for the cultivation of shallow-rooted crops such as: pineapples, sugarcane, vegetables, maize and rice (Dickson & Benneh, 1985).

1.3.5 Relief

The topography of the area is hilly and undulating becoming almost flat in certain areas. It is almost surrounded by mountain ranges, typically is the Buem-Togo Ranges which is an extension of the Akuapem Ranges. The eastern parts of the area are relatively higher with occasional heights ranging between 260 m – 800 m above sea level. The areas consist of the western ridge which comprise of the Odumasi-Abutor range in the south, the Akayoa-Abotoase range in the middle and the Tapa range in the north. The characteristic features of the above hills are their approximate north to south trend, which is sub-parallel to the regional foliation, and the general steeper western scarps with local development of cliff faces (Dickson & Benneh, 1985).

1.4 Objectives of the Research

The main objective of the research is to carry out a comprehensive geological interpretation of the study area using airborne geophysical data namely magnetic and radiometric data.

Specific objectives are to:

- Map the lithology of the study area.
- Map geological structures of the study area.
- Estimate the depth to basement of magnetic body in the area.

1.4.1 Justification of the Objectives

The continued expansion in the demand for minerals of all kinds since the turn of the century have led to the development of many geophysical techniques of ever increasing sensitivity for the detection and mapping of the unseen deposits and structures (Telford et al., 1990). The structural control and the hydrothermal alteration of the rocks and geophysical characterization of mineral deposits can be discerned from integrated interpretation of airborne magnetic and radiometric data (Airo, 2002). In addition, integrated geophysical method offers a quick way of examining large areas, and it should prove useful in the search for mineral deposits in other parts of the world (Airo and Loukola-Ruskeeniemi, 2003).

The Earth's magnetic field of an area is directly influenced by geological structures, geological composition and magnetic minerals, most often due to changes in the percentage of magnetite in the rock. Objects that are underground can warp the simple patterns of the Earth's magnetic field into complex shapes (Grant and Martin, 1966). The magnetic map allows a visualization of the geological structure of the upper crust of the Earth, the presence of faults and folds (Atchuta and Badu, 1981). In exploration geophysics, aeromagnetic maps are important tools for mapping geology (Smith and O'Connell, 2007). A study of these shapes on a magnetic map can reveal much information about the features that are underground. This information can include the location, size and shape, volume or mass, and depth of the features; in some cases, the age of a feature and its material (stone, soil, metal) may be estimated (by logging) (Telford et al., 1990).

Radioactive elements occur naturally in the crystals of particular minerals and it changes across the Earth's surface with variations in rock and soil type (Gregory and Horwood, 1961). The energy of gamma rays is related to the source radioactive element, hence, it can be used to measure the abundance of those elements in an area. Airborne radiometric survey measures the natural radiation in the Earth's surface, which can give the distribution of certain soils and rock type formation. Airborne radiometric survey is also useful for the study of geomorphology and soils. The radiometric data is an excellent tool for mapping and tracing individual lithological units in areas of outcrop (Beltrão et al., 1991). Many times, there is a good correlation between patterns in the radiometric data and un-weathered rocks (Gunn et al., 1997b).

1.5 Structure of the Thesis

The thesis work has six (6) chapters with each chapter addressing a main heading. Chapter one introduces the subject matter, outlining the background of the research, objectives of the research, justification of the objectives of the research, location and accessibility of the research area, physiography, climate and occupation of inhabitants of the research area as well as literature review.

Chapter two gives the general overview of the geological settings. It reviews both the regional and local geology of the area.

Chapter three outlines the main fundamental theory behind airborne radiometric and magnetic survey, taking into account some enhancement techniques applicable to magnetic and radiometric data.

Chapter four gives an overview of the methods used to acquire the datasets and how the enhancement techniques were used in enhancing the datasets. This chapter also outlines the processing steps employed in the data processing.

Chapter five analyses the various maps obtained from the radiometric and magnetic datasets. Interpretations to the deduced maps are also given in this chapter. Finally, this chapter correlates the magnetic and radiometric data to produce an integrated geological map of the study area.

Chapter six draws conclusions from the research and makes recommendations for future work.

CHAPTER TWO

2 Geological Background

2.1 Regional Geological Setting

Most part of Ghana falls within the West African Shield (Fig. 2.1). The main rock units underlying the country are the Birimian, the Tarkwaian, the Dahomeyan Systems, the Togo Series and the Buem Formation. Intruded into the Birimian rocks are Cape Coast and Winneba granitoids (basin type), Dixcove granitoids (belt type) and the rare Bongo granitoids. These Precambrian rocks are overlain by the Voltaian System (Late Proterozoic to Paleozoic) (Wright, 1985). Younger rocks as well as unconsolidated sediments occur at various places along the coast (Fig. 2.2).

The geology of Ghana can be divided into three main geologic provinces (Hasting, 1982):

1) an early Proterozoic Birimian Supergroup and Tarkwaian group of the main West African shield occupying the west and northern parts of the country;
2) a Pan African province covering the Dahomeyan, Togo and Buem formations in the southeast and eastern parts of the country; and
3) Infracambrian/Palaeozoic sedimentary basin situated in the central and eastern parts of the country Fig. 2.1.

2.1.1 Proterozoic Birimian Supergroup

The Birimian Supergroup in Ghana has long been divided into two series: (1) a lower series of mainly sedimentary origin, and (2) an upper series of the greenstones, mainly metamorphosed basic and intermediate lavas and pyroclastic rocks (Junner, 1935). The lower Birimian rocks comprise an assemblage of fine-grained rocks with a large volcano clastic component. Typical lithologies include tuff, aceous shale, phyllite, siltstone, greywacke and some chemical (Mn-rich) sediment. The upper Birimian rocks comprise mostly basalts with some interflow sediment (Eisenlohr and Hirdes, 1992). Recent studies, however, shows that the lavas of the greenstone belts in Ghana and the sediments of the sedimentary sequence in the basins were deposited contemporaneously as lateral facies equivalents (Leube et al., 1990).

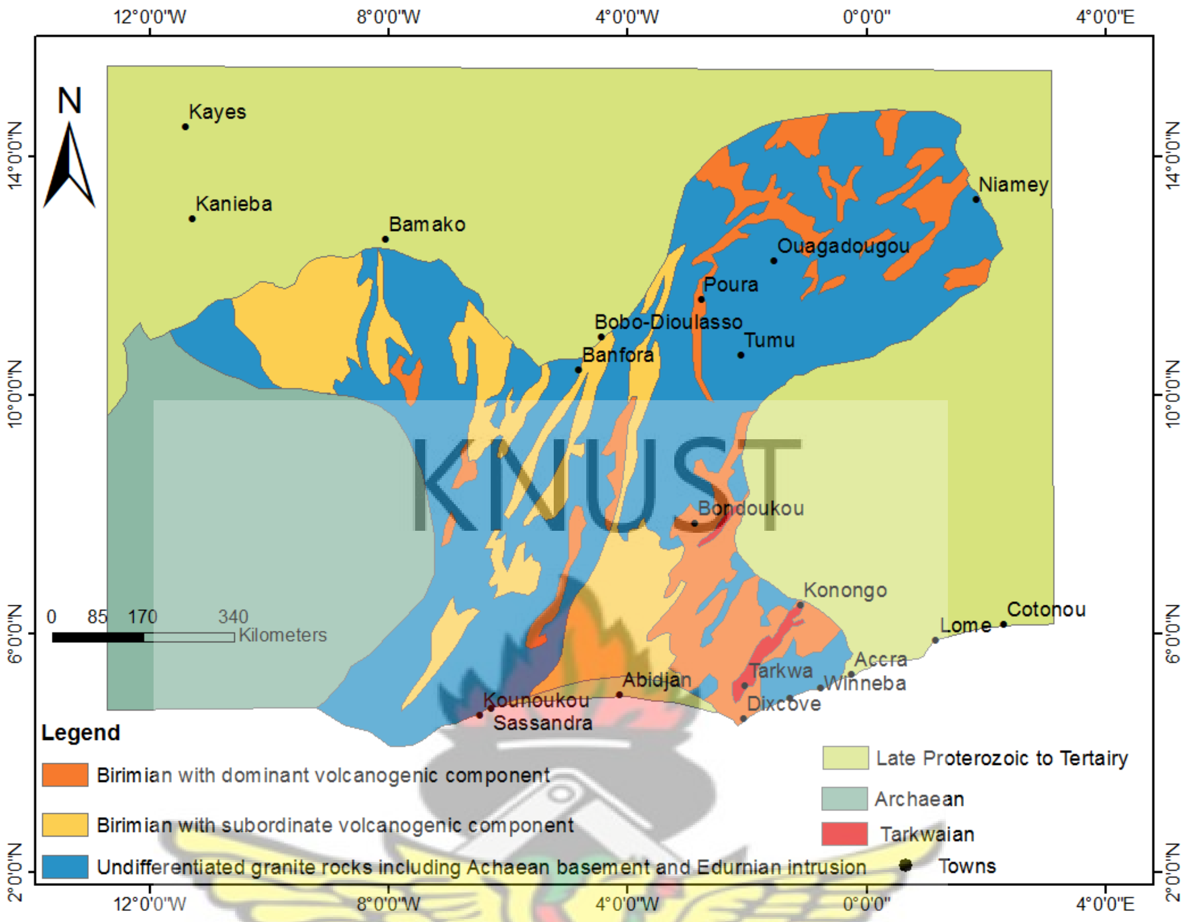

Figure 2.1 Generalised distribution of Birimian supracrustal belts in West Africa (after Wright et al., 1985)

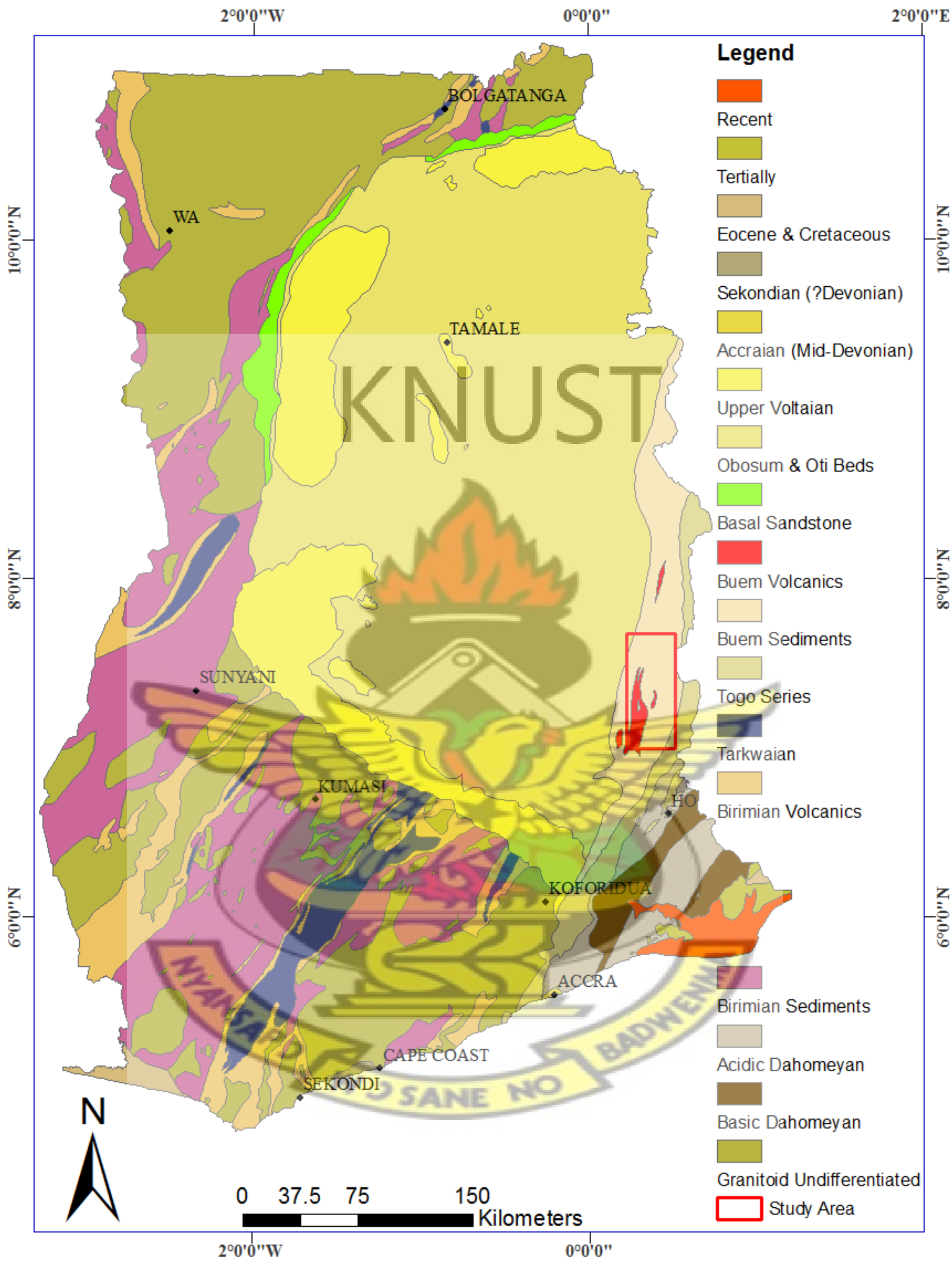

Figure 2.2 Geological map of Ghana showing study area (modified after GSD (1988))

2.1.1.1 Birimian Metavolcanics

There are six volcanic belts in the Birimian, namely the Kibi-Winneba, Ashanti, Sefwi, Bui, Bole-Navrongo and Lawra belts. The belts have a slight keel-shaped outline that is perhaps produced by the associated diapiric, intrusive plutons (Kesse, 1985). The belts consist mainly of metamorphosed basaltic and andesitic lavas, now hornblende- actinolite schists, calcareous chlorite-schists and amphibolites (the greenstones). Minor intrusions of mafic rocks cut the volcanics. Volcaniclastic sediments occur interbedded within the basaltic flows of all volcanic belts (Leube et al., 1990). Metamorphism in most volcanic rocks is confined to the chlorite zone of the greens schist facies. Amphibolite-facies assemblages occur sporadically but especially along the margins of granitoid bodies.

2.1.1.2 Birimian Metasediments

Birimian metasedimentary rocks of Ghana are divided into: (1) volcaniclastic rocks; (2) turbidite-related wackes; (3) argillitic rocks; and (4) chemical sediments. Boundaries between these subdivisions are gradational (Leube et al., 1990). The volcaniclastic sediments comprise chiefly of sand-to silt-sized, partly reworked pyroclastics that is shown by the presence of quartz, idiomorphic plagioclase crystals, chloritised glass fragments, and the absence of heavy minerals (Leube et al., 1990).

2.1.1.3 Birimian Granitoids

Four main types of granitoids are recognised in the Birimian of Ghana. They include Winneba, Cape Coast, Dixcove and Bongo granitoids (Junner 1935; Kesse, 1985). The latter three have been recently termed “Basin”, “Belt” and “K-rich” granitoids. (Leube et al., 1990). The Cape Coast (Basin type) and Dixcove (Belt type) granitoids are widespread in Ghana, the Winneba belt is limited to small areas near Winneba, and the Bongo type crops out in the Bole Navrongo Belt and in the Banso area (Kesse, 1985).

The (Basin type) granitoids occur only within the Birimian sedimentary basins. Some of them are two mica granites. This group also includes gneisses, and these are especially well developed in the metasedimentary basin. They are typically biotite-bearing. It has been suggested that the Basin granitoids, which appear migmatitic in some localities, might represent an older continental basement on which the Birimian supracrustals were deposited. Based on the degree of foliation, early workers assumed that the Basin type granitoids intruded during regional deformation and that Dixcove granites were emplaced after deformation (Kesse, 1985). However, later work by Hirdes et al. (1992) demonstrated, in contrast to long held views that Dixcove granitoids formed at about 2,175 Ma and are about 60 and 90 Ma older than the Cape Coast granitoids. Taylor et al. (1988) suggest that the Cape Coast and Dixcove granitoids are coeval.

Belt type granitoids are metaluminous and typically dioritic to granodioritic in composition. They intrude Birimian volcanic rocks. They are typically hornblende-bearing and are commonly associated with gold mineralisation where they occur as small plutons within the volcanic belts. The granitoids are massive in outcrop, do not have a compositional banding or foliation, and are thus generally considered post-deformation. However, belt-type granitoids have never been shown to intrude or crosscut basin granitoids (Murray, 1960). The granitoids commonly contain basalt xenoliths, and there appears to be a gradational boundary between finer and coarser grained belt granitoids and basalts (Hirst, 1946).

2.1.2 The Tarkwaian System

The Tarkwaian is a Proterozoic supracrustal system overlying the Birimian. It consists mainly of shallow water sediments and is present in all the Birimian volcanic belts (Junner, 1935). It consists of coarse clastic sedimentary rocks that include conglomerates, arkoses, sandstones and minor amounts of shale. The Tarkwaian is usually regarded as the detritus of Birimian rocks that were uplifted and eroded following the Eburnean tecto-thermal event (Eisenlohr and Hirdes, 1992). Economically, the most important unit of the Takwaian is the Banket series which contains economic concentrations of gold in several areas.

2.1.3 Voltaian Basin

Almost one third of Ghana is covered by sediments of the inland Voltaian Basin which covers an area of about 103,600 km^2; it consists mainly of flat lying or very gently dipping sediments sitting on a major Precambrian unconformity (Griffis, et al. 2002). This unconformity marks an erosional surface, which apparently covered the entire Man Shield. The Voltaian Basin area appears to have been the eastern margin of a large West African cratonic block, which had broken away from the former supercontinent Rodinia (Hoffman, 1999). This block would later join up with other cratonic blocks to form a new supercontinent, Gondwana, during the Pan-African thermo tectonic event (approximately 600-550 Ma). The Voltaian Basin is a structural basin. Sedimentary rocks along the eastern margin were folded during erogenic activity associated with a late Precambrian to early Paleozoic thermal event, the Pan-African Thermo-Tectonic Episode (Kennedy, 1964).

Numerous geological studies have been carried out in the Voltaian Basin starting from the early days of the former Gold Coast Geological Survey. Most of these covered only restricted areas but, in 1946, Hirst provided a more comprehensive evaluation of the stratigraphy on a regional basis and established an Upper, Middle and Lower series of units. Shallow marine, quartz rich sediments and a basal conglomerate dominate the Lower series. The very thick Middle series include a great variety of sandstones and shales with some conglomerate interbeds, a few carbonate sequences and clastic units generally identified as glacial tillites. The Upper series is more or less restricted to the central and eastern parts of the basin and it is dominated by massive, quartz-rich sandstones.

More detailed stratigraphical studies have revised the division of the Voltaian Basin sediments modestly and attempted to better define the regional tectonic setting and stratigraphic correlations (Kesse, 1985). The current stratigraphy includes the lower Bombouaka Supergroup, which is approximately 1000 m thick and is dominated by mature sandstones and a central section of siliceous and clay-rich units; these were deposited on a shallow submerged epicontinental marine platform. The succeeding Oti (or Penjari) Supergroup is considerably thicker (average is about 2500 m) and is unconformable with the underlying Bombouaka sediments. The Oti sediments include a distinctive lower sequence with tillite and sandstones, carbonate, and fine grained cherty sediments (silexite). The Oti also includes thick sequences of less mature clastic sediments indicative of a deeper marine depositional environment, probably on a passive continental margin. In places, the tillites actually sit on Birimian basement and indicate extensive local erosion and gouging by Neoproterozoic glaciers that probably correlate with similar events in various other parts of Africa and most likely indicate a major, worldwide glacial event (Hoffman, 1999). The youngest sequence of sediments in the Voltaian Basin, are exposed only in Ghana and are referred to as the Tamale Super group (Affaton et al., 1980). This sequence is only about 500 m thick and features a basal section of sediments that also include glacial tillites. These are overlain mainly by cross-bedded quartz sandstones with subordinate shale and mudstones that are now interpreted to represent a foreland molassic basin (Affaton et al., 1980).

2.1.4 The Togo Series

The Togo Series is an irregular, fault-bounded belt of metamorphic units that comprise the series of hills and ridges (Akwapim) that start from just west and north of Accra and extend along the Ghana-Togo border and into northern Benin where it is called the Atacora Range. The Togo Series consists mainly of metamorphosed sediments (quartzite, schist, phyllite and marble) but there are some metavolcanics as well. Along major faults, slices of higher grade metamorphic (Dahomeyan) and lenses of ultramafic and mafic units can be found. The Togo Series originally consisted of alternating arenaceous and argillaceous sediments, which were converted into phyllites, schists and quartzites in the wake of metamorphism, except in few places, where unaltered shales and sandstones occur. Quartzite, quartz-schist, sericite quartz schist, sericite schist and phyllite are the predominant rocks, but hornstones, jaspers and hematite quartz-schists some of which were formed after the deposition of the sediments also occur in the Togo Series (Junner, 1935). The levels of metamorphism and degree of deformation increase towards the southeast (Wright et al., 1985). To the east of the Togo Series is a generally low-lying area (Accra plains) underlain by high-grade, Dahomeyan metamorphic terrain. The level of metamorphism is largely of amphibolite facies although there are areas of high-grade granulite facies with garnet, pyroxene, and scapolite. The typical rock lithologies include migmatites, gneisses, mica schists, amphibolites, marbles, syenites and granitoids. The Togo Belt marks the western limits of a very large area affected by the Pan-African thermo tectonic event that peaked at about 600-550 Ma and whose effects extend right across Nigeria (Griffis, et al., 2002). The Togo Belt is now recognized to be a collisional belt and suture zone between the West African Birimian craton and an eastern cratonic block that became welded together at a time the supercontinent of Gondwana was being created (Hoffman, 1999).

2.1.5 The Buem Formation

The westernmost Buem Formation consists of a thick, lower sequence of clastic sediments with some carbonate and tillite units succeeded by clastics and volcanics that include mafic flow units and pyroclastics (Kesse, 1985). The formation consists of a thick sequence of shale, sandstone, and volcanic rocks with subordinate limestone, tillite, grit and conglomerate (Dapaah-Siakwan and Gyau-Boakye, 2000). The rocks underlie an elongated area on the eastern part of the country extending northeast to the Republic of Togo. The sandstones overlie the basal beds of shale and the conglomerate and tillite overlie the sandstone (Dapaah-Siakwan and Gyau-Boakye, 2000). Rocks of volcanic origin form the upper part of the Buem formation and include lava, tuff, and agglomerate interbedded with shale, limestone, and sandstone (Dapaah-Siakwan and Gyau-Boakye, 2000). Rocks of this formation are largely inherently impervious, but fracturing and weathering create secondary permeability in them at some locations to form high yielding aquifers. In general, the rocks of the Buem Formation are not metamorphosed, and deformation is expressed as the result of thrust tectonics with development of imbricated thrust systems and duplexes. Folds are not well developed but are expressed as chevron folds in the finest grained material (Kesse, 1985). Folding and faulting also makes it difficult to estimate average thicknesses for the various sequences but the volcanics and closely related clastics are at least 5000 m thick and the underlying clastic sequences are of the same order (Kesse, 1985). The deformation in the Buem Formation includes large-scale thrusting towards the west. Closely associated with the thrust sheets are numerous occurrences of serpentinized ultramafic bodies (Wright et al., 1985). Early workers in the region generally considered the Buem Formation to be older than the Voltaian Basin sediments (Kesse, 1985) but detailed studies by Affaton et al., (1980) indicate that the Buem Formation is probably a lateral equivalent to the Oti Supergroup of the Voltaian Basin. The mafic and ultramafic units probably represent tectonically emplaced slices of paleo-oceanic crust caught up in the suturing of adjacent continental blocks during the Pan-African orogeny (Griffis, et al., 2002).

2.1.6 The Dahomeyan

The Dahomeyan System is a part of the second major tectono-stratigraphic terrain in Ghana; it underlies eastern and south-eastern Ghana. The Dahomeyan is the easternmost rock group in Ghana and differs significantly from other rocks in Ghana in that it is composed of high grade metamorphic rocks. The system consists of four lithologic belts of granitic and mafic gneiss. The mafic gneisses are relatively uniform oligoclase, andesine, hornblende, salite and garnet gneisses of igneous origin and generally of tholeiitic composition (Holm, 1974). The granite gneisses interlayer with the mafic gneiss and are believed to be metamorphosed volcaniclastic and sedimentary rocks. The Dahomeyan System occurs as four alternate belts of acid and basic gneisses trending

SSW to NNE from the coastal plains extending into Togo (Kennedy, 1964). Mani (l978) has suggested the following Dahomeyan stratigraphic scheme:

Table 2.1 Classification of the Dahomeyan Stratigraphy (Modified after Mani, 1978)

Acid Dahomeyan		Pegmatite, aplite, quartz veins, Cape Coast granite, granitic gneiss and migmatite, Granite, gneiss
Alkalic Gneiss		Kpong conglomerate, nepheline gneiss
Basic Dahomeyan	**Basic Intrusive**	Dolerite, norite, chromitiferous pyroxenite
	Metabasics	Garnet-hornblende-gneiss, garnet-hornblende-(pyroxene)-gneiss, hornblende and biotite schist

Intruded in the Dahomeyan are granites, nephelinesyenite and dikes of various compositions (Kennedy, 1964).

2.2 Geology of the Study Area

The study area is mainly dominated by the Buem Formation which defines the eastern limit in Ghana of the Voltaian Basin. It consists mainly of a thick sequence of shale, sandstone, and volcanic rocks. It also includes bedded cherts and siliceous shales (silexites), limestones, dolomites and, north of Togo, some banded iron formation (BIF). Volcanic formations, of alkaline to calc-alkaline affinity, are interbedded in the formation (Delor, et al., 2009). In general, the rocks of the Buem Formation are not metamorphosed, and deformation is expressed as the result of thrust tectonics with development of imbricated thrust systems and duplexes. Folds are not well developed but are expressed as chevron folds in the finest grained material. Close to their contact, the area is the folded and metamorphosed with the Togo series and the Voltaian formation (Delor, et al., 2009).

It is acknowledged that infill material of the Buem was probably derived from the Voltaian Basin and from the Togo Group (Delor, et al., 2009).

2.2.1 Volcanic Group

The volcanic group includes many closely intermingled volcanic rock types: various facies of basalts, microgabbros, andesites or trachytes, and coarse-grained polymictic pyroclastites or agglomerates (Geotech Airborne Limited, 2009). The volcanic group of rock occurs along the western margin of the study area (Fig. 2.3). The rocks area better exposed on the Abutor Hill Range southwest of Kwamekrom and in stream valleys northwest and southwest of Odumasi (Blay, 2003). The volcanic rocks are poorly exposed in the lowland area west of Tapa-Abotoase. West of Akayao and the hill range of which Owisa is a peak, they are not exposed but their presence is indicated by characteristic dark brown clayey nature of the soil and a few scattered fragments of basalt and andesite (Blay, 2003). The Abutor-Odumasi Range is formed by hard resistant volcanic agglomerate, vesicular basalt and pink jasper. Some of these east-west valleys are marked by faults (Blay, 2003).

Two volcanic rock types occur in the area, namely, agglomerate and amygdaloidal basalt, which exhibit pillow lava structure (Jones, 1990). Both types are so closely intermingled that it is not possible to map them separately. The agglomerates vary in colour from pale-green to dark greenish-grey and are hard and massive. These are also very coarse and contain angular rock fragments of basalt, pink jasper and baked greenish shale. The basaltic types are coloured greenish-black to greyish-black. They are massive, fine-grained, and are cut by random calcite veinlets. Generally the basalts are vesicular in texture (Blay, 2003). The sediments enclosing the volcanics are red shales, feldspathic to quartz arenite sands, conglomerates, jasper and minor limestone (Jones, 1990). The Buem volcanic rocks are mainly documented to the south of the Kpandu area. The corresponding volcanic component of the Buem was described from bottom to top as basalt pillow lavas, feldsparphyric basalts, olivine-phyric and aphyric basalts, rhyolitic flows, agglomerates and tuffs (Delor, et al., 2009).

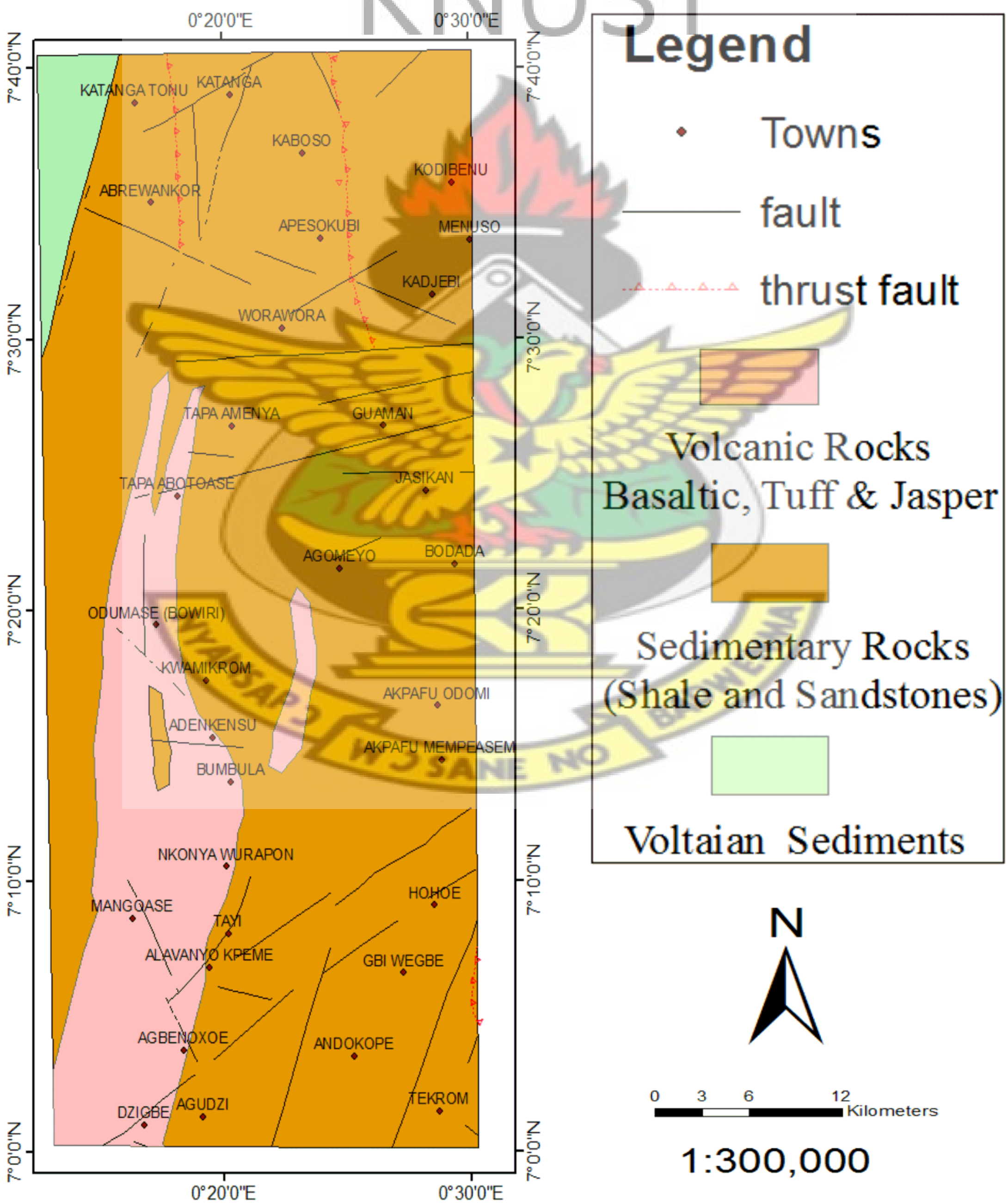

Figure 2.3 Geology map of Study Area (modified after GSD, 1988)

2.2.2 Arenaceous Group

The arenaceous rocks include medium-to coarse-grained feldspathic sandstones, quartzitic sandstones, gritty quartzites, quartz-schist and poorly exposed conglomerate. The conglomerate occurs mainly as boulders south of Tepa-Abotoase. Generally, the arenaceouse rocks outcrop in the graphically higher ground (Blay, 2003). Minor thin band of vary-coloured shales and siltstones occur interbedded with the sandstone. The gritty quartzite and quartz-schist occur close to or within the Buem-Togo contact zone. Thin argillites were found interbedded with the arenites (Blay, 2003).

The Buem sandstones in some parts of the area are poorly exposed. The best exposed in those area are found in and around Tetaman and across the hill range of Borada where they are interbedded with thin-bedded shale. Good exposures of coarse-grained pebbly, haematitic, quartz-veined sandstone are also found along the southwest path from Sokpo to Akpafu-Tadzi. There are also well exposed sandstones on the western ridge south of Akayao. The path from Tapa-Amanya north-westwards to Tepa and Akaniem and from Tapa to Odei also have comparatively good sandstone exposures. From Tapa westward to either Odei or Akaniem, the sandstones become steadily coarse-grained until the foot of the scarp face where coarse-grained and pebbly type outcrop (Blay, 2003). The sandstones range from yellow-orange feldspathic sandstones to grey-white quartz arenites with well-rounded and spheroidal quartz grains. The sandstones are frequently cut by quartz veins (Jones, 1990).

In the west-central ridge area the sandstones are fairly well exposed except along the Kabo Forest Hill. The Togo Plateau is formed by hard, massive, feldspathic and quartzitic sandstone which can be traced geographically into the Nkonya and Alavanyo area to the south of the study area. Bell (1962) mapped and referred to them as quartzites. The sandstones form high cliffs on the scarp face. In Jasikan town, the sandstones are gritty, rather schistose and are cut by small quartz veins. Identical types outcrop between Jasikan and Tetaman along the main road. These sandstones are also deformed and brecciated. They contain clayey and other rock fragment (Osae et al., 2006).

The Buem arenaceous rocks of the study area are poorly sorted sandstones consisting of sub-angular and sub-rounded grains of quartz, albite, microcline, and in some cases shales and phyllitic rock fragments. Towards the Togo boundary and at the foot of the hill ranges, the sandstones are essentially quartzites. The Buem sandstones do not resemble either the Voltaian sandstone or the Togo Series sandstones. The lenticular shape of the sandstone bodies and paucity of sedimentary structures in the massive sandstones suggest their deposited as alluvial fan deposits (Jones, 1990). Osae et al., (2006) classified Buem sandstones as quartz arenite and feldspathic arenite. He said the feldspathic arenites is generally composed of argillaceous materials and the quartz arenites are typically cemented with quartz, hematite (Fe_2O_3), and sericite. He added that the quartz arenites are depleted of K_2O and TiO_2 but enriched in Fe_2O_3 as compared to the feldspathic arenites.

2.2.3 Argillaceous Group

This argillaceous group are of massive shaly rock with interbedded siltstones, thin-bedded sandstones and impure limestone members. The shales are reddish-brown with occasional yellow or green bands showing bedding (Jones, 1990). Except places where minor shale is found to be interbedded with the arenaceous Buem rocks. The Buem argillaceous rocks are restricted to lower topographic level and in stream valleys where they are better exposed (Blay, 2003).

In the area, the shale outcrops only in Nuboiasn Tsi streams west of the Helu-Soba motor road. The shales exposed in the two streams are intensely minor folded and deformed and may be termed metashales (Blay, 2003). In the Nsuta, Guaman and Atonko areas, massive, deformed pale yellow, purple and greenish micaceous shales outcrop. The road linking Odomi and Jasikan exposes quite a good section of the pinkish, greenish and pale yellow shale. The greenish types are more micaceous and siliceous and show evidence of having been tectonically deformed. The Papase massive shale is beautifully exposed at Kwamekrom. Streams south of Papase are underlain by pale yellow and purple shales with minor interbedded fine grained shaly sandstones (Blay, 2003). The only sedimentary structures seen in the shales were dessication cracks and ripples west of Kwamikron (Jones, 1990).

2.2.4 Geological Structures in the Study Area

The foliation of the rocks in the study area is parallel to the bedding. The rocks are generally not metamorphosed except towards their boundary with the Togo and the Voltaian. Reference to the geological map shows that, the strike and dip of the bedding plane vary from place to place (Bell and Crook, 2003). Junner (1940) believed that the sandstones of the Kpandu Hills and Dayi Plateau were strongly folded and showed greater dips than the volcanics. The shape of the minor folds is essentially isoclinal. The folding is interpreted to be represented by open to close asymmetric folds. Stereographic analysis of the area revealed a north-northwest fold trend, with fold axes plunging at south-southeast (Blay, 2003). Stereographic analysis of the area revealed the following fault trend: north faults, north-northeast faults and south-east fault. The most important ones are the north fault, which are recognised as thrust fault (Blay, 2003). The other faults are essentially cross faults. They are mostly normal fault with, in some case, fairly large strike slip movement as deduced from topographic displacement of north trending hill (around the Alavanyo hills) (Blay 2003).

CHAPTER THREE

3 THEORETICAL BACKGROUND

3.1 Magnetism

The principle underlying the operation of the Magnetic Method is based on the fact that when a ferrous material is placed within the Earth's magnetic field, it develops an induced magnetic field. The induced field is superimposed on the Earth's field at that location creating a magnetic anomaly. Detection depends on the amount of magnetic material present and its distance from the sensor. The anomalies are normally presented as profiles or as contour maps.

Ninety percent of the Earth's magnetic field looks like a magnetic field that would be generated from a dipolar magnetic source located at the center of the Earth and aligned at 11.5^{o}, with the Earth's rotational axis. The remaining 10 % of the magnetic field cannot be explained in terms of simple dipolar sources. The main field (90 %) is the largest component of the magnetic field and is believed to be caused by electrical currents in the Earth's fluid outer core. For exploration work, this field acts as the inducing magnetic field. Crustal magnetic field is the portion of the magnetic field associated with the magnetism of crustal rocks. This portion of the field contains both, magnetism caused by induction from the Earth's main magnetic field and from the remnant magnetization of both surface and crustal rocks. Relatively small portion of the observed magnetic field is generated from magnetic sources external to the earth. This field is believed to be produced by interactions of the Earth's ionosphere with the solar wind.

3.1.1 The Earth Magnetic Field

From the point of view of geomagnetism, the earth may be considered as made up of three parts: core, mantle and crust. Convection processes in the liquid part of the iron core give rise to a dipolar geomagnetic field. The mantle plays little part in the earth's magnetism, while interaction of the (past and present) geomagnetic field with the rocks of the Earth's crust produces the magnetic anomalies. Magnetic field in SI units is defined in terms of the flow of electric current needed in a coil to generate that field (Reeves et al., 1997). As a consequence, units of measurement are volt-seconds per square metre or Weber/m^2 or Teslas (T). Since the magnitude of the earth's magnetic field is only about 5 x 10^{-5} T, a more convenient SI unit of measurement in geophysics is the nanoTesla (nT = 10^{-9} T). The geomagnetic field varies from less than 22000 nT in southern Brazil to over 70000 nT in Antarctica south of New Zealand. Magnetic anomalies as small as about 0.1 nT can be measured in conventional aeromagnetic surveys and may be of geological significance. One nT is numerically equivalent to the gamma which is an old (c.g.s.) unit of magnetic field (Reeves et al., 1997).

3.1.2 The Geomagnetic Field

The definition of the main geomagnetic field at any point on the earth's surface as a vector quantity requires three scalar values (Fig. 3.1), normally expressed either as three orthogonal components (vertical, horizontal-north and horizontal-east components) or the scalar magnitude of the total field vector and its orientation in dip and azimuth. With the exception of a few specialised surveys, aeromagnetic surveys have always measured only the scalar magnitude of F, making the latter system more convenient for present purposes.

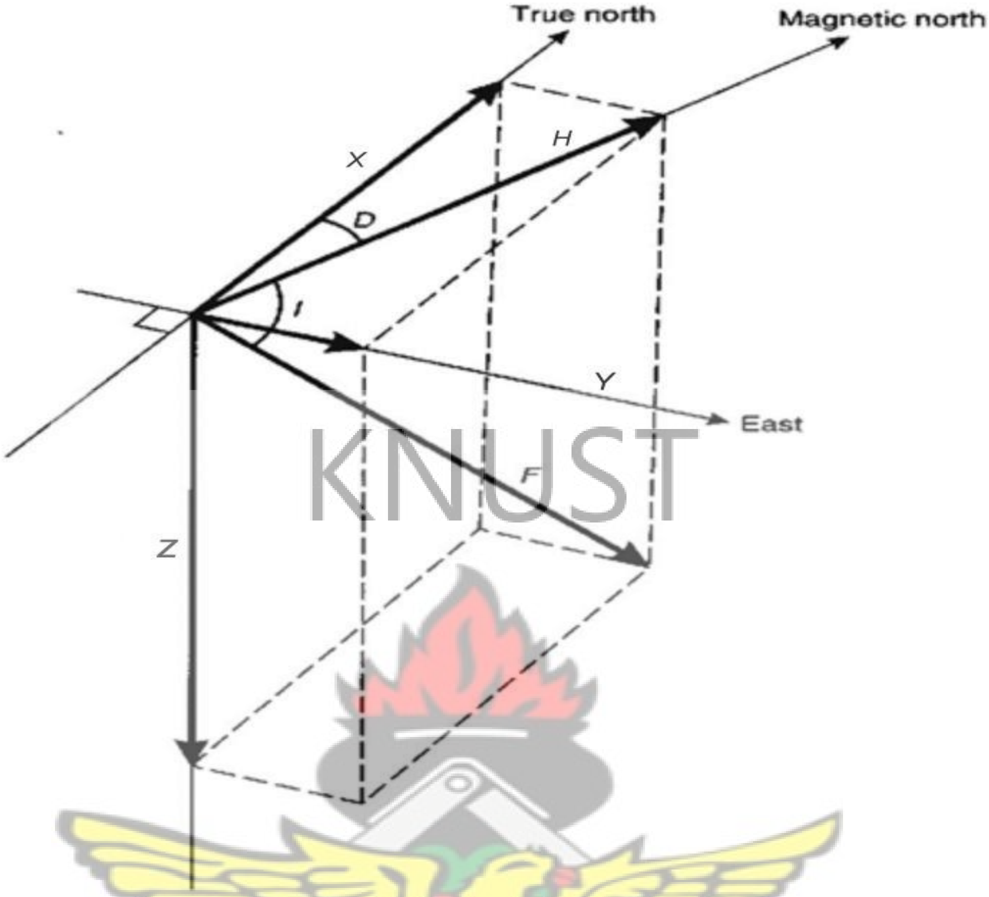

Figure 3.1 Elements of Earth's Magnetic Field; Z: Vertical component H: Horizontal component

The angle the total field vector makes above or below the horizontal plane is known as the magnetic inclination, I, which is conventionally positive north of the magnetic equator and negative to the south of it (-90° ≤ I ≤ +90°). The angle between the vertical plane containing F and true (geographic) north is known as the magnetic declination, D, which is reckoned positive to the east and negative to the west. The value of D is commonly displayed on topographic maps to alert the user to the difference between magnetic north, as registered by a compass, and true north (Reeves et al., 1997).

Since mapping of local variations in F attributable to crustal geology is the purpose of aeromagnetic surveys, it is the definition of the 'normal' or global variation in F that must be subtracted from observed F to leave the (time invariable) magnetic anomaly that concerns us here. As often in geophysics, the need to define the normal before being able to isolate the 'anomaly' is clear. Unlike the simple case of the gravity field, however, the time-variations of the magnetic field are also quite considerable and complex and therefore need to be addressed first (Reeves et al., 1997).

Equations relating the three (3) vectors and two (2) angles include:

$$\begin{aligned}
&H = F\cos(I)\\
&Z = F\sin(I) = H\tan(I)\\
&X = H\cos(D)\\
&Y = H\sin(D)\\
&X^2 + Y^2 = H^2\\
&X^2 + Y^2 + Z^2 = F^2 = H^2 + \Delta Z
\end{aligned} \tag{3.1}$$

3.1.2.1 Temporal variations

The variations in F with time over time-scales ranging from seconds to millions of years have a profound effect on how magnetic surveys are carried out, on the subtraction of the main field from the measured field to leave the anomaly, and in the interpretation of the resulting anomalies. These variations are described briefly, starting with variations of short time-span (some of which may be expected to occur within the duration of a typical survey) and ending with those of significance over geological time (Reeves et al., 1997).

3.1.2.2 Diurnal variations

Diurnal variations arise from the rotation of the earth with respect to the sun. The 'solar wind' of charged particles emanating from the sun, even under normal or 'quiet sun' conditions, tends to distort the outer regions of the earth's magnetic field, as shown in Figure 3.2. The daily rotation of the earth within this sun-referenced distortion leads to ionospheric currents on the 'day' side of the planet and a consequential daily cycle of variation in F that usually has an amplitude of less than about 50 nT (Reeves et al., 1997).

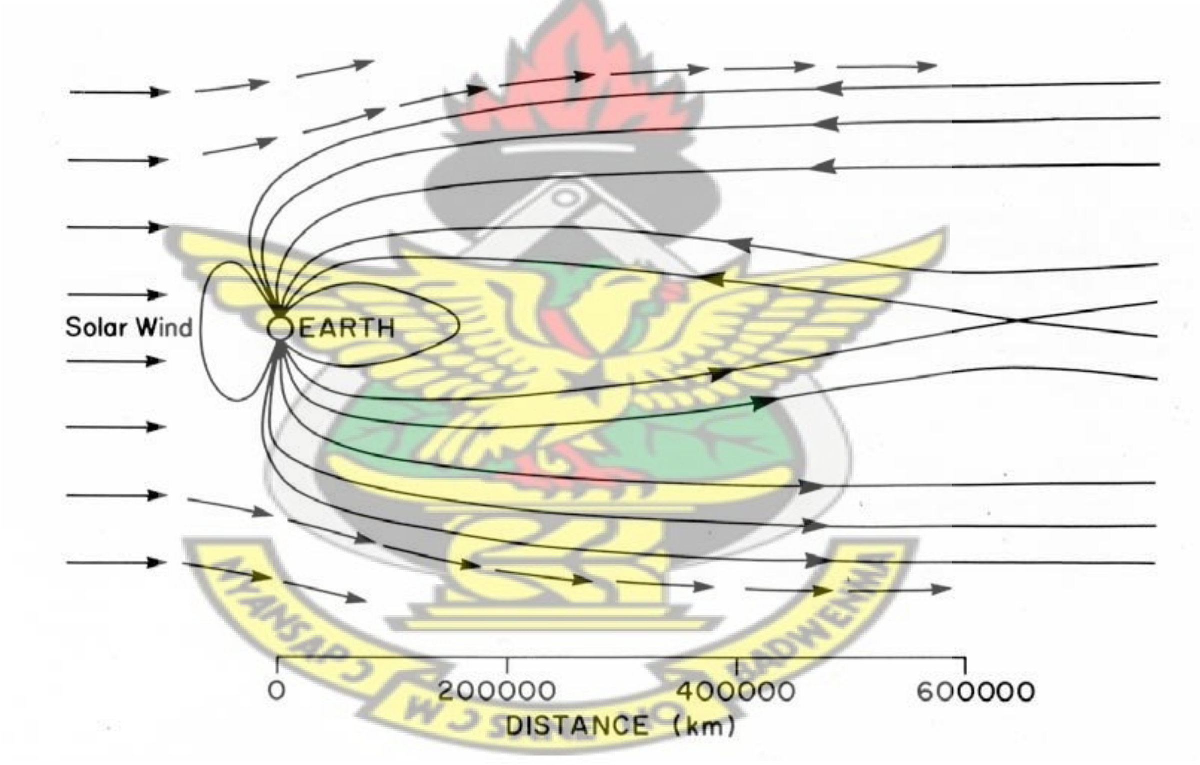

Figure 3.2: The solar wind distorts the outer reaches of the earth's magnetic field causing current loops in the ionosphere (Reeves et al., 1997)

The main variation occurs towards local noon when peaks are observed in mid-latitudes and troughs near the magnetic equator. Surveys have to be planned so as to allow for corrections to be made for diurnal (and other) variations

3.1.2.3 Secular variation

Variations on a much longer time-scale hundreds of years are well documented from historical data and the accurate magnetic observatory records of more recent decades. The variation is due to slow movement of eddy currents in Earth’s core. The main manifestation of secular variation globally is changes in size and position of the departures from a simple dipolar field over years and decades. The effects of these changes at a given locality are predictable with a fair degree of accuracy for periods of five to ten years into the future, but such predictions need to be updated as more recent magnetic observatory and earth satellite recordings become available (Reeves et al., 1997).

As an approach to standardisation of main field removal in aeromagnetic surveying, a mathematical model for the global variation in F is formalised from all available magnetic and, more recently, satellite observations worldwide every five years in the International Geomagnetic Reference Field (IGRF) (Reeves et al., 1997).

3.1.3 The International Geomagnetic Reference Field (IGRF)

The magnitude of F will fall between 20 000 and 70 000 nT everywhere on earth and it can be expected to have local variations of several hundred nT (sometimes, but less often, several thousand nT) imposed upon it by the effects of the magnetisation of the crustal geology. The 'anomalies' are usually at least two orders of magnitude smaller than the value of the total field. The IGRF provides the means of subtracting on a rational basis the expected variation in the main field to leave anomalies that may be compared from one survey to another, even when surveys are conducted several decades apart and when, as a consequence, the main field may have been subject to considerable secular variation.

The IGRF removal involves the subtraction of about 99% of the measured value; hence, the IGRF needs to be defined with precision if the remainder is to retain accuracy and credibility. The IGRF is published by a working group of the International Association of Geomagnetism and Aeronomy (IAGA) on a five-yearly basis. A mathematical model is advanced which best fits all actual observational data from geomagnetic observatories, satellites and other approved sources for a given epoch (Reeves et al., 1997). The model is defined by a set of spherical harmonic coefficients to degree and order 13. Software is available which permits the use of these coefficients to calculate IGRF values over any chosen survey area. It is normal practice in the reduction of aeromagnetic surveys to remove the appropriate IGRF once all other corrections to the data have been made. From the point of view of exploration geophysics, undoubtedly the greatest advantage of the IGRF is the uniformity it offers in magnetic survey practice since the IGRF is freely available and universally accepted (Reeves et al., 1997).

3.1.4 Magnetic Susceptibility

Magnetic susceptibility is a measure of the ease with which particular sediments are magnetized when subjected to a magnetic field. The ease of magnetization is ultimately related to the concentration and composition (size, shape and mineralogy) of magnetisable material contained within the sample (Wemegah et al., 2009). Magnetisable minerals include the ferromagnetic minerals (strongly magnetisable) and any of the paramagnetic (moderately magnetisable) minerals and other substances (Wemegah et al., 2009).

The ratio between the induced magnetization and the inducing field if expressed per unit volume, volume susceptibility (κ) is defined as $\kappa = M/H$, or $\kappa = J/H$ where M or J (also referred to as the intensity of magnetization) is the volume magnetization induced in a material of susceptibility (κ), by the applied external field H (Clark, 1997). Although susceptibility has no units (dimensionless), to rationalize its numerical value to be compatible with the SI or rationalized system of units, the value in chg.'s equivalent units should be multiplied by 4π .

Telford et al. (1990) indicate that although there is great variation, even for a particular rock, and wide overlap between different types, sedimentary rocks have the lowest average susceptibility and basic igneous rocks have the highest. In every case, the susceptibility depends only on the amount of ferrimagnetic minerals present, mainly magnetite, sometimes titanomagnetite or pyrrhotite. The values of chalcopyrite and pyrite are typical of many sulphide minerals that are basically nonmagnetic.

3.1.5 Magnetism of Rocks and Minerals

Many rocks that contain iron-bearing minerals act as tiny magnets. As magma or lava cool, these minerals begin to form. At this point the molten rocks have not completely solidified, so the magnetic minerals floating in the molten mass become aligned to the magnetic field. When the rock finally solidifies, these minerals acquire the magnetic field present. Sedimentary rocks also have a magnetic record (Reeves et al., 1997). As iron bearing sedimentary minerals is deposited from the water column, they also become aligned with the exiting magnetic field. Local changes in the main field result from variations in the magnetic mineral content of near surface rocks. Magnetic anomalies are caused by magnetic minerals (mainly magnetite and pyrrhotite) contained in the rocks. Substances can be divided on the basis of their behaviour when placed in an eternal field (Telford et al., 1990).

In diamagnetic materials, all the electron shells are complete and so there are no unpaired electrons. The electrons orbit in such a way so as to produce a magnetic field which opposes the applied field, giving rise to a weak, negative susceptibility (Telford et al., 1990). The most common diamagnetic earth materials are graphite, marble, quartz and salt (Reeves et al., 1997). Unpaired electrons of incomplete electron shells produce unbalanced spin magnetic moments and weak magnetic interactions between atoms in paramagnetic materials. Paramagnetic materials have weak positive susceptibility but one which decreases inversely with the absolute temperature according to the Curie-Weiss Law (Reeves et al., 1997). Ferromagnetism decreases with increasing temperature and disappears entirely at the Curie temperature. Truly ferromagnetic materials occur only rarely in nature but include substances such as cobalt, nickel and iron, all of which have parallel alignment of moments. In ferrimagnetic materials (of which magnetite, titanomagnetite and ilmentite are prime examples) the sub-lattices are unequal and anti-parallel. Spontaneous magnetization and large susceptibility are characteristics of ferrimagnetic materials, such as in the case pyrrhotite (Telford et al., 1990). The majority of naturally occurring magnetic minerals exhibit either ferrimagnetic or imperfectly anti-ferromagnetic characteristics (Reeves et al., 1997).

3.1.6 Aeromagnetic Survey

An aeromagnetic survey is a common type of geophysical survey carried out using a magnetometer aboard or towed behind an aircraft. The principle is similar to a magnetic survey carried out with a hand-held magnetometer, but allows much larger areas of the Earth's surface to be covered quickly for regional reconnaissance. The aircraft typically flies in a grid-like pattern with height and line spacing determining the resolution of the data (and cost of the survey per unit area).

As the aircraft flies, the magnetometer records tiny variations in the intensity of the ambient magnetic field due to the temporal effects of the constantly varying solar wind and spatial variations in the Earth's magnetic field, the latter being due both to the regional magnetic field, and the local effect of magnetic minerals in the Earth's crust. By subtracting the solar and regional effects, the resulting aeromagnetic map shows the spatial distribution and relative abundance of magnetic minerals (most commonly the iron oxide mineral magnetite) in the upper levels of the crust. Because different rock types differ in their content of magnetic minerals, the magnetic map allows a visualization of the geological features of the upper crust in the subsurface, particularly the spatial geometry of bodies of rock and the presence of structures (faults and folds). This is particularly useful where bedrock is obscured by surface sand, soil or water. Aeromagnetic surveys are widely used to aid in the production of geological maps and are also commonly used during mineral exploration.

3.1.7 Data Enhancement Techniques

Enhancements of magnetic field data are processing operations designed to preferentially emphasize the expression of a selected magnetization at the expense of others. Airborne geophysical data can be enhanced by a range of linear and non-linear filtering algorithms which selectively enhance the anomalies due to one group of geological sources relative to anomalies due to other groups of geological sources (Milligan & Gunn, 1997). Mathematical enhancement techniques are complemented by a range of imaging routines which can be specified to visually enhance the effects of selected geological sources. Fourier transforms are particularly useful in the transformation from the frequency domain to the wave number domain and also for the calculation of derivatives (Telford et al., 1990). Conversely, some enhancement operations distort the data, and care must be taken to ensure that enhanced data is not used inappropriately.

3.1.7.1 Horizontal derivative

This process involves a phase transformation as well as an enhancement of high frequencies. The phase transformation generally has the result of producing anomaly peaks approximately located over the edges of wide bodies and the enhancement of the high frequencies sharpens these peaks to increase the definition of the body edges (Milligan & Gunn, 1997). On a profile, the horizontal derivative may be calculated only in the forward (or in the reverse) direction along the profile itself. With gridded data, the derivative may be computed in any azimuth from 0 to 360°. Some interpreters use this quality of the horizontal derivatives to map body outlines. The process becomes extremely ambiguous for narrow bodies, however, and it is difficult to see what advantage horizontal derivatives have over vertical derivatives, which give peaks over the tops of sources and indicate source outlines by steep gradients and inflections (Milligan & Gunn, 1997).

3.1.7.2 Vertical derivatives

Vertical derivative (or alternatively named "vertical gradient") filters preferentially amplify short-wavelength components of the field at the expense of longer wavelengths (Foss, 2011). Vertical derivative filters are generally applied to gridded data using FFT (Fast Fourier Transform) filters. Various vertical derivatives of the magnetic field can be computed by multiplying the amplitude spectra of the field by a factor of the form:

$$\frac{1}{n}\left[\left(u^2+v^2\right)^{\frac{1}{2}}\right]^n \qquad \textbf{(3.2)}$$

Where n is the order of the vertical derivative, (u, v) is the wavenumber corresponding to the (x, y) directions respectively. The first vertical derivative (or vertical gradient) is physically equivalent to measuring the magnetic field simultaneously at two points vertically above each other, subtracting the data and dividing the result by the vertical spatial separation of the measurement points. The second vertical derivative is the vertical gradient of the first vertical derivative and so on. The formula for the frequency response of these operations shows that the process enhances high frequencies relative to low frequencies, and this property is the basis for the application of the derivative process which eliminates long-wavelength regional effects and resolves the effects of adjacent anomalies. First vertical derivative data have become almost a basic necessity in magnetic interpretation projects. This is derivative of the anomaly with respective of depth of the source gives a better resolution of the anomaly itself. Computation of the first vertical derivative in an aeromagnetic survey is equivalent to observing the vertical gradient directly with a magnetic gradiometer and has the same advantages, namely enhancing shallow sources, suppressing deeper ones, and giving better resolution of closely-spaced sources. The second vertical derivative has even more resolving power than the first vertical derivative, but its application requires high quality data as its greater enhancement of high frequencies results in greater enhancement of noise. Higher orders of derivatives are virtually never used to produce interpretation products (Gunn et al., 1997a).

3.1.7.3 Vertical continuation of the field

The amplitude of a magnetic field above a source varies with elevation as an exponential function of wavelength. This relationship can be readily exploited with FFT filters to recompute the field at a higher elevation ("upward continuation") or lower elevation ("downward continuation") (Foss, 2011). A potential field measured on a given observation plane at a constant height can be recalculated as though the observations were made on a different plane, either at higher or lower elevation. As described by Gunn (1997), the process has a frequency response of $e^{-h}\left(u^2+v^2\right)^{1/2}$ (where h is elevation). This means that upward continuation smooth out high-frequency anomalies relative to low-frequency anomalies. The process can be useful for suppressing the effects of shallow anomalies when detail on deeper anomalies is required. Downward continuation on the other hand sharpens the effects of shallow anomalies (enhances high frequencies) by bringing them closer to the plane of observation.

For upward continuation (where z is positive downward) (Telford et al., 1990)

$$F(x, y, -h) = \frac{h}{2\pi} \iint \frac{F(x, y, 0)\partial x \partial y}{\left\{(x - x') + (y - y') + h^2\right\}^{1/2}} \qquad \textbf{(3.3)}$$

where $F(x, y, -h)$ = Total field at the point $P(x', y', -h)$ above the surface of which $F(x, y, 0)$ is known. h = elevation above the surface.

3.1.7.4 Reduction to the pole

Reduction to the pole (RTP) is a standard part of magnetic data processing method, especially for large-scale mapping. RTP operation can transform a magnetic anomaly caused by an arbitrary source into the anomaly that the same source would produce if it is located at the pole and magnetized by induction only. Interpretation of magnetic data can further be helped by RTP in order to remove the influence of magnetic latitude on the anomalies, which is significant for anomalies caused by crust. Reduction to the pole is the process of converting the magnetic field from magnetic latitude where the Earth's field is inclined, to the field at a magnetic pole, where the inducing field is vertical (LUO et al., 2010). When the Earth's field is inclined, magnetic anomalies due to induction have forms that are asymmetrically related to their sources, but when the inducing field is vertical, the induced anomalies are directly over their sources (Milligan & Gunn, 1997). Fourier transform is applied to transform RTP from the space domain into the wavenumber domain. The RTP operation in wavenumber domain can be expressed as

$$A_p(u,v) = \frac{A_c A_p(u,v)}{\left(sinI + icosIcos(D-\theta)\right)^2} \quad \textbf{(3.4)}$$

where $A_p(u,v)$ be the Fourier Transform of these observed magnetic data, $A_c(u,v)$ be the Fourier Ttransform of the vertical magnetic field, I and D is the inclination and declination of core field, (u,v) is the wavenumber corresponding to the (x, y) directions respectively and $\theta = \arctan\left(\frac{u}{v}\right)$ (LUO et al., 2010).

Reduction-to-the-pole (RTP) is a useful and effective operation designed to transform a total magnetic intensity (TMI) anomaly caused by an arbitrary source into the anomaly that this same source would produce if it were located at the pole and magnetized by induction only (Li, 2008).

3.1.7.5 Analytic signal

Analytical signal of TMI has much lower sensitivity to the inclination of the geomagnetic field than the original TMI data, and provides a means to analyse low latitude magnetic fields without the concerns of the RTP operator. Analytical signal is a popular gradient enhancement, which is related to magnetic fields by the derivatives. Roest et al., (1992), showed that the amplitude of the analytic signal can be derived from the three orthogonal gradient of the total magnetic field using the expression:

$$|A(x,y)| = \sqrt{\left(\left(\frac{\partial m}{\partial x}\right)^2 + \left(\frac{\partial m}{\partial y}\right)^2 + \left(\frac{\partial m}{\partial z}\right)^2\right)} \quad \textbf{(3.5)}$$

where A(x,y) is the amplitude of the analytical signal at (x,y) and m is the observed magnetic anomaly at (x,y).

While this function is not a measurable parameter, it is extremely interesting in the context of interpretation, as it is completely independent of the direction of magnetisation and the direction of the Earth's field (Milligan & Gunn, 1997). This means that all bodies with the same geometry have the same analytic signal. Analytic signal maps and images are useful as a type of reduction to the pole, as they are not subject to the instability that occurs in transformations of magnetic fields from low magnetic latitudes. They also define source positions regardless of any remnant magnetization in the sources (Milligan & Gunn, 1997).

3.1.7.6 Tilt Angle Derivative

Since the amplitude of magnetic signature depends on magnetic field strength and to some extent the depth of magnetic sources, lower amplitude signature may be suppressed at the expense of higher amplitudes. For this reason, the edge-detection filters area normally applied for delineating linear features without necessary diminishing the long-wavelength anomalies (Oruc & Selim, 2011). The Tilt derivative filter, TDR (a very good edge-detection filter) brings out short wavelength and reveals the presence of magnetic lineaments. Verduzco et al. (2004) showed in his work that tilt derivative filter also performs an automatic-gain-control (AGC) filter which tends to equalize the response from both weak and strong anomalies. Hence, the filter provides an effective way to trace out along striking anomalies.

The tilt angle (Miller and Singh, 1994) is defined as

$$T = \tan^{-1}\left(\frac{\partial f / \partial z}{\sqrt{(\partial f / \partial x)^2 + (\partial f / \partial y)^2}}\right) \quad \textbf{(3.6)}$$

where f is the magnetic or gravity field.

The gradient of the tilt angle has some interesting properties. It is a dimensionless ratio but it responds equally well to shallow and deep sources and to a large dynamic range of amplitudes for sources at the same level (Cooper & Cowan, 2006). The tilt angle is positive when over the source, passes through zero when over, or near, the edge where the vertical derivative is zero and the horizontal derivative is a maximum and is negative outside the source region. The TDR values are restricted to values between $-\pi/2$ and $+\pi/2$ and is much simpler to interpret (Cooper & Cowan, 2006).

3.2 Radiometric

Radiometric, also known as Gamma-Ray Spectrometry, is a measure of the natural radiation in the earth's surface, which can tell us about the distribution of certain soils and rocks. Geologists and geophysicists routinely use it as a geological mapping tool to in identifying different certain rock types. Radiometric is also useful for the study of geomorphology and soils. A radiometric survey measures the spatial distribution of three radioactive elements (potassium-K, thorium-Th and uranium-U) in the top 30-45 cm of the earth's crust (Gregory & Horwood, 1961). The abundances of K, Th and U are measured by detecting the gamma-rays produced during the natural radioactive decay of these elements. The basic purpose of radiometric surveys is to determine either the absolute or relative amounts of U, Th, and K in the surface rocks and soils. Changes in the concentration of the three radioelements U, Th, and K accompany most major changes in lithology; hence the method can be used as a reconnaissance geologic mapping tool in many areas (Wilford et al., 1997). On regional scale airborne gamma-ray spectrometry data have often been used to identify several features, such as: limits of geologic provinces, fold belts, sedimentary basin and tectonic and structural detail of shear zones and overprinted structural trends (Direen et al., 2001).

3.2.1 Basic Radioactivity

Radioactivity is the process where an unstable atom becomes stable through the process of decay, or breakdown, of its nucleus. During decay, energy is released in the form of three types of radiation; alpha, beta and gamma (Gunn et al., 1997b).

- Alpha radiation is helium nuclei, which are absorbed by a few cm of air;
- Beta radiation is electrons, which can travel up to a metre in air; and
- Gamma rays are parcels of electromagnetic radiation (similar to visible light).

Gamma rays can travel for up to 300 m through air, but are stopped by water and other molecules (e.g. in soil, rock). The energy of each gamma ray is characteristic of the radioactive element it came from. They have much shorter wavelengths than most other electromagnetic rays. Gamma rays can penetrate up to 30 cm of rock and several hundred metres of air, and are the only choice available for the remote sensing of terrestrial radioactivity (Gunn et al., 1997b).

3.2.2 Geochemistry of the Radioelements (K, U &Th)

3.2.2.1 Potassium

Potassium (K) is a major component of the Earth's crust (2.35%). It is an alkali element and shows a simple chemistry. The major hosts of K in rocks are potassic feldspars (principally orthoclase and microcline with -13% K) and micas (biotite and muscovite with typically 8% K). Potassium is absent from mafic minerals. Consequently K is relatively high in felsic rocks (granites, etc.), but low in mafic basalts and very low in dunites and peridotites (Fertl, 1983). The potassium content of sedimentary rocks is highly variable but tends to be higher in shales than in carbonates or sandstones (Dickson & Scott, 1997). The weathering behaviour of the K-bearing minerals determines the radioelement contents of weathered rocks and soils. During weathering, the major K hosts will be destroyed in the order biotite-K-feldspar- muscovite. Potassium released during weathering can be taken up in the formation of K-bearing minerals such as illite or adsorbed in minor amounts into other clays, e.g. montmorillonite, under suitable conditions. The efficient uptake of K by clays is reflected in the low concentration of K in sea water (380 ppm) (Dickson & Scott, 1997). Potassium is detected in a gamma-ray survey by measurement of the 1.46 MeV gamma-ray emitted by the decay of ^{4O}K. This isotope constitutes 0.02% of natural K and is, therefore, a direct measurement of the K content in the ground.

3.2.2.2 Thorium

Thorium is a minor component of the Earth's crust (~12 ppm), occurring only in valence state $Th^{4+.}$ Thorium may be present in allanite, monazite, xenotime and zircon at levels

>1000 ppm or as trace amounts in other rock-forming minerals (Dickson & Scott, 1997). Major Th-bearing minerals (monazite and zircon) are stable during weathering and may accumulate in heavy mineral sand deposits. Thorium freed by the breakdown of minerals during weathering may be retained in Fe or Ti oxides-hydroxides and with clays. As with U, Th may also be transported and adsorbed on colloidal clays and iron oxides. Like U, Th does not emit gamma-rays during its decay, but is also the parent of a decay series which ends in stable ^{208}Pb (Dickson & Scott, 1997).

3.2.2.3 Uranium

Uranium is a minor component of the Earth's crust (~3 ppm). Its chemistry is dominated by two valence states U^{4+} and U^{6+}. The more reduced form, U^{4+}, is generally contained in insoluble minerals. Uranium may be present in rocks as the oxide and silicate minerals, uraninite and uranothorite; in major U-bearing minerals such as monazite, xenotime and zircon; as trace amounts in other rock-forming minerals; or along grain boundaries, possibly as U oxides or silicates. Of the major U-bearing minerals, only zircon and monazite are stable during weathering. Uranium is the parent of a decay series which ends in stable ^{206}Pb. Uranium itself does not emit gamma-rays during its decay and the most energetic gamma-rays emitted by its daughter isotopes come from ^{214}Bi which occurs late in the decay series (Dickson & Scott, 1997).

3.2.3 Disequilibrium

Disequilibrium in the U decay series is a serious source of error in gamma-ray spectrometric surveying. When radioactive decay results in an unstable daughter product with a half-life shorter than that of the parent, a situation will eventually be reached where the daughter product is decaying as rapidly as it is being produced. If this is true for all the daughters in a decay series, then the series is said to be in secular equilibrium, and the total activity decreases at the same rate as that of the original parent. The equal activity under equilibrium conditions does not imply equal concentration, since the relevant half-lives must be considered when calculating the relative concentration of members of a decay series. Disequilibrium occurs when one or more decay products are completely or partially removed or added to the system, and it may take days, weeks or even millions of years to restore equilibrium, depending on the half-lives of the radioisotopes involved. Thorium rarely occurs out of equilibrium in nature, and there are no disequilibrium problems with K, since it only exhibits a single photo-peak. However, in the U decay series, disequilibrium is common in the natural environment (Minty, 1997).

Accurate estimates of U from gamma-ray spectrometry, where we rely on the abundance of isotopes such as ^{214}Bi and ^{214}Pb, which occur far down in the radioactive decay chain, require equilibrium conditions that are frequently not present. These estimates are, therefore, usually reported as ‘equivalent uranium’ (eU), reminding us that the accuracy of these is dependent on the presence of equilibrium conditions. Thorium is also usually reported as ‘equivalent thorium’ (eTh), although the Th decay series is almost always in equilibrium (Minty, 1997).

3.2.4 The radioactivity decay law

While it is impossible to predict the exact moment at which a particular atom will decay, each radioisotope has a characteristic rate of disintegration, which is proportional to the number of nuclei present. Thus the number of nuclei (dN) which decay during a short time $(dt)$is proportional to the number of nuclei present *(N).* That is

$$\frac{dN}{dt} = -\lambda N \qquad \textbf{(3.7)}$$

Or

$$N = N_o e^{-\lambda t} \qquad \textbf{(3.8)}$$

where λ is the decay constant, $N_o$is the number of radionuclides present at time t= 0, and N is the number of nuclides present after a time t. A related constant is the previously mentioned 'half-life'.

When $N = \frac{1}{2} N_o$ we have

$$t_{\frac{1}{2}} = \frac{0.693}{\lambda} \qquad \textbf{(3.9)}$$

Usually, the activity of the source (number of disintegrations per unit time) is measured, and the activity also decreases exponentially over time with the same half-life.

3.2.5 Measurement of Gamma Radiation

Radioactive elements occur naturally in the crystals of particular minerals. The abundance of minerals changes across the earth's surface with variations in rock and soil type. Since the energy of gamma rays is related to the source radioactive element, they can be used to measure the abundance of those elements in an area. So by measuring the energy of gamma rays being emitted in an area, we can infer the presence of particular minerals in the earth's surface.

Gamma rays can be measured on the ground or from a low flying aircraft. The gamma rays are detected by a spectrometer, which counts the number of times each gamma ray of particular energy intersects it. The energy spectrum measured by the gamma ray spectrometer is in the range 0 to 3 MeV and energies of geological interest lie between 0.2 and 3 MeV. Peaks in the spectrum (Fig. 3.3) can be attributed to potassium (K), thorium (Th) and uranium (U), the number of gamma ray counts across the whole spectrum is referred to as the total count (TC) (Milsom, 2003).

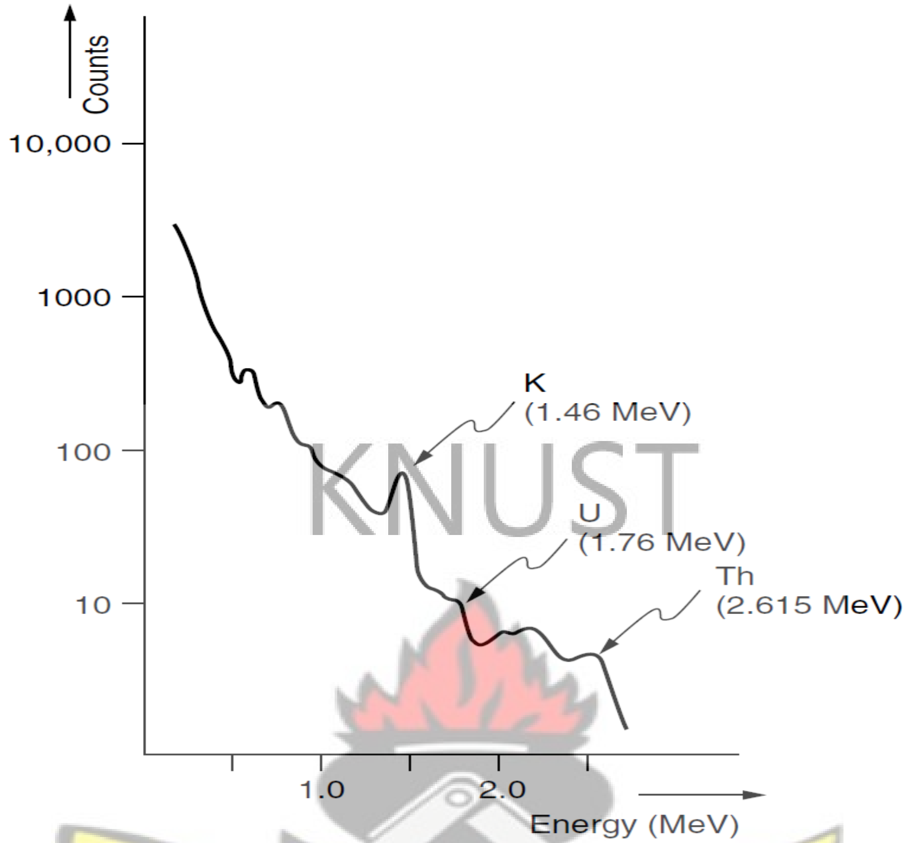

Figure 3.3 A natural gamma-ray spectrum. (Vertical scale (numbers of counts) is logarithmic) (Milsom, 2003)

3.2.6 Display of Radiometric data

Radiometric data are commonly displayed as a map, with colours representing sample values. Normally, red areas in the maps correspond to high gamma ray counts and the blue areas corresponding to low counts. Another way to display radiometric data is to combine three datasets on the one picture using a red-green-blue ternary ratio. Each of the datasets are displayed using a different basic colour, which when combined make a colourful display with each shade representing different relative amounts of potassium, thorium and uranium. Usually the colours are displayed as: Red = potassium, Green = thorium and Blue = uranium. Thus, bright Blue areas on the map show areas where the Uranium count is very high relative to both of the other element count rates; bright Red indicates areas of high potassium count rate and bright Green indicates area with high

Thorium count rate. Colours other than the three primary colours indicate areas with various, well defined proportions of Th, U, and K. Generally, the different colours on the map correspond closely with different rock types when compared with geological samples collected on the ground. In fact, the Ternary map has proven to be so useful that it has become a standard method of presenting radiometric data. Also, the ratios maps, U/Th, U/K and Th/K, are often more diagnostic of changes in rock types, alteration, or depositional environment than the values of the radio-isotope abundances themselves, which are subject to wide variations due to soil cover (Dickson & Scott, 1997). For example, the U/Th ratio map has particular value in exploration for uranium deposits because it has been found to increase locally within regions containing uranium ores (Minty, 1997).

CHAPTER FOUR

4 MATERIALS AND METHODS

4.1 Data Acquisition

The main data set used in this study is an airborne geophysical survey data acquired during 1997- 1998 by the Geological Survey of Finland (GKT) in collaboration with the Geological Survey of Ghana and the Ghana Minerals Commission. Different areas were surveyed by the Geological Survey of Finland using a fixed wing aero-plane (Cessna Titan 404 (C-FYAU)). The GPS (Global Positioning System) was used for navigation. The nominal line separation was 400 m with tie lines separation of approximately 5 km. The terrain clearance was flown at a constant height of 70 m. The survey line direction was chosen (East-West) to intersect the main geological strike direction (South- North) perpendicularly (Amoako et al., l998).

The magnetic system used was the Scintrex Cesium SC-2 magnetometer coupled helium sensor. The output from the magnetometer was sampled at 0.2 s to a resolution of 0.01 nT with noise envelope of 0.1 nT. The sensor was kept at a constant height of 45 m above the ground. The Exploranium spectrometer, model GR-820 with 256 spectral channels and Exploranium detector GPX-1024, 1024 cubic inches of NaI (Tl) (Sodium iodide crystals treated with thallium) were coupled in the aero-plane was used for the radiometric data collection. The survey produced high resolution airborne geophysical information for geological mapping and mineral exploration purposes.

4.2 Data Processing

This section gives an overview of the processing of the airborne data. The processing of airborne data for this research involved the application of enhancement technique, the application of a gridding routine, and removal of the Earth's background magnetic field. Some corrections like background correction (Aircraft, Radon and Cosmic), stripping, microlevelling, removing diurnal variation of the Earth's magnetic field, aircraft heading, instrument variation, lag error between aircraft and the sensor and inconsistencies between flight lines and tie lines were done by the Geological survey of Finland (GKT) (the contractors) . The geophysical data set for the study area was co-registered to Universal Transverse Mercator Coordinate System, zone 31 of North hemisphere.

The main software used for the processing and enhancement of the airborne geophysical data were the Geosoft® (Oasis Montaj) and the Discover 12. The ArcGIS was used to create the GIS environment for the integration of the interpreted results. The Airborne geophysical datasets namely magnetic and radiometric were obtained from the Ghana Geological Survey Department (Accra) by Department Physics KNUST (Kwame Nkrumah University of Science and Technology, Kumasi) on the 1st November, 2012. The methodology applied involved the acquisition of two different Geophysical Airborne data sets (magnetic and radiometric), building of databases (projects), data processing and interpretation.

4.2.1 Gridding

Gridding interpolates the data from the measurement locations to nodes of a regular mesh, creating a new and fundamentally different construct of the data (Foss, 2011). The dataset was gridded to a 100 m interval using the minimum curvature technique described by Briggs, (1974). Once a grid was produced it was displayed as an image. The minimum curvature technique gridding was applied to both the radiometric and magnetic data. The minimum curvature technique takes the randomly distributed survey data and interpolates it onto a regular grid. The images were produced in the Geosoft® software package, and exported in the GeoTIF format, including associated files that contain spatial reference information. The images were viewed with any image viewing software and as they were spatially referenced, it was possible to be displayed in a GIS environment. Gridding the data provided a way for the application of filters since filtering requires equally spaced data points.

4.2.2 Enhancement of Aeromagnetic Dataset

Airborne magnetic dataset can be enhanced by a range of linear and non-linear filtering algorithms. A range of imaging routines can be specified to visually enhance the effects of selected geologic sources using mathematical enhancement techniques (Milligan and Gunn, 1997). The following discussion describes some enhancement techniques used and their results. Because it is known that significant concentrations of mineral deposits are correlated with high frequency magnetic responses, high-pass and horizontal gradient were applied to the aeromagnetic data in order to enhance high frequencies and define body edges. All the enhancement techniques were performed with the Geosoft® (Oasis montaj 7.3) and MapInfo- Discover 2012.

The *MagMap extension* in Geosoft®, which offers a number of utilities for processing of magnetic data, was used on the magnetic-anomaly grid (total field intensity minus the

Definitive International Geomagnetic Reference Field) for the processing and applying filters. The necessary filters were applied and it was displayed as an image using the *GRID AND IMAGE* tool. Two-Dimensional Fast Fourier Transformation (2D-FFT) filters were applied to enhance the quality of the data. The 2D-FFT filters used included Reduction to the Pole, First Vertical and Horizontal Derivatives, Downward and Upward Derivative, and Analytic Signal. Since one of the axioms of the Fourier domain processing is that the signal must be periodic. And in order to mimic periodicity in the preprocessing stage, the grid was extended to be continuous along both coordinates. The system pads the edges of the grid with dummy values. The reason the grid was expanded is to allow adequate space for ensuring smooth periodicity. The dummy area was interpolated so that the filled grid is periodic along both coordinates.

4.2.2.1 Reduction to the Pole (RTP)

Reduction to pole (RTP) filter, for low geomagnetic latitudes was applied to the magnetic anomaly data (Remnant Magnetic Intensity: RMI). The approach utilizes an azimuthal filter in the frequency domain to minimize the directional noise caused by the low geomagnetic latitude (Philips, 1997). The calculation of inclination and declination were made using the central coordinates of the area. It was found out that the study area had inclination of -11.1^{o}, declination of -3.4^{o} to and an average total field of 32644 nT.

This is a post-processing technique performed on the gridded data that removes the asymmetry in RMI data that is caused by the non-vertical inclination of the Earth's magnetic field. This simplifies the images so that induced magnetic anomalies from vertical sources are located over the geological body responsible, rather than being skewed and offset to one side.

4.2.2.2 First Vertical and Horizontal Derivatives

The RTP grid data was subjected to first vertical derivative (1VD) filter. This filter allows small and large amplitude responses to be more equally represented. The 1VD grid in gray-scale helped enhance linear features in the area. The RTP grid is also enhanced by the application of first horizontal gradient or derivative (1HD) which is critical when trying to map linear features such as fault and/or dikes from the magnetic data. The filter provides higher resolution and better accuracy at wider spacing. The horizontal derivative aided in identifying geologic boundaries of formations in the study area. Higher derivative images with different filter such as 2VD and 2HD produced interesting results but several distortions were noted to occur in the images due to the increase in the noise level introduced in the data by this process. These images were therefore not used in the interpretation but were only used as a guide in the interpretation from the first derivative images. This is a post-processing technique performed on the gridded data that quantifies the spatial rate of change of the magnetic field in the vertical direction. It essentially enhances the high frequency anomalies relative to low frequencies.

4.2.2.3 Downward and Upward Continuation (DC and UC)

The appropriation of the magnetic intensities from deeper structures, led to applying the UC filter to suppress the effects of shallow anomalies. The RMI grid was continued to 100, 200, 400 and 800 m to see deeper signature coming from deeper structures. This helped high frequency anomalies relative to low frequency anomalies to be smoothed out.

The downward continuation filters enhanced responses from shallow depth sources by effectively bringing the plane of measurement closer to the source. However, the data contain short wavelength noises that appear as signals coming from very shallow sources in the continuation. Since short-wavelength signal can appear to be from shallow sources, it has to be removed to prevent high magnitude and short wavelength noise in the processed data. To do this, we applied Butterworth filter (a low-pass filter) to remove the short wavelength noise (as determined by the radially averaged energy spectrum) before applying the downward continuation filter. The energy spectrum generated form the *MagMap* was a good for determining the depth to which the data can be continued downward.

4.2.2.4 Analytical Signal Amplitude

The analytical signal amplitude was calculated from the residual magnetic field and gridded to visualize the distribution of the magnetic signature irrespective of the direction of the magnetization. The analytical signal amplitude is independent of the direction of the magnetization of the source, and is related to amplitude of magnetization. The most significant concentrations of mineral deposits in this area are correlated with high analytical signal amplitudes (Silva et al., 2003).

4.2.3 Depth to Basement

Attempt was made to estimate the depth to basement of the magnetic body. The Geosoft oasis montaj *Depth to Basement extension* which determines the position (distance along the profile and depth), dip (orientation) and intensity (susceptibility) of magnetic source bodies for a magnetic profile was used. The *Werner deconvolution function* which uses the horizontal and vertical derivatives in the calculation in the depth to basement of the magnetic anomaly was employed. The anomaly profile selected was perpendicular to the geological structure generating the field. The *Werner Deconvolution function* assumes the source bodies are either dikes or contacts with infinite depth extent and uses a least-squares approach to solve for the source body parameters in a series of moving windows along the profile (Ku & Sharp, 1983). Solutions derived from the total field profile are designated "Dike" solutions and solutions derived from the horizontal gradient are designated "Contact" solutions.

Each *Werner Deconvolution* calculation operates on a segment of the anomaly profile referred to as a window, and produces a single solution at each window. Several parameters in the dialog (Appendix A.1) which controls the number of solutions generated by *Werner deconvolution* was set accurately to generate the desired solution. The Window Expansion Increment which determines the number and size of steps between the minimum and maximum length was set to 500. The distance which the Werner operator moves along the profile between calculations was set to 200 in other to restrain the number of solutions generated. Solutions caused by noise in the input profile were eliminated by setting an amplitude threshold for the anomalies (setting the "Residual cut-off" to 0.1). The calculated solutions are saved in an Oasis montaj database (GDB), allowing for viewing in profiles or 2D plots (Appendix A.2).

4.2.4 Airborne Radiometric Data

Airborne radiometric data are normally used as an aid to lithological mapping. There is a good correlation between patterns in the radiometric data and unweathered rocks. This information compliments magnetic, electromagnetic and geochemical data normally acquired during mineral exploration programs (Gunn et al., 1997b). This is one of the most cost-effective and rapid techniques for geochemical mapping of the radioactive elements: potassium, uranium and thorium. This section describes briefly some enhancing techniques such as Ternary Image, Ratio Maps, Potassium and Thorium and Uranium Maps which were used on the radiometric dataset. The goal is to recognize and understand radiometric signatures associated with the host rocks important to mineralization.

4.2.4.1 Total Count (TC), Potassium (K), Thorium (Th) and Uranium (U) Channels

By employing the Grid and Image tool in Geosoft® software, the total count image was created after micro-levelling the entire data set to remove any apparent residual errors. These images were generated by employing mini-curvature gridding since the data were collected in grid window with the grid depending on the instrumentation, cost of exploration and the type of plane used in the survey. The images were then correlated with the geological units, patterns and trends. Thorium is generally considered very immobile. (Silva et al., 2003). Ostrovskiy (1975) refers to a decrease in Th and an increase in K for the alteration environment in variety of ore deposits. It is for this and many more reasons that led to the developing of the Th image map.

4.2.4.2 Ternary Images and Ratio Maps

A ternary RGB colour model was created using Geosoft® software for which potassium, thorium and uranium were assigned to the red, green and blue respectively because the blue tends to reduce the poorest signal-to-noise ratio of uranium channel. The resulting images to be discussed later on comprise colours generated from the relative intensities of the three components and represents subtle variations in the ratios of the three bands. A histogram equalization to give the best colour variation was used to enhance the contrast of the individual histograms of K, Th and U before combining to composite image.

Magnetic and radiometric interpretations were made independently in order to extract the maximum information from each method. A number of groups with specific signatures (e.g. high magnetic, high K.) were identified during the interpretation process and assigned to specific layers in the ArcGIS environment. This structure gave the possibility to combine different layers in the interpretation process.

CHAPTER FIVE

5 RESULTS AND DISCUSSION

The result from the airborne magnetic and radiometric datasets are presented and discussed in this chapter. The airborne magnetic and radiometric data generated high resolution images that show major lithologies and structural features that may be present in the study area. Interpretation of these images was carried out visually to identify the individual lithologies and delineate geological structures. High radiometric element patterns, anomalous high magnetic zones and low magnetic areas suspected to have resulted from underlining rocks were delineated. To improve the available geological map and reduce the level of its subjectivity, a qualitative interpretation of the bedrocks from the available geophysical datasets was performed. This process involved comparing the existing geology map with that generated from a GIS environment and making inference to structure and geology.

5.1 Digitized Elevation Map (DEM)

The digitized elevation map that shows the highlands and lowlands in the study area is displayed in figure 5.1. The elevation ranges from 50 to 818 m with a mean value of 178 m. On the average, a greater portion of the area falls within low lands (VL in Fig. 5.1) which coincide with the Lake Volta and its river channels.

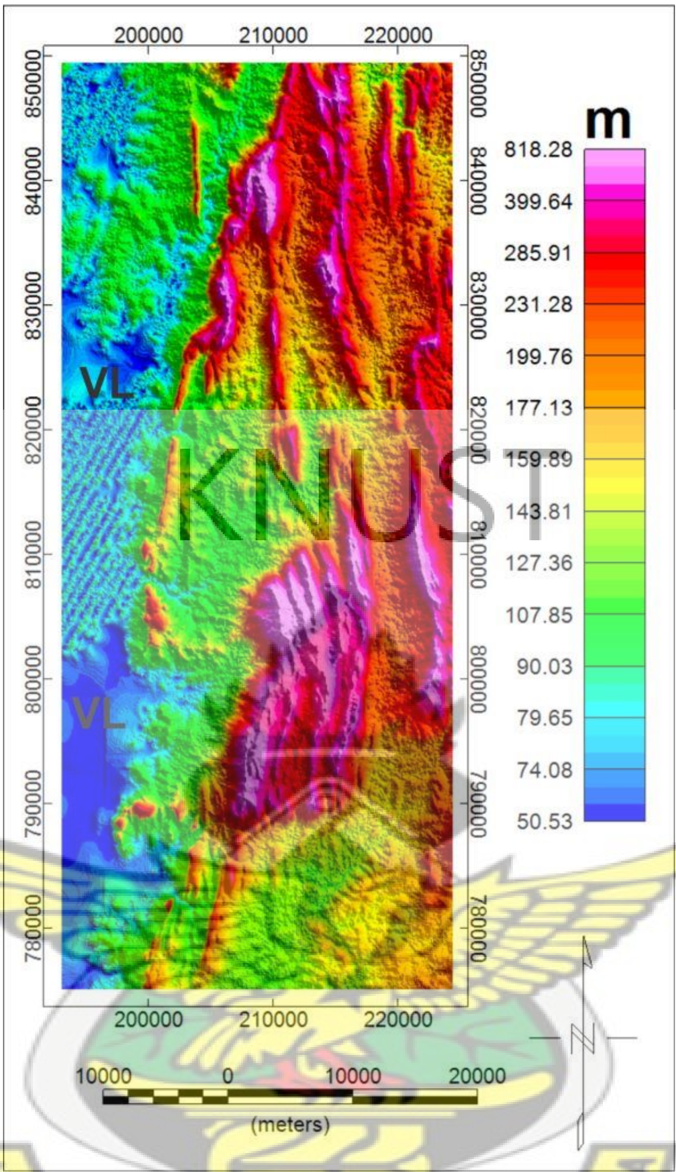

Figure 5.1 Digital Elevation Map of the area

The high elevations shown at the eastern part of the area are partly associated with the Buem-Quartzose sandstone (BS) described by Delor et al., (2009); Osae et al., (2006); Bell & Crook, (2003) and Jones, (1990). The relatively low elevations (green in Fig. 5.1) coincided with the Buem Shale (BS) delineated from the analytical signal image (Fig. 5.5). By comparing vertical derivative images (Fig. 5.6a) and tilt angle images (Fig. 5.9) with the DEM (Fig. 5.1) it become obvious that most of the structures delineated coincide with the high elevated regions.

5.2 Magnetic

An airborne magnetic survey is a supportive geophysical method in mapping subsurface bedrock geology (lithology) and structures due to variations in magnetic susceptibility of rocks (Gunn et al., 1997a). According to Reeves et al., (1997), where the bedrock geology cannot be mapped due to thick jungle, swamp, deep weathering or sand cover, aeromagnetic data can give information on the hidden geology using methods of inference that are similar to those used in photo geological interpretation (such as enhancement filters). One of the main goals for the use of the magnetic data is to delineate geological structures and to some extent delineate lithology (Gunn et al., 1997a) by gridding and appling enhanement tools.

Rocks of the study area showed different aeromagnetic responses that can be related to their lithology and tectonic activities that have resulted in the geological structures (e.g. folds, faults and fractures) in the area. Linear features (geological structures) associated with the volcanic rocks, sandstones and shale are observed as moderately low and low magnetic signature. The pink colours or characters in the presented figures (Figs. 5.2 - 5.12) are areas of high magnetic signature, whereas the blue characters represent areas of low magnetic signature.

5.2.1 Residual Magnetic Intensity, RMI

The residual magnetic data was gridded with a 100 m grid space to show the spatial distribution of magnetic anomaly. The amplitude of a magnetic anomaly is directly proportional to magnetisation which depends on magnetic susceptibility of the rocks (Gunn et al., 1997a). Close to the earth’s equator low (points of low magnetic equator) susceptible magnetic features appear as high magnetic anomalies and vice versa (Gunn et al., 1997a). The RMI image show high magnetic susceptible areas in low magnetic values (blue) while less magnetic susceptible areas are depicted as high magnetic values (pink colour) except for the analytical signal image (Fig. 5.4) and reduction to the pole image (Fig. 5.3) where high magnetic susceptible areas are shown as high anomalies.

Residual magnetic intensity level in the study area ranges from -922.27 to -1515.95 nT with the mean value of -1256.33 nT. Negative anomalies were observed in the area which may be due to the present of low magnetic rocks (e.g. shale, sandstone, limestone) in the area, that are noted for low magnetic signatures. By removing the regional magnetic anomaly form the measured anomaly, negative RMI values were obtained. The residual magnetic field intensity data was gridded using the minimum curvature method (Fig. 5.2). To highlight the appearance of anomalies near surfaces, the colour-shade grid with illumination inclination of 45^{o} and declination at 45^{o} was applied. The residual magnetic image (Total Magnetic Intensity (TMI) -IGRF) showed the difference in locations of high and low magnetic intensities (Fig. 5.2). It also shows the difference in locations of high and low magnetic intensities and many crustal magnetization patterns.

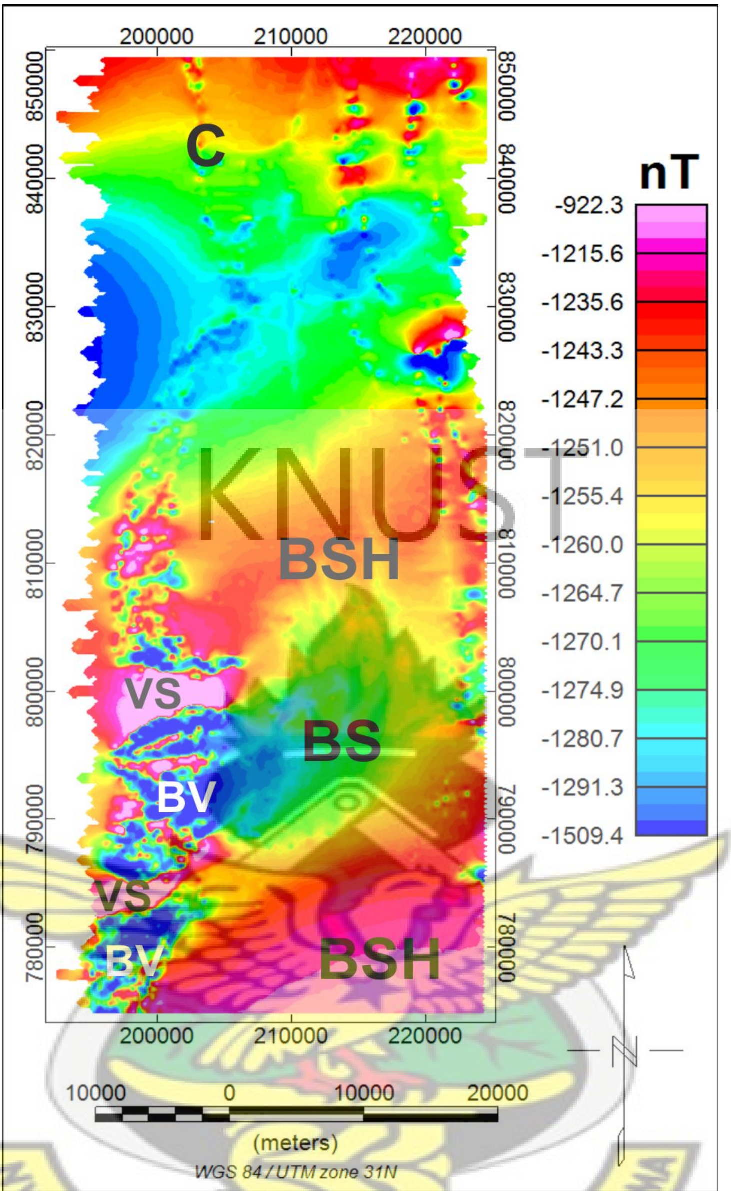

Figure 5.2 Residual Magnetic Intensity, RMI grid map.

The RMI map displays different regional magnetic zones (BV, BS, BSH, C and VS in Fig. 5.2), with most of them trending in the north-south direction and some been polygon features (BS, VS). The magnetic zone division was based on the intensity, shape, and pattern in magnetic signatures. At the western lower corner, there exists a high magnetic signature zone (BV Fig. 5.2) which is cut by low magnetic signature (VS in Fig. 5.2). This feature trends almost in the south-north direction. From the RMI image, the high magnetic susceptible body, BV, observed at the lower left corner of Figure 5.2 is interpreted as the Buem volcanic rocks which are known for its high magnetite content (Jones, 1990). This intruding body VS (low magnetic signature) that cuts the BV body is suspected to be sediments from the Voltaian basin which is known to have low magnetic response. The most prominent relatively low magnetic intensity with a polygon feature is observed at the central zone (BS in Fig. 5.2) of the area. This feature at the central zone (BS in Fig. 5.2) of the area has its magnetic intensities ranging from -1277 to -1260 nT. This feature, BS, is observed at the lower side of the map which is interpreted as the Buem sandstone (Osae et al., 2006). The relatively high magnetic signature observed in the sandstone (BS in Fig. 5.2) is described in a publication by Osae et al., (2006). He indicated that the sandstone has some iron oxide element in them and this may explain its relatively high magnetic signature.

Additionally, the boundary between the central zone (BS in Fig. 5.2) and the southern zone is displayed by a sharp magnetic contrast. To the west upper corner (F in Fig. 5.2), the zone is characterized by a high magnetic signature with its magnetic intensities ranging from -1216 to -922 nT. Relatively low magnetic signature (BSH in Fig. 5.2) with intensities ranging from -1254 to 1246 nT is also observed just close to the circular feature (BS in Fig. 5.2). The feature, BSH which is also observed around BS and VS is delineated as the well-known Buem shale described by Jones (1990). Jones (1990) described the shale in the area to be noted of having low magnetic signature.

5.2.2 Reduction to the Pole, (RTP)

A reduction to the pole, RTP filter was applied to the RMI grid in order to locate the observed magnetic anomalies directly over the magnetic source bodies that caused the anomaly. It was also applied to remove the influence of magnetic latitude on the residual anomalies (Murphy, 2007). The RMI grid was transformed into reduction to the pole (RTP) grid using the 2D-FFT (Fast Fourier Transform) filter in Geosoft Oasis Montaj software. The parameters used for the transformation are an inclination of -11.1^{o} and declination of -4.9^{o} which represent the mean value for the area.

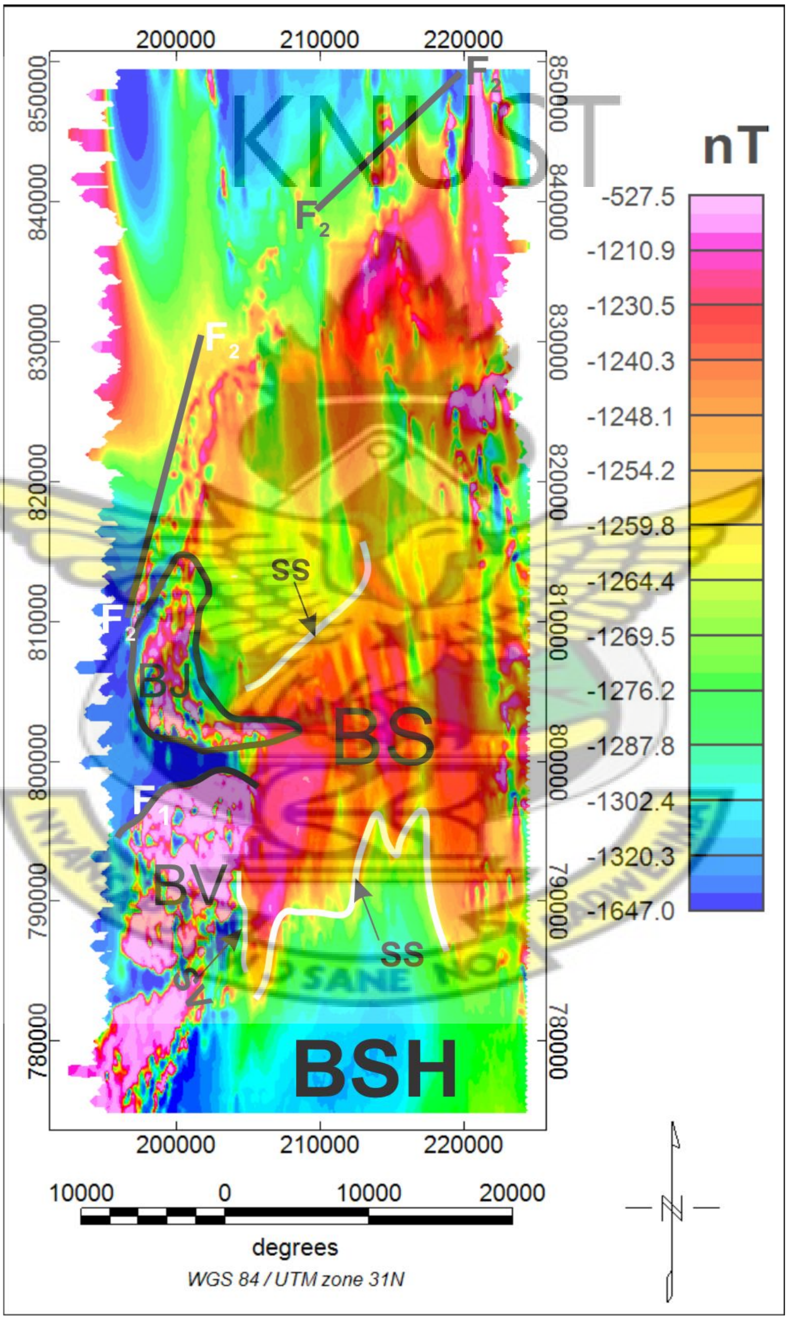

Figure 5.3 Reduction to the pole (RTP) image using an inclination of -11.1 and declination of -4.9^{o}

The RTP magnetic anomaly map (Fig. 5.3) shows both low and high magnetic frequencies representing points of low and high magnetic signatures respectively in the area. Both RMI (Fig. 5.2) and the reduction to the pole RTP image (Fig. 5.3) display similar magnetic features, but in the RTP image the highs (pink colour) of the RMI are seen as lows (blue colour). The RTP map shows more significant features such as structures and lithology in the magnetic signature than the residual magnetic intensity map. At the centre zone (BS in Fig. 5.3) some features observed in the RMI are now seen as linear features trending in the south-north direction. Moreover, other features (e.g. the low magnetic signature (VS in Fig. 5.3) and high magnetic signature (BV in Fig. 5.3) which are not clearly seen in the RMI image (Fig. 5.2) are seen in the RTP. Another clear example is the linear magnetic signature (BS in Fig. 5.3) at the centre of the area. Also observed are some high (pink) features in the RMI image remained high (pink) in the RTP image. Example is the magnetic signature BJ found at the western part of the area. This feature is interpreted as the jasper in accordance to what Jones (1990) reported. He described the jasper in the area (around Kwamekrom) to be interbedded with some iron oxide which is responsible for its association with high magnetic signature in that area. The RTP image displays the highest magnetic intensity at the western part of the area (BV in Fig. 5.3) with the average peak to peak at about -1148 nT. These high magnetic anomalies are seen to trend in the south-north direction. Clear lithological boundaries are also observed in the image. These boundaries are observed from the sharp contrast in the magnetic signature on adjacent magnetic bodies. The high frequency magnetic anomaly at the western part of the area was interpreted as the magnetite-rich formation (BV) and was delineated as the volcanic rocks (Blay, 2003). A clear idea about the shape of the Buem sandstone (BS) at the southern central portion of the area is noted in the RTP image which is interpreted to be a dome shaped. The folding F_1 of the Buem volcanic rock (BV) (located at the south western corner which trends south-northeast) caused by the collision between the Buem and the Voltaian (Kennedy, 1964) is well defined in the RTP image (Fig. 5.3). The structures SS, SV and F_2-F_2 representing faults and folds which were not clearly seen in the RMI grid are well delineated in the RTP grid. Some magnetic contrasts observed in Fig. 5.3 are interpreted as the lithological contacts. Prominent is the contact (white lines, SS in figure 5.3) between the Buem sandstone and the Buem shale (delineated as displayed by a fairly sharp magnetic contrast).

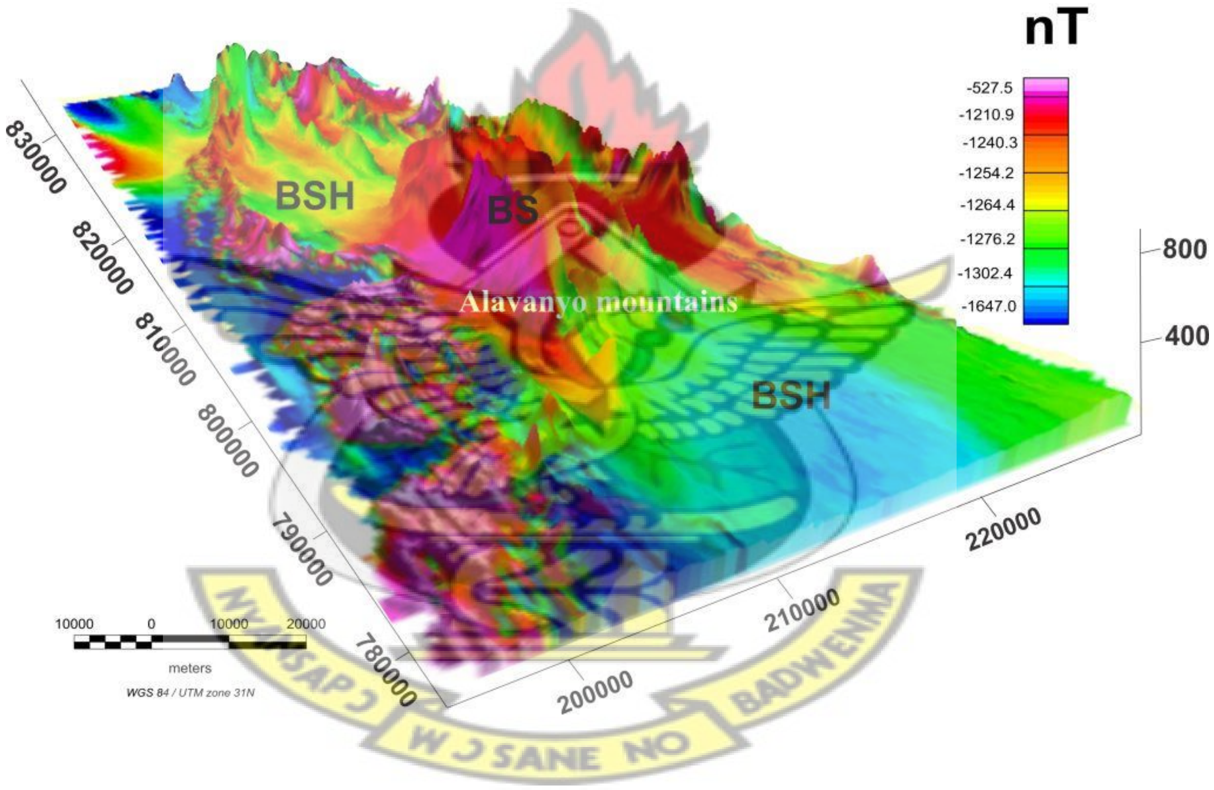

Figure 5.4 RTP image drape over DEM viewed in 3D (Red - high magnetic signature and blue- low magnetic signature)

Interestingly, the relatively high magnetic signature (BS) located at the south-central part of the area was seen to have a close relation with the topography of the area. Draping the RTP image over the digital elevation map (DEM) and viewing it in 3D helped to visualize the relation between the sandstone and the elevation of the area. From figure 5.4 it is seen that sandstones (relatively high magnetic signature) are normally associated with the high elevations in the area (prominent is the BS in Fig. 5.4). This confirms the description Jones (1990) gave concerning the sandstone in the area as being found in areas of high elevation. Another obvious location where this observation can be clearly seen is the Alavanyo mountain range (Blay, 2003).

5.2.3 Analytical Signal

To know the source positions of the magnetic anomaly regardless of direction and remnant magnetization in the sources effect that is mostly associated with the RTP, the analytical signal filter was applied to the RMI grid. The significant characteristic of the analytical signal, AS is that it is independent of the direction of the magnetization of the source. Moreover, the amplitude of the analytical signal can be related to the amplitude of magnetization (Silva et al., 2003). Asadi and Hale (1999) used the analytical signal of total magnetic intensities to delineate intermediary magmatic rocks in the Takab area of Iran.

Figure 5.5 (analytical signal map) shows that, the most prominent features are the high analytic signal amplitude that runs in an approximately south–north (SN) direction along the western border of the area. Three major magnetic zones (high magnetic anomalous zone) define by (BV), intermediate magnetic anomalous zone (BS) and low magnetic anomalous zone (BSH and VS) were delineated (Fig. 5.5). The high magnetic signatures (BV) of the analytical map are the volcanic rocks (Bell & Crook, 2003) which are found around the south-western part of the area and trend in the south–north direction (Fig. 5.5).

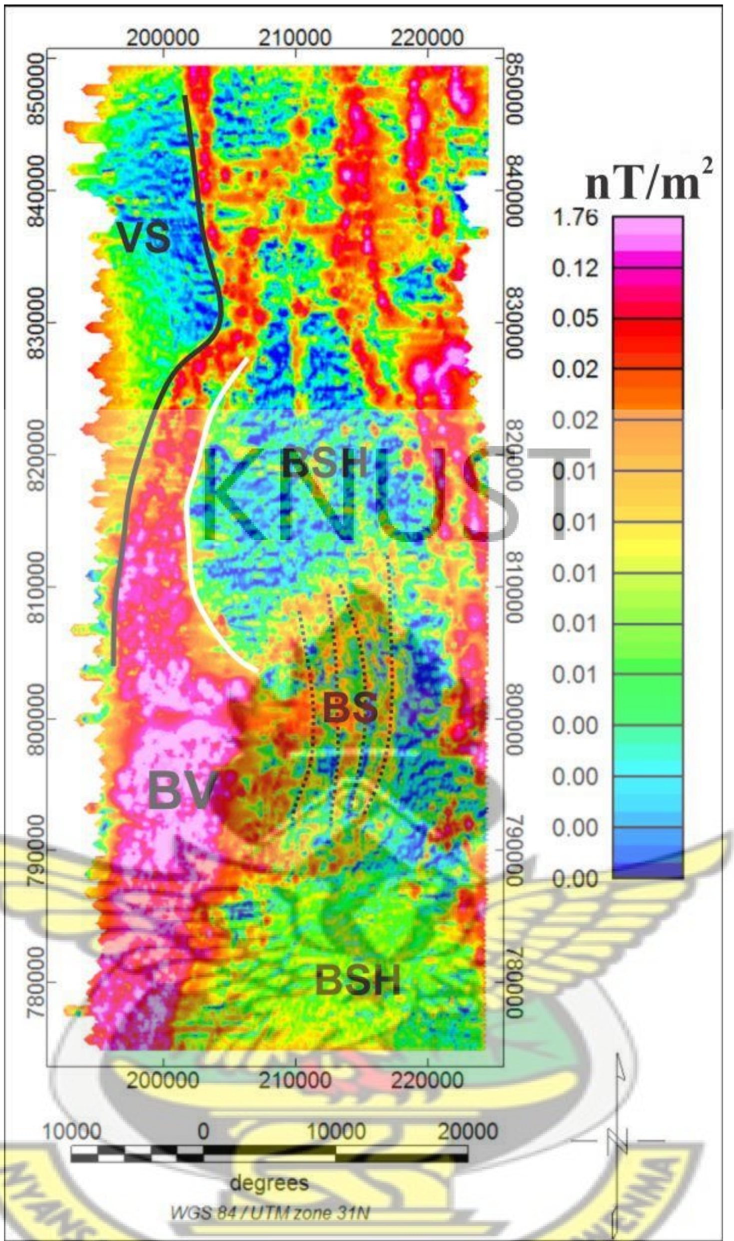

Figure 5.5 Analytic signal image of residual magnetic intensity

According to Jones (1990), ferruginous quartzite occurs throughout the Buem formation, and this ferruginous material is considered to be responsible for the intermediate magnetic signature (BS). The low magnetic signature was delineated to be the Buem shale (BSH) and Voltaian sediment (VS) (Fig. 5.5). Additionally, the black and white lines in figure 5.5 which portrays a sharp magnetic contrast are lithological contacts. The white line is the volcanic-shale boundary (contact) and the black line represent the Buem Formation-Voltaian Formation contact. Osae et al., (2006) described the outcrop of the Buem sandstone as having a lense shape body (thick in the middle and thin at the edge) and overlap in lines to form a range of hills. This discription of the sandstone is shown in figure 5.5 as doted black lines around BS. In general, the analytical signal image (Fig. 5.5) revealed the different lithological units and geological structures in the area.

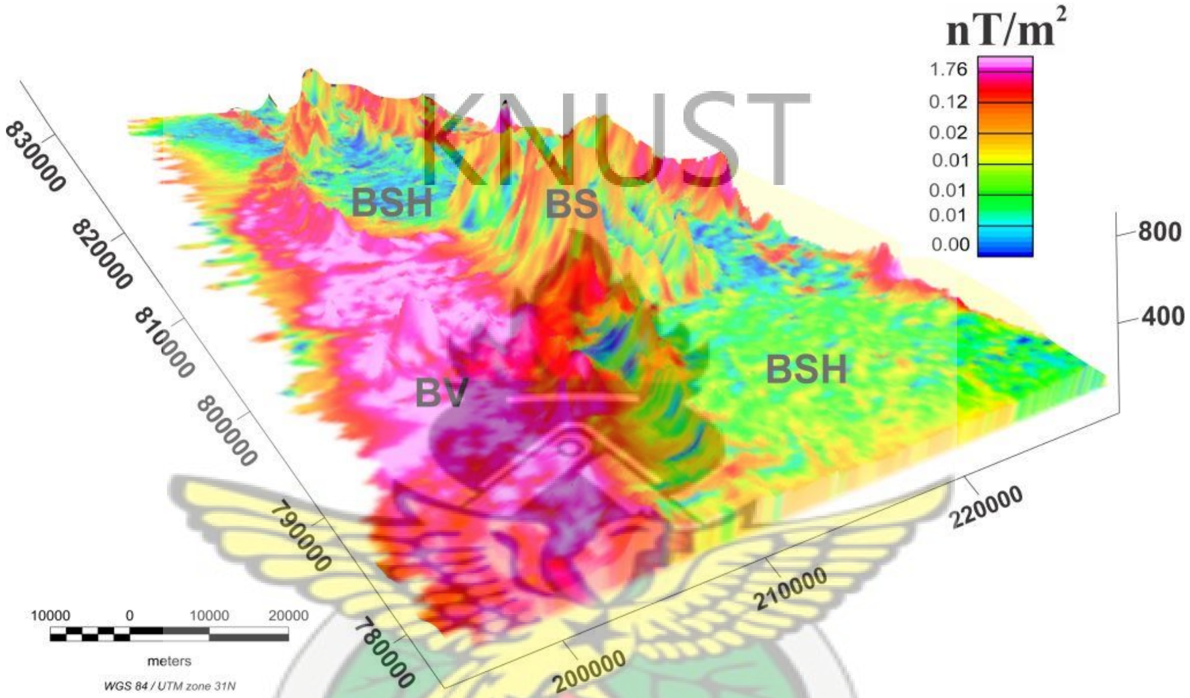

Figure 5.6 Analytical signal image draped over DEM viewed in 3D

Analytical signal image was draped over the digital elevation map (DEM) (Fig. 5.6) and there appears to be a greater correlation between the highlands in the area and the high magnetic signature observed. These relatively high magnetic signature observed to be associated with the highlands are interpreted as the Buem sandstone in accordance with Osae et al., (2006) description of the Buem sandstone.

5.2.4 First Vertical Derivative (1VD)

To observe the near surface source magnetic features that are associated with geological structures, the first vertical derivative filter was applied to the RTP grid. The colour and grey scale vertical gradient images of the residual magnetic intensity (Fig. 5.7 a & b) enhanced the image by showing major structural and lithological detail which were not obvious in RMI image (Figure 5.2). Thus the colour and grey-scale images complement each other.

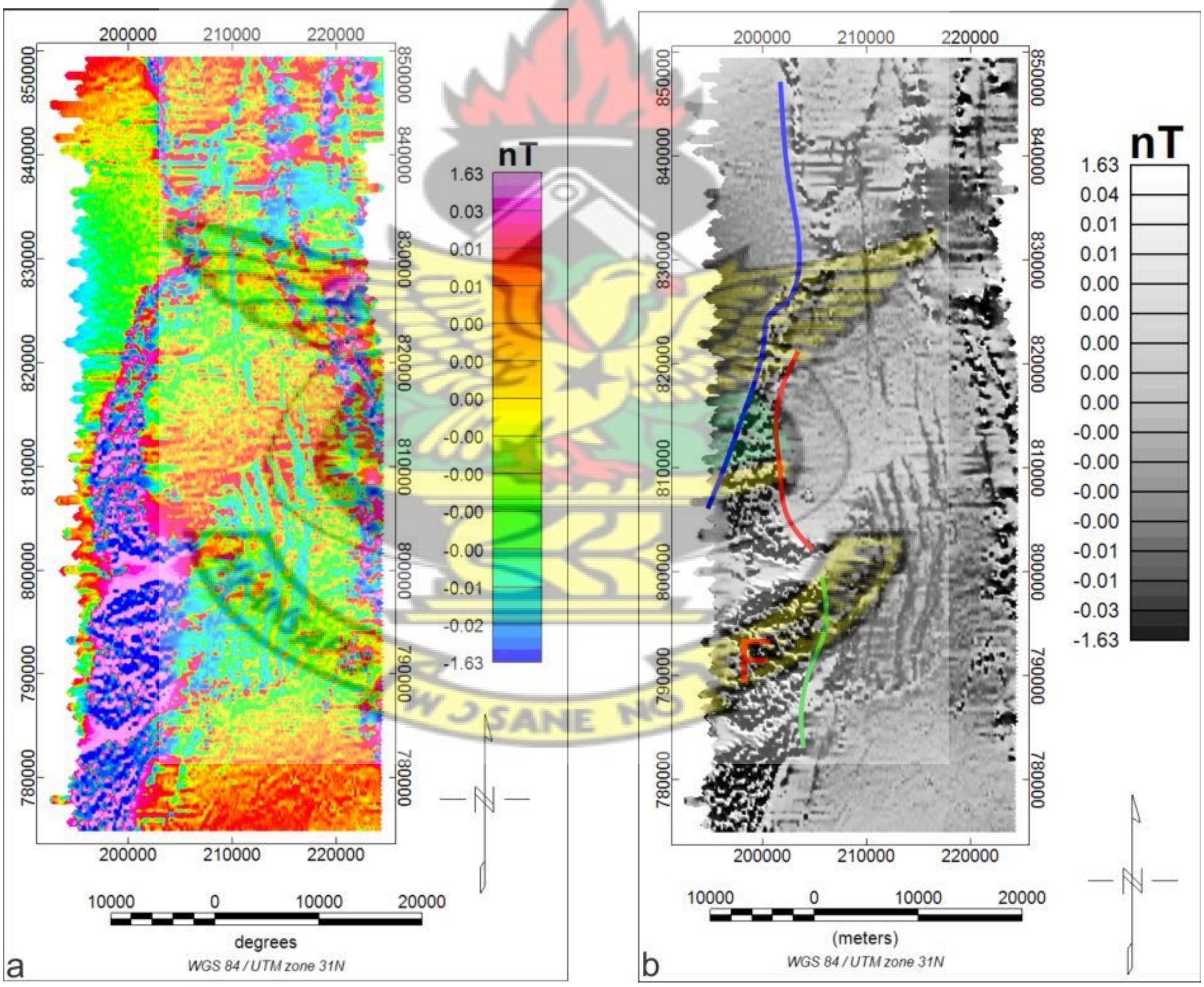

Figure 5.7 First vertical derivative map of the RTP grid. (a) colour shaded map (b) grey scale map

The grey-scale of first vertical derivative (Fig. 5.7b) displayed the near surface source magnetic features associated with geological structures. Lithological contacts were clearly delineated by the coloured lines In Fig. 5.7b. The red line is the volcanic-shale contact, the blue is the Beum-Voltaian contact and the green is the volcanic-sandstone contact. The structure F within the volcanic formation is a fold which is caused by the collision between the Buem and the Voltaian (Kennedy, 1964). The 1VD filter helped decrease broad and more regional anomalies and rather enhanced local magnetic responses which are interpreted as structures in the area. Most of the structures delineated in the area coincided with already delineated structures in the geological map of the area (Fig. 2.3). Prominent among these delineated structures are the thrust faults (in the Fig. 2.3) at the northern and the eastern part of the area. These thrust faults coincided with the delineated fault (in Fig. 5.7) which trends in the south-north direction.

5.2.5 Upward continuation

Figures 5.8 b-d show the RTP (grid) continued upward to 100 m and 400 m and 800 m, respectively; i.e. they show images of the magnetic intensity that would be obtained assuming the data were recorded at heights of 100 m and 400 m higher than the original datum the data was collected. In physical terms, as the continuation distance is increased, the effects of smaller, narrower and thinner magnetic bodies progressively disappear relative to the effects of larger magnetic bodies of considerable depth extent. As a result, upward-continuation maps give the indications of the main tectonic and crustal blocks in an area.

Comparing the figures, the 100 m upward continuation for the RTP image (Fig. 5.8b) shows similar features as seen in the RTP image (Fig. 5.8a). Thus the magnetic body producing the anomaly may be at a deeper depth other than the 100 m depth. Moreover, comparing the 400 m and 800 m upward continuation images (Fig. 5.8c and Fig. 5.8d respectively) with the RTP image and 100 m upward continuation image (Fig. 5.8a and Fig. 5.8b respectively) it is seen that most sharp feature in the Fig. 5.8a & b are not seen in Fig. 5.8c & d. Prominent is the sharp linear feature (L in Fig. 5.8a & b) at the western side of the area which is not visible in the other images. This may indicate that the signature is coming from a magnetic body at shallow depth than the 400 or 800 m.

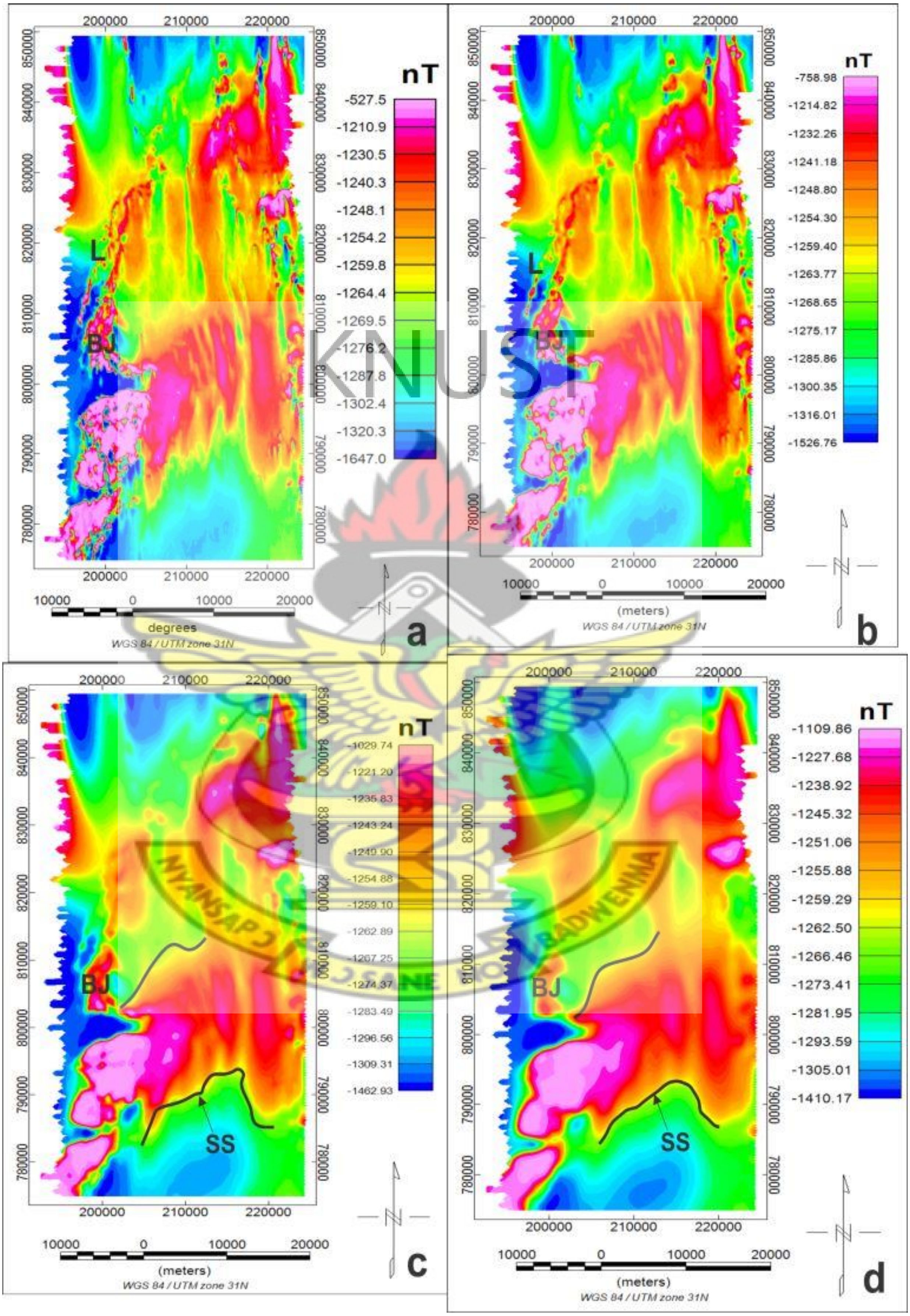

a
nT
-527.5
-1210.9
-1230.5
-1240.3
-1248.1
-1254.2
-1259.8
-1264.4
-1269.5
-1276.2
-1287.8
-1302.4
-1320.3
-1647.0
L
BJ
degrees
WGS 84 / UTM zone 31N
b
nT
-758.98
-1214.82
-1232.26
-1241.18
-1248.80
-1254.30
-1259.40
-1263.77
-1268.65
-1275.17
-1285.86
-1300.35
-1316.01
-1526.76
(meters)
WGS 84 / UTM zone 31N
c
nT
-1029.74
-1221.20
-1235.83
-1243.24
-1249.90
-1254.88
-1259.10
-1262.89
-1267.25
-1274.37
-1283.49
-1296.56
-1309.31
-1462.93
SS
(meters)
WGS 84 / UTM zone 31N
d
nT
-1109.86
-1227.68
-1238.92
-1245.32
-1251.06
-1255.88
-1259.29
-1262.50
-1266.46
-1273.41
-1281.95
-1293.59
-1305.01
-1410.17
(meters)
WGS 84 / UTM zone 31N

Figure 5.8 (b-d) RTP (grid) been continued upward to 100 m and 400 m and 800 m (a) RTP image

Additionally, lithological contacts (SS) are also observed in the Fig. 5.8c and Fig. 5.8d. Prominent contact is the shale-sandstone (SS) contact (marked by black lines in Fig. 5.8c and Fig. 5.8d) at the southern part of the area. Other prominent bodies believed to be situated at a deeper depth other that the 800 m is also observed in the other images. A clear example is the dome shaped body labelled BJ in Fig. 5.8 which is seen in all the images. Upward continuation of the RMI provided insights into crustal geology (lithology and contacts) of the area.

5.2.6 Tilt derivative

To determine structures (fault and folds), the contacts and edges or boundaries of magnetic sources, and to enhance both weak and strong magnetic anomalies of the area, the TDR filter was applied to both the RMI and the RTP grid. The tilt angle derivative filter attempts to place an anomaly directly over its source. Verduzco et al., (2004) showed in their work that tilt derivative filter performs an automatic-gain-control (AGC) filter which tends to equalize the response from both weak and strong anomalies, hence, providing an effective way to trace out along striking anomalies. Tilt angle derivative (TDR) of RMI locates the edges of formations, especially at shallow depths by using the theory that the zero contours are the edges of the formation (Salem et al., 2007). It is observed that the zero contours estimate the location of abrupt changes in magnetic susceptibility values. The zero contour lines in this grid (Fig. 5.9b) are represented by a yellow colour.

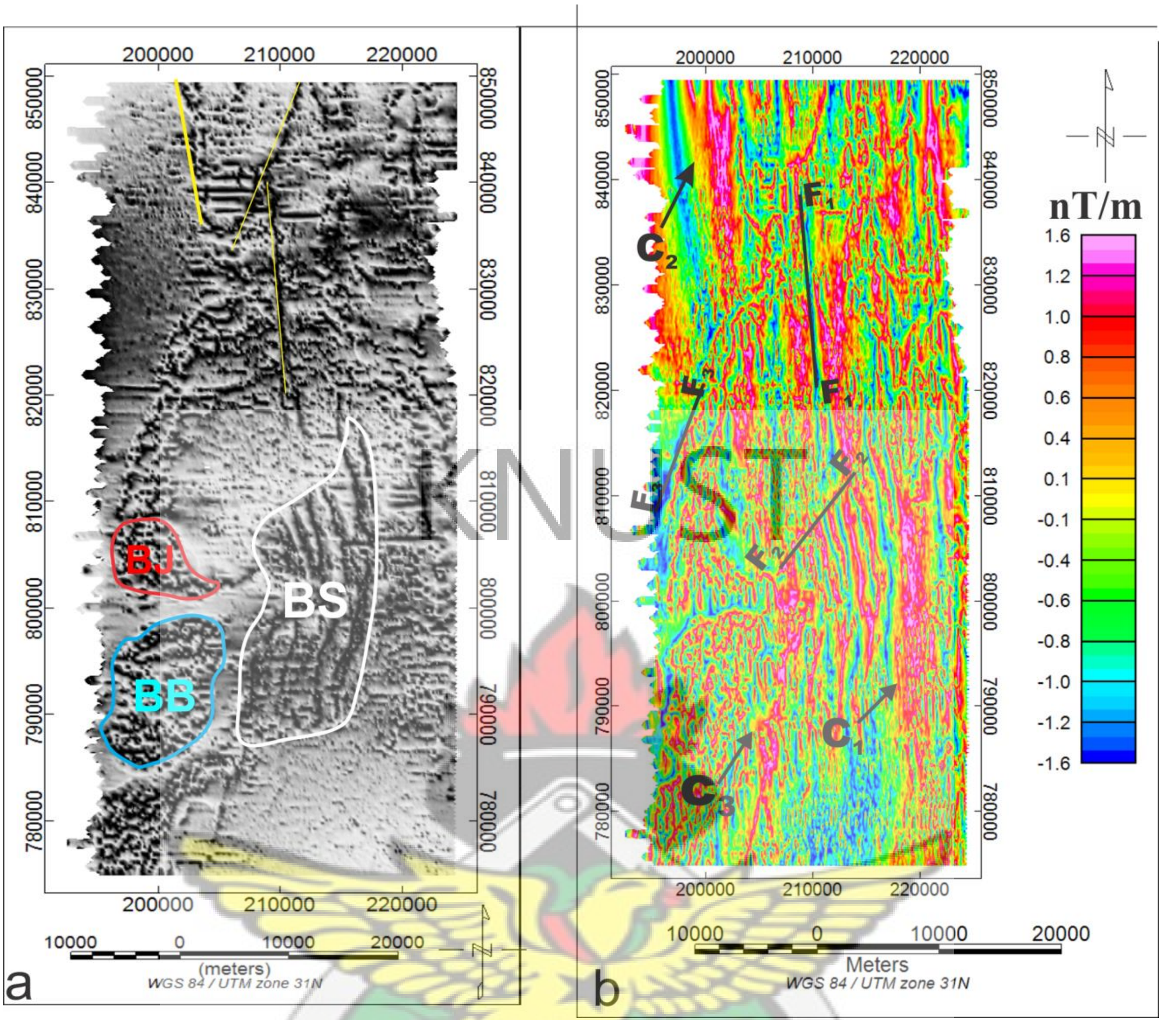

Figure 5.9 Till angle derivative, TDR (a) TDR derived from RTP image displaced in grey scale (b) TDR derived from RMI

Figure 5.9a displays most structural feature of the area such as the faults, contacts and to some extent the shape of some lithology. Some lithologies (e.g. BJ, BB and BS in Fig. 5.9a) in the area are accentuated. Prominent of these features are the ones marked with blue polygon, BB (in Fig. 5.9a) at the south-western part of the area and this is interpreted as the basalt with some associated volcanic rocks as described by Jones (1990). The jasper which Jones (1990) described to be around Kwamekrom is clearly delineated (marked with a red polygon, BJ, in Fig. 5.9a). Junner (1940) reported that the sandstones in the area are strongly folded and showed greater deformation (faulted) than the Buem volcanics. This observation is seen in the polygon marked white, BS, at the central part of the area. This feature, BS, marked with white polygon and which coincides with the sandstone in the area is seen to be highly faulted and deformed. This deformation and folding may be as a result of the thermo-tectonic event that occurred about 600 m.a. ago (Jones 1990). According to Jones (1990) a number of thrust faults relating to the eastern Pan- African orogenic event occur in the northern part of the area. Moreover, according to Villeneuve and Cornée (1994), the Buem and Togo rocks form part of the Dahomeyide Belt, a nappe complex thrust over the Volta Basin. The linear anomalies are clearly seen at the northern part (marked with yellow line in Fig. 5.9a) and are interpreted as a thrust faults. These thrust faults can also be inferred from the regional geological map of the area (GSD, 1988). Appling the filter on the RTP grid gave a clear picture of the magntic body and structures in the area as compared to the filter applied on the RMI grid (comparing Fig. 5.9a and Fig. 5.9b). The TDR image (Fig. 5.9 a & b) shows different lineaments and contacts in the area. Most of the lithological contacts in the area were delineated from the Fig. 5.9b (TDR on RTP image). Noticeable lithological contacts observed are; the shale-sandstone contact (C_1 in Fig. 5.9b) at the southern part of the area, the Buem-Voltaian contact (C_2 in Fig. 5.9 b) at the north-western part of the area and the volcanic-shale contact at the south-western part of the area (C_3 in Fig. 5.9b). Some structural lineaments (faults) e.g. F_1- F_1, F_2 – F_2 and F_3 - F_1 were delineated by observing the abrupt change between the positive and negative magnetic anomalies (Fig. 5.9b). Faults and folds are also delineated from the TDR and are displayed in the structural map produced (Fig. 5.11). Some of these features are inferred from other publications and published maps of the area. In Fig. 5.9b a lot of noise believed to be from the shallow surface are observed which show that appling TDR on RTP on dataset from the study area can really help in delineating geology (lithology) and structures.

5.2.7 Summary

In attempt to identify the structures and geology of the area, recognizable patterns from the RMI and enhanced maps were first observed and related to their possible physical causes. Furthermore the geophysical interpretations were properly correlated with available geological publications, topography and geological data of the area to actually confirm the interpreted structures. From the results of enhanced aeromagnetic maps, we were able to distinguish the magnetic responses in the geology due to the difference in magnetic susceptibilities, structures and deformation styles of the magnetic units in the area. The area was divided into magnetic domains (regions) based upon the magnetic intensities, structural styles, and geological features. Boundaries of the individual lithological domains coincide with the abrupt changes in the magnetic intensities and orientations were delineated. The division was also on the basis on interpreted subsurface geology and structure, lineament patterns, and circular features described in the previous sections (section 5.1.1 – 5.1.7).

Figure 5.10 shows the interpreted geological structures in the area delineated from the magnetic dataset and superimposed on the TDR image. This map gives a rough idea about the geological structural and lithology deformation of the area.

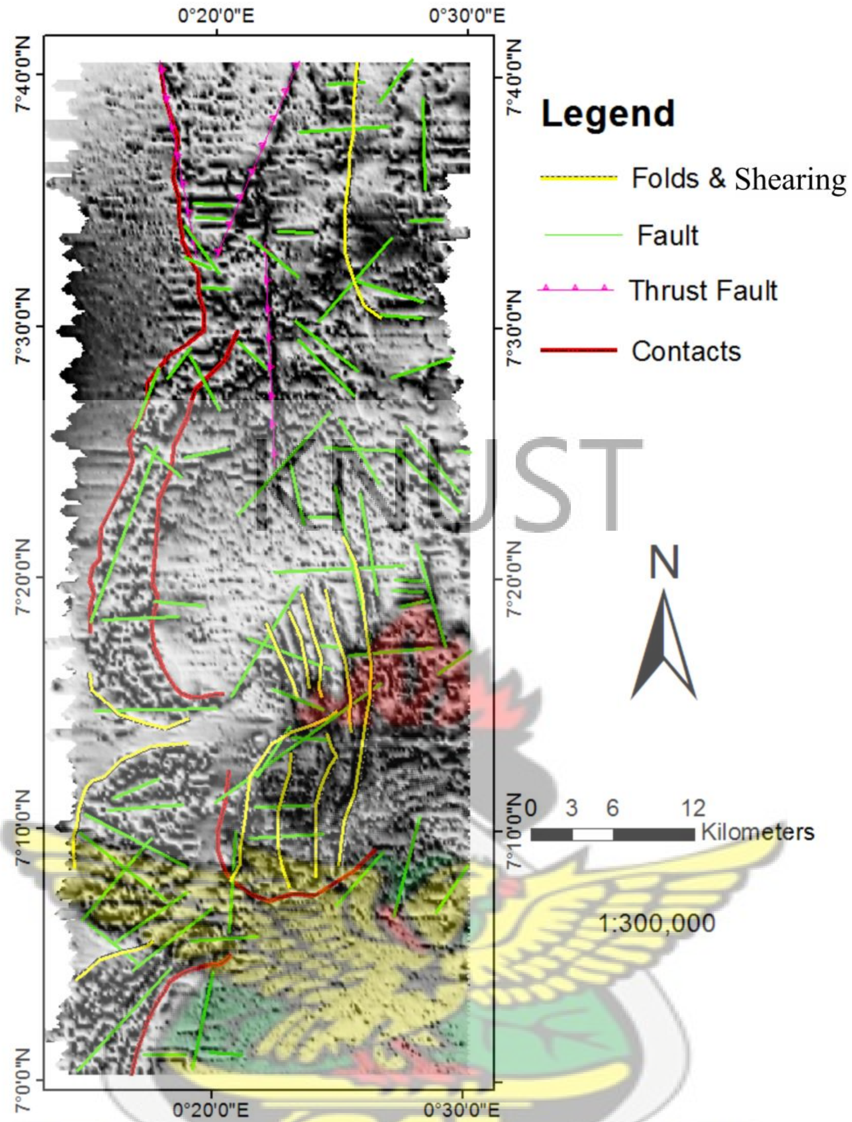

Figure 5.10 Interpreted fault, folds and contacts superimposed on the TDR image displayed in greyscale

The interpreted magnetic structural map, Fig. 5.11, is integrated information from the first vertical derivative map (Fig. 5.7), the residual magnetic intensity, RMI map (Fig. 5.2), analytical signal map (Fig. 5.5) and Tilt derivative map TDR map (Fig. 5.9). Fig. 5.11 reveals enhanced structural features that include faults, folds, lithological contacts and fracture systems in the area.

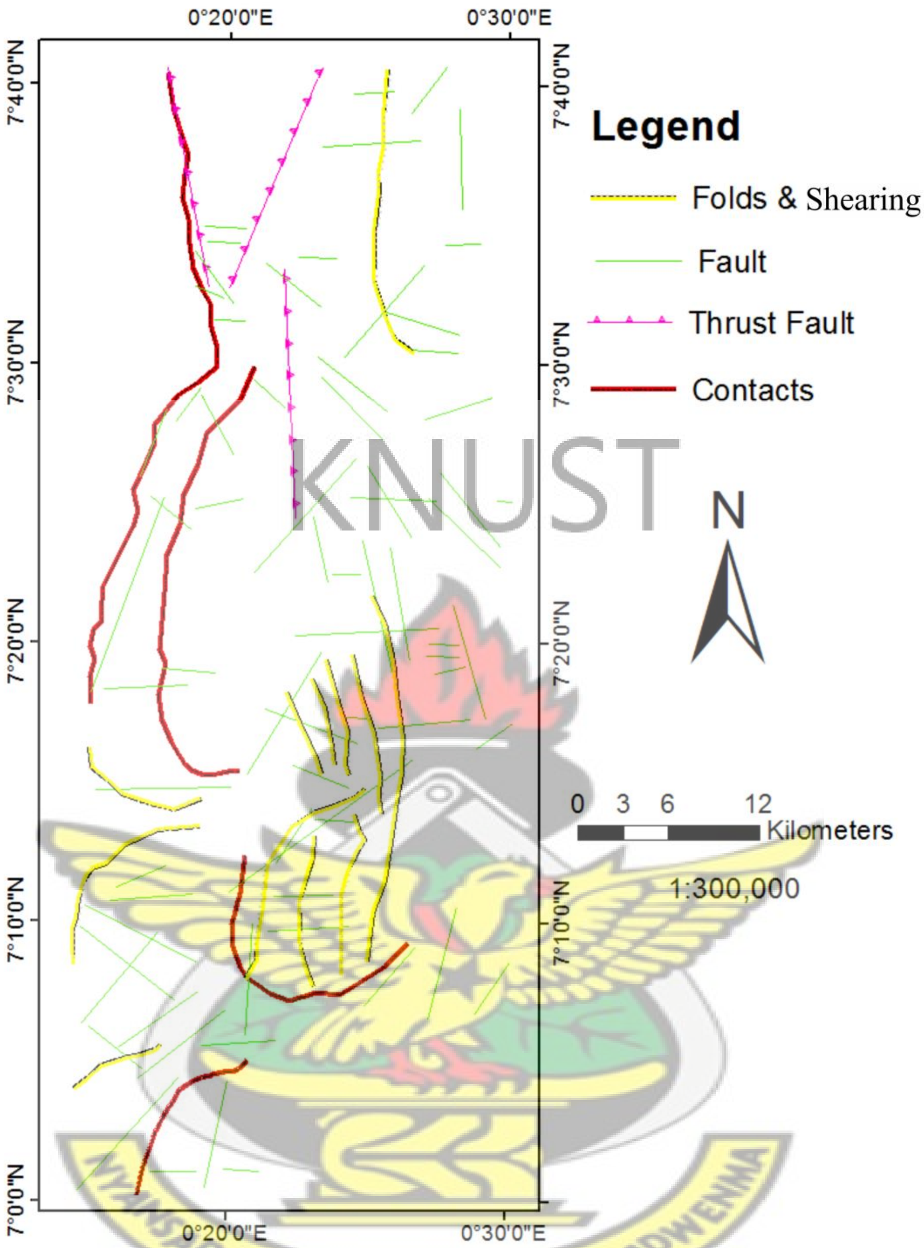

Figure 5.11 Interpreted structural map from the aeromagnetic dataset

Lineaments were analysed in order to extract further information on the distribution and nature of the lineaments and for this purpose a conventional technique called rose diagram was applied. A Rose Diagram was used to display graphically different tendencies for structures like joints or fault planes representing the angular relationships of the geologic map data. The purpose of this study is to analyse the spatial distribution of lineaments extracted from aeromagnetic images according to their length and orientation in order to contribute to the understanding of the faults of the study area.

The Fig. 5.12 is a Rose Diagram representation of the regional strike of the delineated lineament from aeromagnetic data by using a polar plot where the distance from the centre of the plot is proportional to the sum of the line lengths in that orientation. Structural lineament orientation or azimuth direction on the structural lineament map (Fig. 5.11) were measured (using a script (Appendix A.3) in ArcGIS 10) and plotted as a rose diagram using StereoNett software.

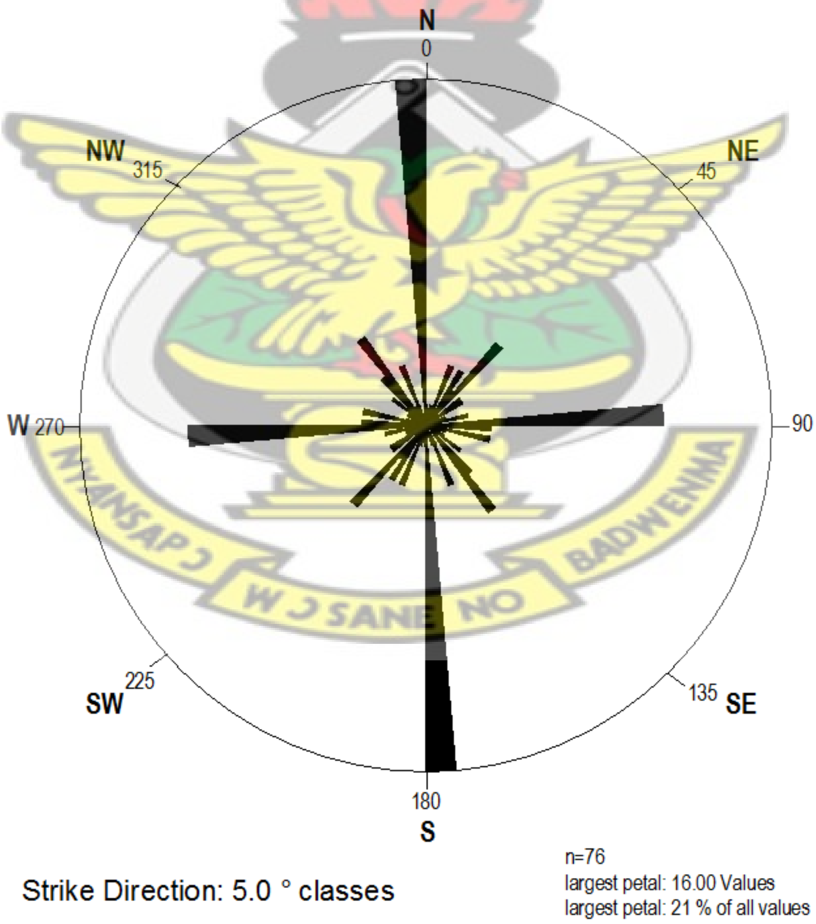

Figure 5.12 Rose diagram showing the lineaments orientation of the study area

The rose (azimuth-frequency) diagram (Fig. 5.12) depicted most (major) of the lineament extracted trends in the north-south (N-S) and east-west (EW) direction with the minor trending in northeast southwest (NE-SW) and northwest-southeast (NW-SE) direction. According to Junner (1940); Jones (1990); Blay (2003) the the structures in the area are complex and most of lineatemt trends in the N-S direction. This accounts for the observedstructures in the Rose diagram which show that the largest petral is 21 % of the delinaeted lineaments and represent lineaments trending in the north-south direction. The Fig. 5.12 also indicates that out of delineated lineaments plotted 11% represented the second largest petal striking in the east-west (EW) direction, with 6% also striking in the northeast-southwest (NE-SW) and another 6 % trending in the northwest-southeast (NW-SE) direction. From the rose diagram it is seen that the area is dominated by a north-south and east-west trending lineament.

Figure 5.13 is the interpreted lithological map of the area from the aeromagnetic data showing the shale, sandstone, jasper, basalt and it associate volcanic rocks, Volcanic domain, part of the Voltaian sediments, and some geological structures. The strike of the rock formation South-North, SN (Bell & Crook, 2003) of the area is observed.

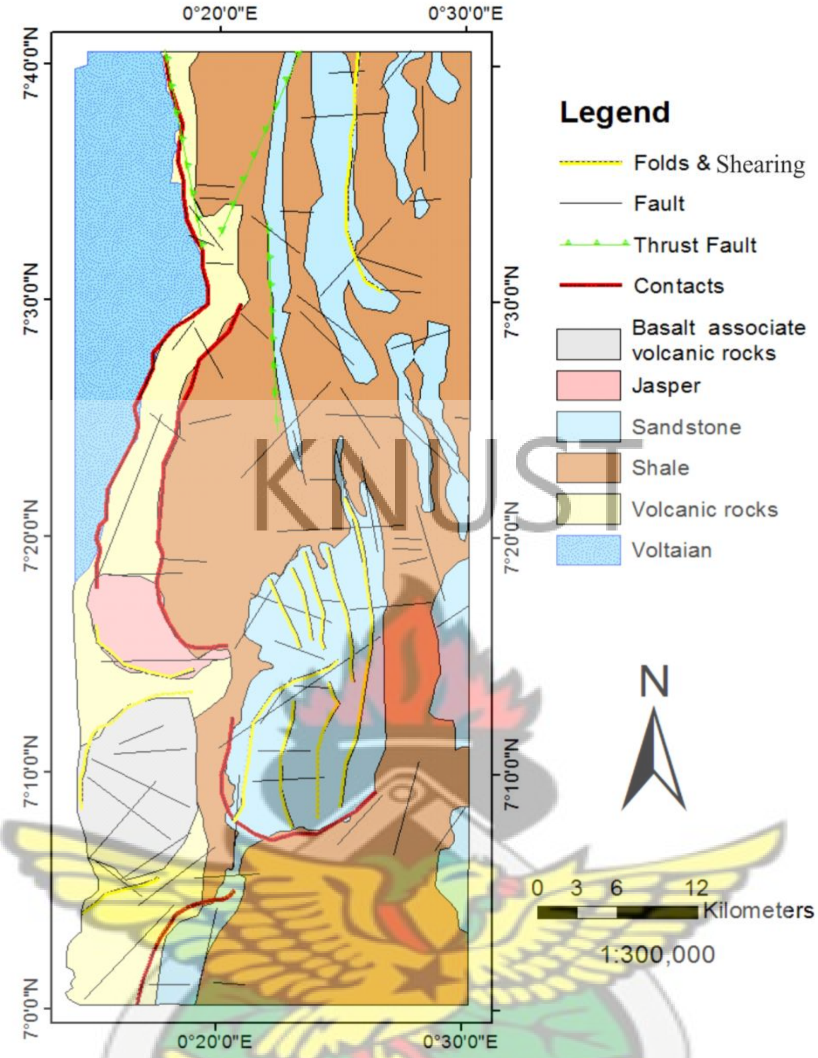

Figure 5.13 Interpreted lithological map from aeromagnetic dataset

The interpreted geological map (Fig. 5.13) from aeromagnetic dataset shows the lithological units and their contacts and the structures in the Buem formation. The map (Fig. 5.13) also depicts most of the observations and feature described in the previous section (section 5.1.1 – 5.1.7).

5.3 Radiometric Data

Radiometric data has many uses including soil mapping and to some extent structural mapping but its main use is mapping lithological units and alterations by determining the spatial correlation existing between the radiometric data and the rocks (Gunn et al., 1997b). The spatial correlation of the radiometric data involves measuring of naturally occurring radioactive elements that exist in minerals forming rock and soil (Telford et al., 1990). The images generated from the data were analysed and interpreted to provide geological meaning to the radiometric dataset. Interpretation of these figures and maps were carried out visually to identify and characterize lithology and delineate possible surface geological structures. High radiometric elemental patterns and irregular low magnetic zones are interpreted to have resulted from possible mineral deposits or rock alterations (Gunn et al., 1997b).

5.3.1 Potassium

The potassium, K, map (Fig. 5.14) shows different degrees of potassium concentrations that reflects different lithological units and alterations in the area. Potassium radiation fundamentally comes from potash feldspars, which are mainly common in felsic igneous rocks (e.g. granite) and are low in mafic rocks (e.g. basalts and andesite) (Gunn et al., 1997b). Rock alterations can also result in high K concentrations (Wilford et al., 1997).

A number of potassium anomalies are evident in the radiometric image Fig. 5.14. The colour blue corresponds with low K values whilst the pink corresponds with very high K values. The colour red represents moderately high to high K values and the shades of orange to yellow colour represent or are associated with moderately low K values.

Low potassium concentration is observed at the left side of the image (VL), and similar observation is seen at the upper left corner of the area. This observation coincides with the Volta Lake (from Fig 1.1) which is observed in the study area. Low concentration was recorded because water body shields the potassium radiation from the underlying rocks hence, reducing the intensity of the signal at that point. Since radiometric survey uses the assumption of residual of soil the top 30 cm soil is able to adsorb most of the radiated radioactive element from the underlying rocks or the lithology. High concentration of K is also observed at the south-west corner (B in Fig. 5.14) of the area. B is suspected to be basalt described by Jones (1990); Osae et al., (2006) as being alkaline and having high concentration of K. High concentration of potassium concentration is found at the central (BSH in Fig. 5.14) part of the area. This coincides with the shale region mapped in the analytical signal map (Fig. 5.5) of the magnetic data. This shows that the shale in the area has high concentration of K and this can be attributed to the description given by Osae et al., (2006) concerning Buem shale. Osae et al., (2006) described shale in the area as emitting more gamma rays than other sedimentary rocks in the area. Similar observation at the center of the area is seen at the southern part (BSH) of the area and this can also be attributed to the Buem shale.

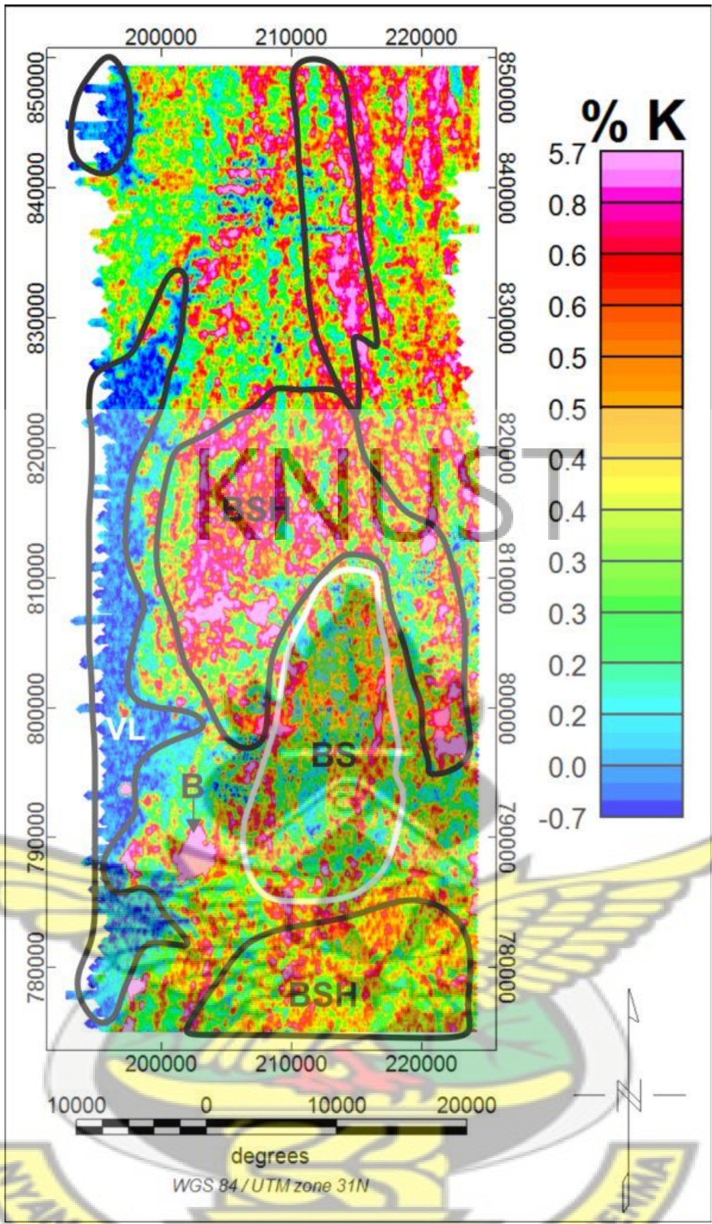

Figure 5.14 Gamma spectrometric image for Potassium (K) concentration

A relatively medium concentration of K is observed at the center (BS) of the area just below the Buem shale and this feature also coincides with the Buem sandstone which was clearly mapped in the Residual Magnetic Intensity map (Fig. 5.2). The relatively medium concentration of K in the sandstone confirms the discription Osae et al. (2006) gave concerning the sandstone and shale in the Buem as having relatively low concerntration of K. Within the sandstone, (BS in Fig. 5.14) there are some high potassium concerntration which looks almost like a linear feature. This can be attributed to linear sturcture in the area. It was also observed that the high concentration of potassium coincides with the elevated region in DEM (Fig. 5.1). The lithological contacts are not clearly seen in the potassium image.

5.3.2 Thorium

Anomalies in the thorium data in Fig. 5.15 helped map the lithology and lithological boundaries of the area. The thorium, Th map shows three distinct regions of thorium concentration in the area. These Th concentration zones are represented by pink colour, relatively high concentration of the Th concentration represented by green colour and low Th concentration represented by blue colour (Fig. 5.15). The high concentration in Th marked by black polygon (Fig. 5.15) correspond to the shale and other weathered sediment in the area. These weathered sediments are believed to have originated from the rock (sandstone) in the high elevated lands in the region (Jones, 1990). The assertion is approved by (Fig. 2.3) and this coincides with the high elevated lands in the area (from DEM Fig. 5.1). Prominent of this relatively high Th anomaly is observed around the Alavanyo high lands. Moreover, the low concentration of Th marked by white polygon observed at the western part of the area coincides with the Volta Lake in the area. This indicates the fact that the water body shield the emission of radiation from radiogenic element (thorium) of the underlying lithology.

Weathered sedimentary rocks from the high elevated lands (from DEM Fig. 5.1) for most part of the area are depicted by high Th radiogenic emissions (red colour). This indicates the relatively high clay content of the weathered sediment and the adsorption of Th by the essential clay minerals of the weathered sediments (Blay, 2003). The low K signature recorded may be due to continued weathering and leaching of the sandstone (associated with the high elevated lands) in most part of the area.

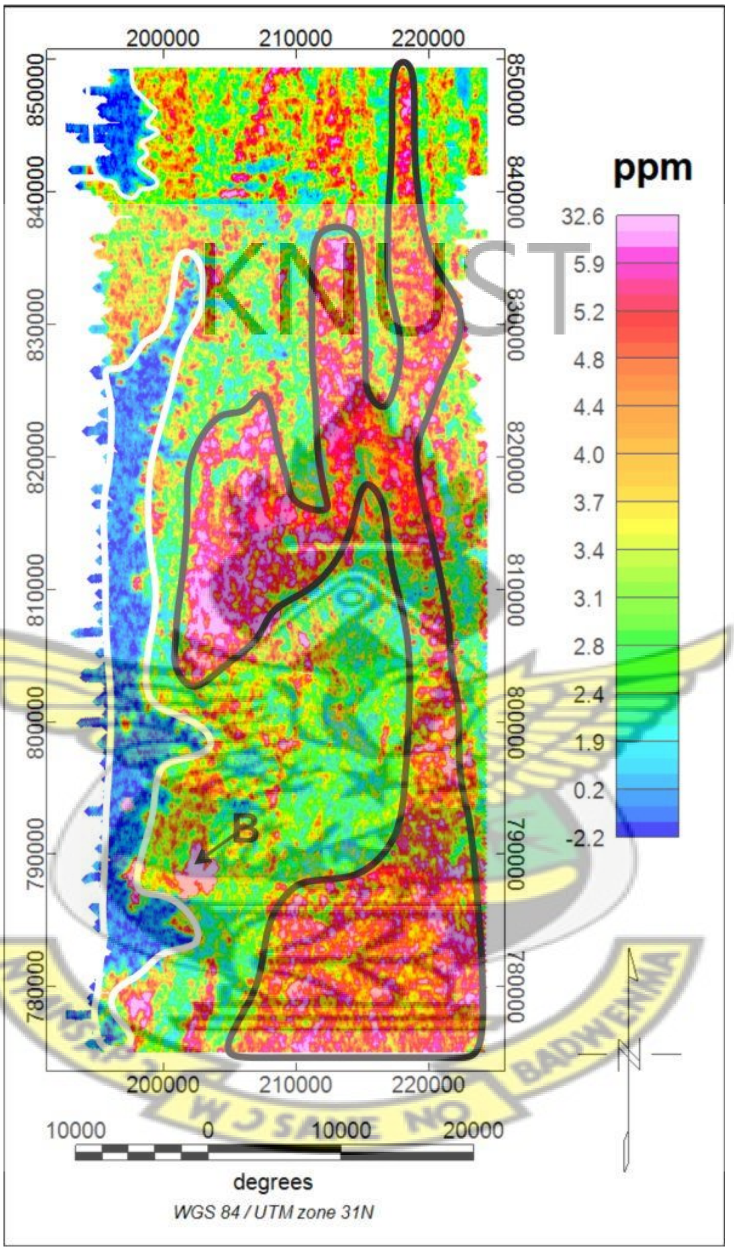

Figure 5.15 Gamma spectrometric image for thorium (eTh) concentration

5.3.3 Uranium

The uranium image shows good definition in mapping the Volta Lake (marked by black polygon in Fig. 5.16) and certain geological formations such as B and BSH. The feature B, registered high uranium concentration. Interestingly, the circular body (B) which is observed in the Th and potassium map is also observed in the uranium map. The feature coincides with the Basalt which Jones (1990) described to be located around that part of the area. High concentration of uranium is also observed at the central part of the area marked with a white polygon. This feature coincides with the shale in the area. Thus the shale is broadly represented by high U concentration (white polygon in Fig. 5.16).

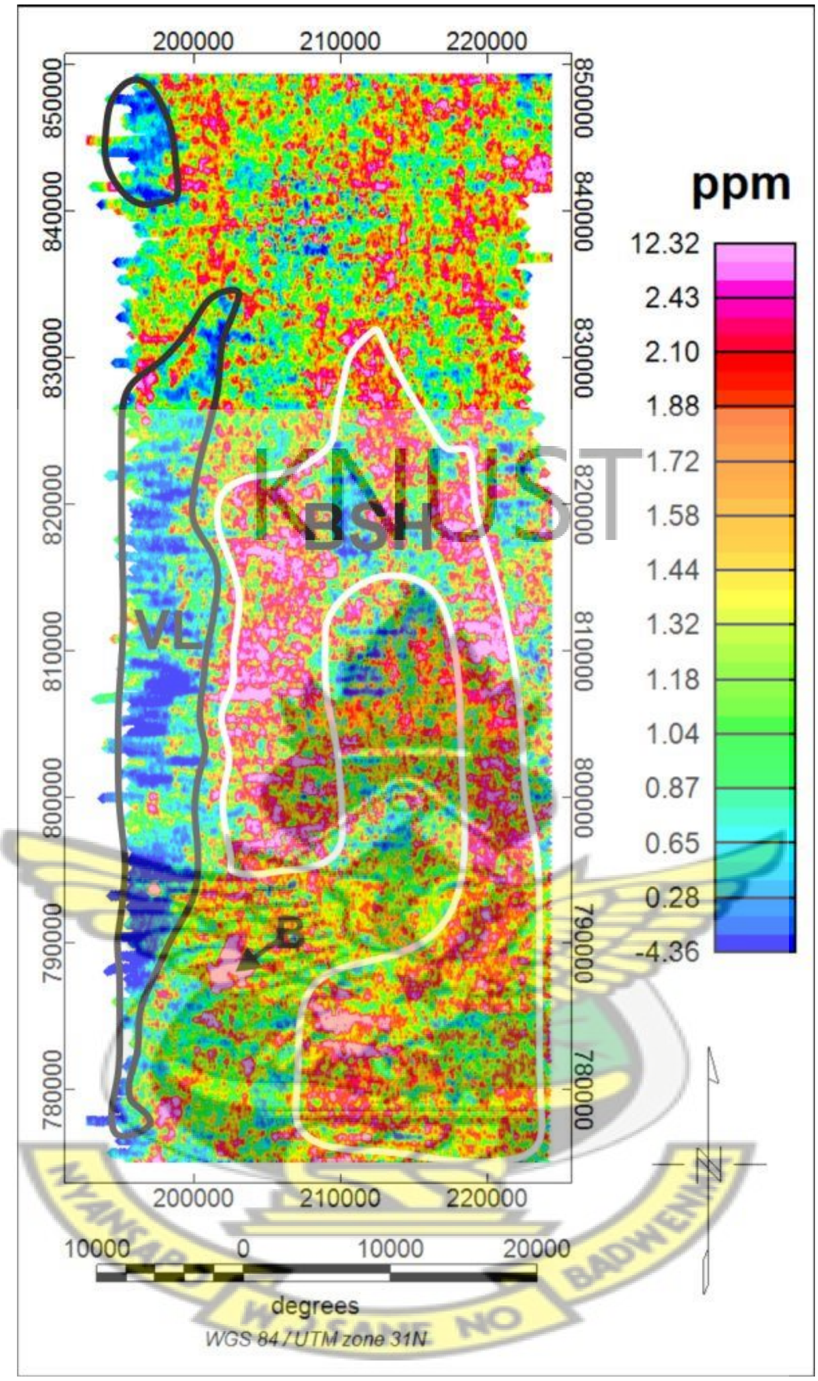

Figure 5.16 Gamma spectrometric image for Uranium (eU) concentration

Unlike the K and the Th maps, the uranium, U map could not clearly delineate the distinct boundary between most of the lithology of the area. The obvious boundary between the sandstone and the shale which are clearly seen in the Th map (Fig. 5.15) and Potassium map (Fig. 5.14) was not observed the uranium map. This is because the image (Fig. 5.16) shows short wavelength anomalies corresponding to noise caused by the variations in atmospheric radon concentrations during the course of the survey resulting in significant streaking in the image. This is a typical feature found in uranium images (Minty, 1997), in spite of the processing steps the dataset was subjected to.

5.3.4 Ternary map

The radiometric data are displayed as a ternary map with combined intensities of potassium (K), thorium (Th), uranium (U) concentration given in red, green, and blue colour respectively. The ternary radiometric map (Fig. 5.17) shows different colour combinations which indicate the K, Th and U concentrations. The radiometric responses in the ternary map, to some extent, correspond with the surface geological map of the study area (Fig. 2.3). Low concentrations of U, Th, and K radioactive elements are displayed by black colours with the magenta colour corresponding to high potassium with low uranium and thorium concentrations. Those with the low content of K but high contents of U and Th are characterized by green colour and the yellow colours are characterized by high potassium and thorium with low uranium. Additionally, the blue colour corresponds to regions of high uranium with low potassium and thorium.

From the ternary map, the Volta Lake can easily be delineated as having low concentration of the three radiogenic elements (depicted by a black colour in Fig. 5.17). The contact between the shale and sandstone (C in Fig. 5.17) in the area is also observed. The high concentration of K, Th and U, marked with the black polygon coincide with the shale and weathered sediment in the area which Osae et al. (2006) and Jones (1990) described to be in the area. Osae et al. (2006) and Jones (1990) described the shale in the area as emitting more gamma rays than other sedimentary rock in the area. The high K with low U and Th concentration which was depicted by a magenta colour coincides with sandstone in the area and interestingly it also coincides with the high elevated land in the area. Osae et al. (2006) reported that the sandstones in the area are normaly found at the highlands or the elevated regions in the area.

Figure 5.17 Ternary map of Study area (RGB=KThU)

The feature (B in Fig. 5.17) with high concentation of the K, U and Th is observed at the south western part of the area. The feature is seen in all the three radiogenic maps and is interpreted as the basalt that Osae et al. (2006) and Jones (1990) described in the area.

They also reported that the basalt is an alkaline basalt and accounts for its high K concentration.

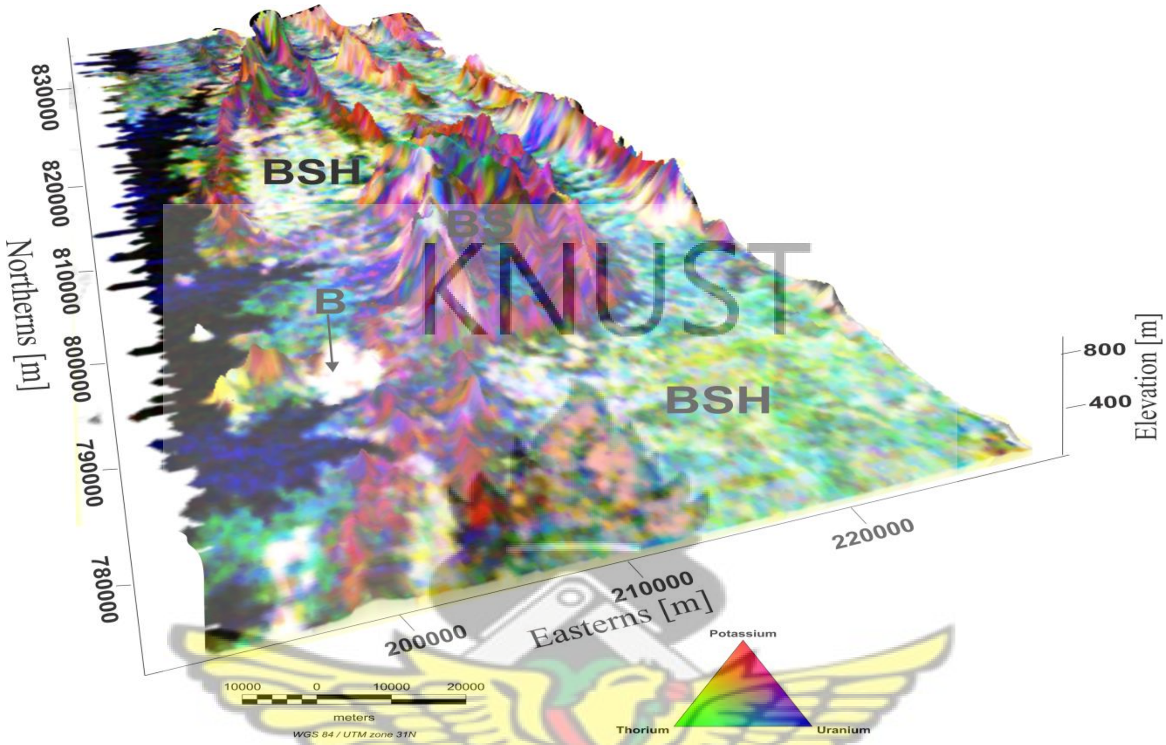

Figure 5.18 Ternary map draped over DEM and viewed in 3D

The ternary image was draped with the DEM of the area (Fig. 5.18) to observe the behaviour of the three radiogenic elememts, K, U and Th with the elevation. It was observed that the high elevated regions in the area coincided with the high K concentration as well as low U and Th concentration (magenta colour in Fig. 5.18) and this was interpreted as sandstone. Moreover, lowlands were seen to coincide with high concentration of all the three radiogenic elememts, K, U and Th. It was also observed that the black coloured region which was interpreted as the Lake Volta lay in a low elevated region. The basalt which was found at the southern part of the area also coincided with the low elevated regions.

5.3.5 Summary

Interpreted lithological map from the radiometric dataset combines information from the uranium image (Fig. 5.16), potassium image (Fig. 5.14), thorium image (Fig. 5.15) and the ternary image (Fig. 5.17) alongside published articles and geological map of the area. The area was divided into radiometric domains (regions) based upon the concentration, shape and abrupt change of radiometric concentration in the radiometric image. Boundaries of the individual lithological domains are seen as abrupt changes in the signature of radiometric concentration.

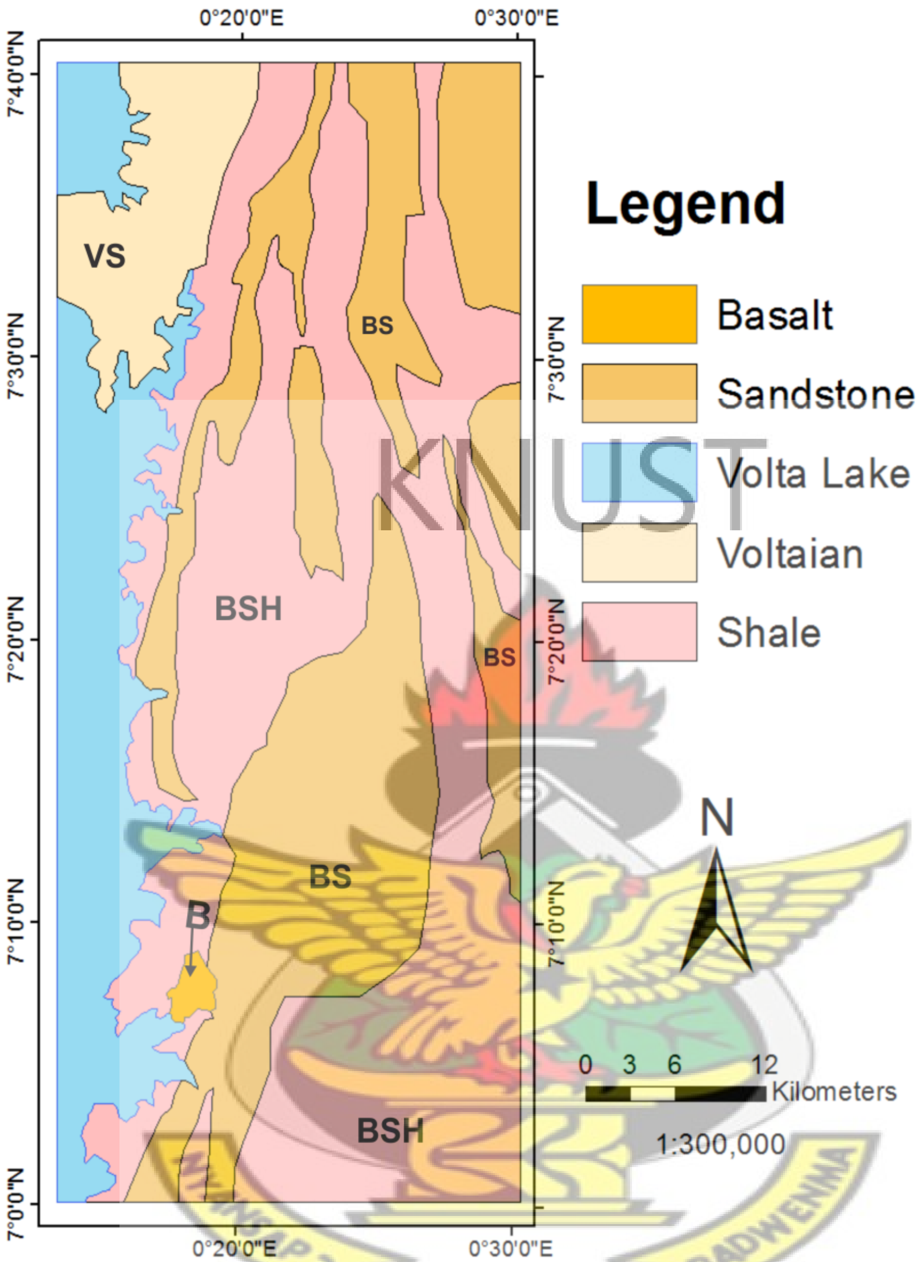

Figure 5.19 Interpreted lithological map from the radiometric dataset

The interpreted lithological map Fig. 5.19 of the area from the radiometric dataset shows the shale (BSH), sandstone (BS), basalt intrusion (B) and part of the Voltaian sediment (VS). The map Fig. 5.19 also depicts most of the observations and feature described in the previous sections (section 5.2.1 – 5.2.4).

5.4 Proposed Geological map

Information from aeromagnetic dataset, airborne radiometric dataset and published literature of the area were put together to produce a regional geological map of the study area (Fig. 5.20) which consists mainly of the Buem formation and the Voltaian sediment.

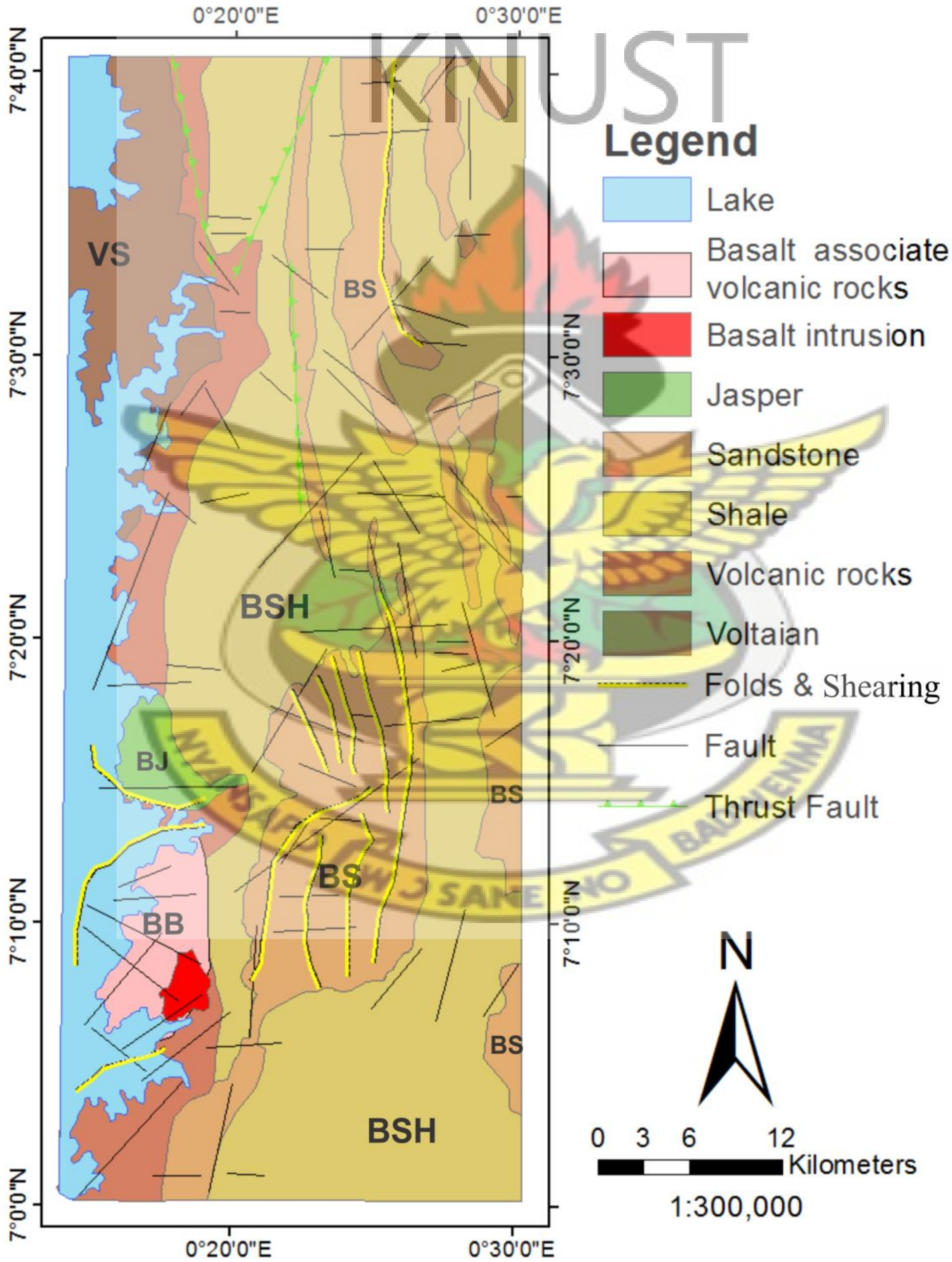

Figure 5.20 Proposed Geological map of the study area

The integrated geological map (figure 5.20) shows the various lithological units and the geological structures in the area. It can be observed from this map (fig. 5.20) that the Buem sandstones (BS) are associated with different regimes of tectonic activities producing faults and folds. This can be attributed to the thermo-tectonic event that occurred within the Buem formation about 600 m.a. (Kennedy, 1964; Jones, 1990; Osae et al., 2006).

5.5 Quantitative interpretation

Attempt was made to estimate the depth to basement of the magnetic body. The Geosoft oasis montaj *Depth to Basement extension* which determines the position (distance along the profile and depth), dip (orientation) and intensity (susceptibility) of magnetic source bodies for a magnetic profile was used. The *Werner deconvolution function* which uses the horizontal and vertical derivatives in the calculation in the depth to basement of the magnetic anomaly was employed. It assumes the source bodies are either dikes or contacts with infinite depth extent and uses a least-squares approach to solve for the source body (Ku & Sharp, 1983).

Three profiles were chosen across the residual aeromagnetic intensity map of the area to estimate the depth to magnetic bodies and possibly the intensity (susceptibility), namely A-A_1, B-B_1 and C-C_1 (Fig. 5.21). They were taken perpendicular to the most prominent strike direction (N-S) of the anomaly to obtain the best estimate of body parameters from the selected profiles. The afore-mentioned profiles lines were plotted and displayed on analytical signal image (Fig. 5.21). Two depth source models (Dike and contacts model) were assumed and their depths to basement were estimated using the *Werner deconvolution function*.

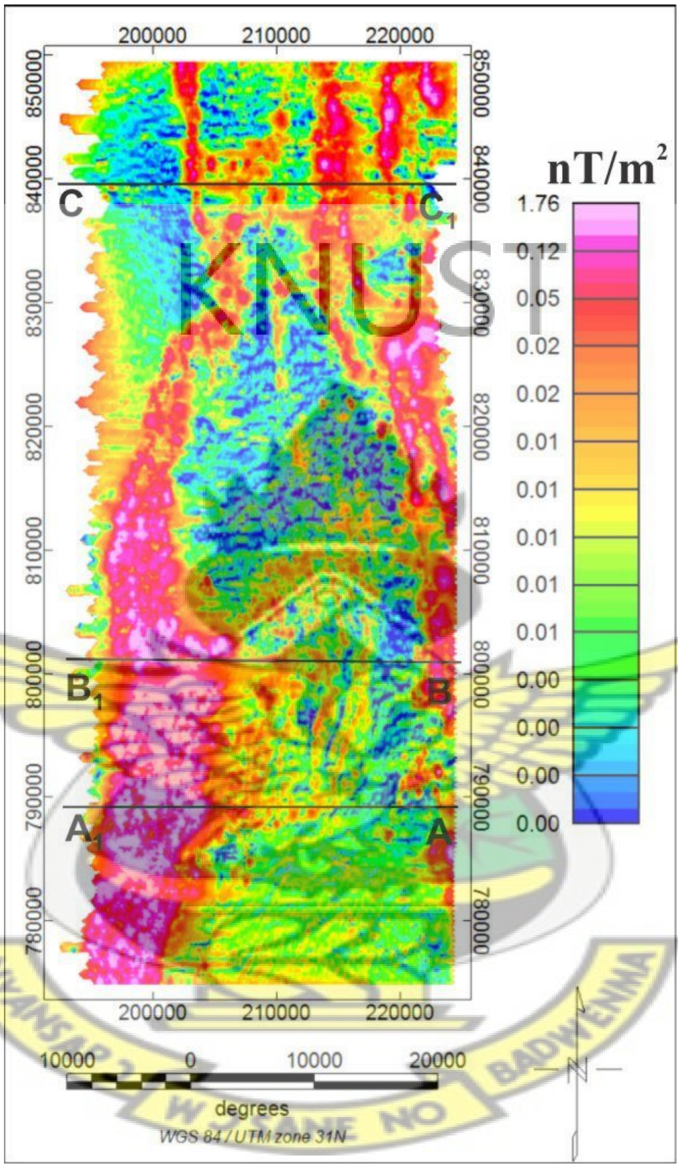

Figure 5.21 Profiles lines A-A_1, B-B_1 and C-C_1 displayed on analytical signal image

The profile A-A_1 (Fig. 5.22) is a 30-km section of a flight line which cuts the shale, sandstone and the basalt in the area and runs east to west. For profile A-A_1, 106 solutions were generated with the dike model and the model for the contact generated 72 and 34 solutions respectively. The depth to basement of A-A_1 ranged from 103.11 m to 857.99 m and the magnetic anomaly values varied from -1140.27 nT to -1327.13 nT. The depth to basement of the contact model was shallow (103.11 to 717 m) as compared to the dike model (114.41 to 857.99 m).

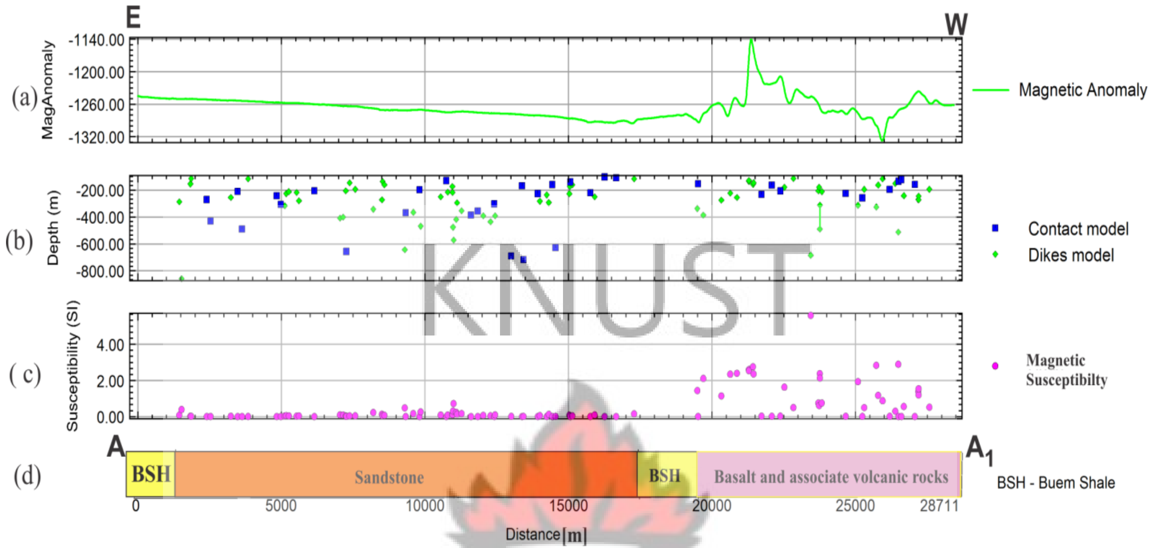

Figure 5.22 Werner deconvolution solutions from a magnetic profile A-A_1 over the study area: (a) residual magnetic intensity profile [nT], (b) depth [m], (c) susceptibility contrast [SI]. (d) A simplified geological section of the interpreted geological map

The profile B-B_1 (Fig. 5.23) is also a 30-km section of a flight line which cuts the sandstone, shale and the jasper in the area and runs east to west. Additional, for profile B-B_1, 139 solutions were generated with the dike model and the contacts model generated 98 and 41 solutions respectively. The depth to basement of B-B_1 ranged from 100.36 m to 1866.34 m with the magnetic anomaly values varying from -1214.33 nT to -1397.33 nT. The depth to basement of the contact model was shallow (100.36 to 983.71 m) as compared to the dike model (101.5 to 1866.334 m).

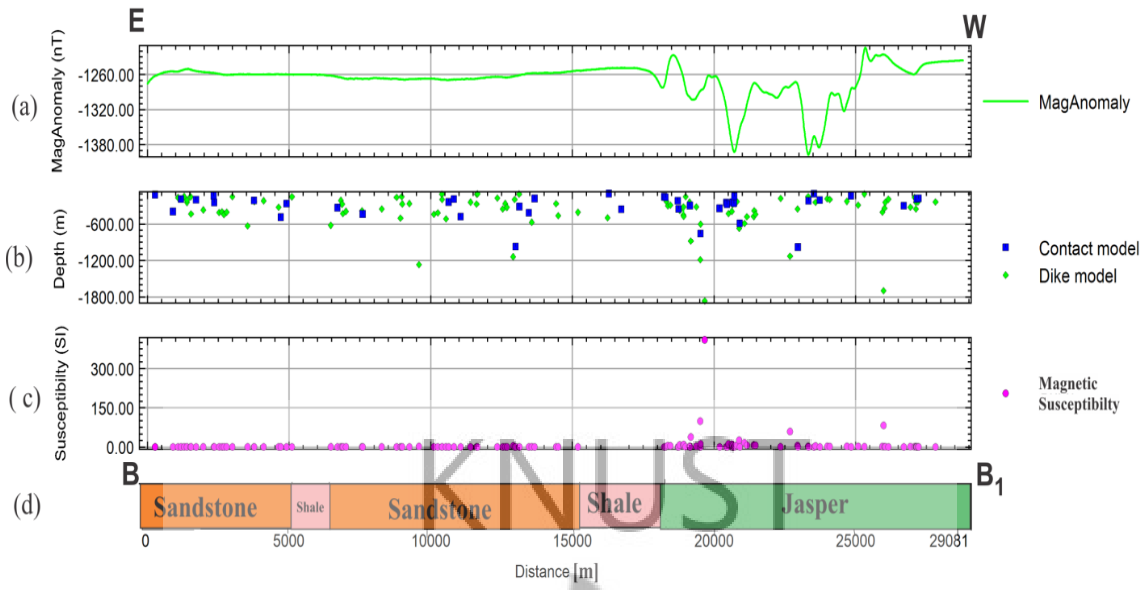

Figure 5.23 Werner deconvolution solutions from a magnetic profile B-B_1 over the study area: (a) residual magnetic intensity profile [nT], (b) depth [m], (c) susceptibility contrast [SI]. (d) A simplified geological section of the interpreted geological map

The profile C-C_1 (Fig. 5.24) is also a 30-km section of a flight line which cuts the Voltaian, shale and the sandstone in the area and runs west to east. Profile C-C_1 generated 73 solutions with the dike model and the contacts model generated 45 and 28 solutions respectively. The depth to basement of C-C_1 ranged from 113.82 m to 1605.24 m with the magnetic anomaly values varying from -1270.13 nT to -1302.81 nT. The depth to basement of the contact model was shallow (113.82 to 846.28 m) as compared to the dike model (131.82 to 1605.24 m).

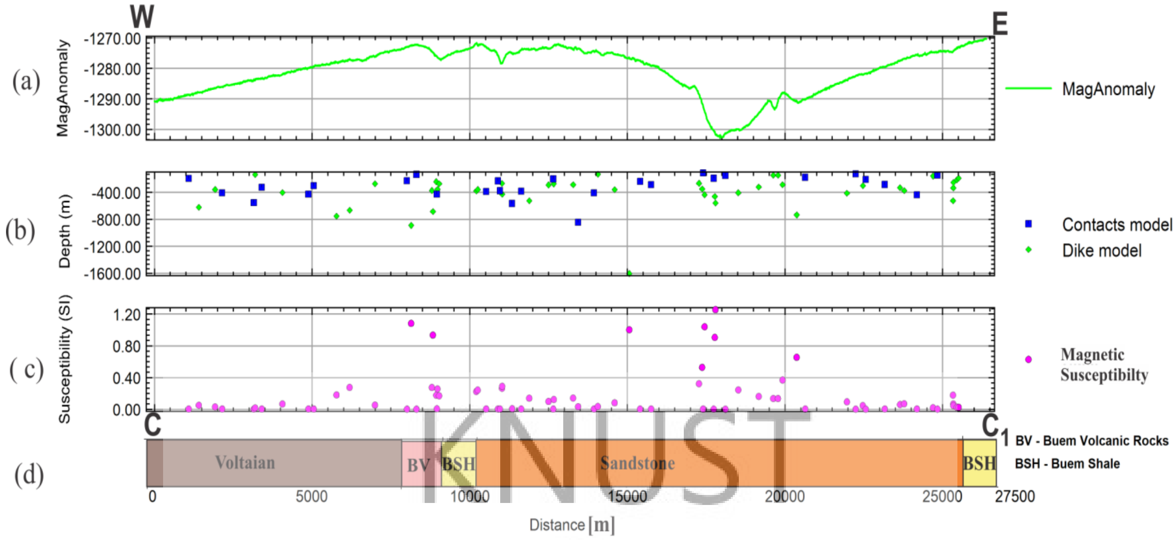

Figure 5.24 Werner deconvolution solutions from a magnetic profile C-C_1 over the study area: (a) residual magnetic intensity profile [nT], (b) depth [m], (c) susceptibility contrast [SI]. (d) A simplified geological section of the interpreted geological map.

From the three profiles it is observed that the depth to basement of the contact model was shallow (ranging from 100.36 m to 983.709 m) as compared to the dike model (ranging from 101.15 m to 1866.34 m) and this confirms a similar observation Mushayandebvu et al., (2001) made in their work work on Great Dyke of Zimbabwe and Teisseyre–Tornquist Zone, Poland.

CHAPTER SIX

6 CONCLUSION AND RECOMMENDATIONS

6.1 Conclusion

In order to map the lithology and geological structures of the study area, airborne radiometric and magnetic datasets collected over the area were processed and enhanced. The magnetic image enhancing filters applied to the residual magnetic intensity (RMI) using Geosoft (Oasis Montaj) are reduction to the pole (RTP), analytic signal, first vertical derivative (1VD), Tilt derivative (TDR) and upward continuation (UC). These filters helped define the lithological boundaries, intersection of geological structures, faults, folds and contacts. The tilt derivative (TDR) proved very useful in the delineation of the contacts and the most of geological structures in the area. The radiometric data provided geochemical information of uranium (U), thorium and potassium (K) and proved valuable in delineating bedrock lithology of the area such as the Buem shale, sandstone, and part of the Voltaian sediments. The radiometric dataset was also valuable in the delineation of the Volta Lake and the lithological contacts of the various rock formations. The interpretation of the high-resolution airborne magnetic dataset has provided a synopsis of the regional geology (lithology) as well as further insight into structural controls of the area. It also shows a detailed assessment of various lithology and north-south striking of the geology in the area.

Most of the delineated structures found within the sandstone, (BS) (at the central and eastern part of the area), volcanic rocks and the basalt (western part of the area) strike mostly in the N-S and E-W direction. The jasper deposits which for the past years proved difficult in mapping using this data has been successfully mapped from the enhanced magnetic dataset. This deposit occurs at the western part of the study area, around Kwamekrom and Odumase Township (Fig. 1.1), labelled BJ on the interpreted geological map (Fig. 5.20). The relatively high magnetic signature that the jasper produced compared with the shale and the sandstone as a result of it being interbedded with iron oxide (Jones, 1990) helped in delineating the deposit. The Buem sandstone delineated (at the central and eastern part of the area) produced relatively high magnetic signature. This may be due to the presence of high composition of magnetic minerals mainly magnetite in this unit.

The depth to basement of the formations within the study area was determined using the contact model and the dike models. The contact model produced shallow depth ranging of 100.36 m to 983.709 m while the dike model on the other hand produced depth range of 101.15 m to 1866.34 m for the basement rock. This is because dike model anomaly occurs at a greater depth than the contact model (Mushayandebvu et al., 2001). The dike model seems to best fit the study area. The aeromagnetic dataset proved valuable in the delineation of most of the lithologies and structures in the area and estimating the depth to basement of the magnetic body with the radiometric dataset proving to be a valuable tool for mapping lithology and water bodies.

6.2 Recommendations

Based on this study, the following recommendations are made:

Ground thrusting is highly recommended to actually confirm the delineated structure and lithology delineated. Ground geophysical and geological drilling surveys are recommended where possible to validate airborne geophysical measure since they have better depth and lateral resolutions.

High structural connectivity regions such as the sandstone region (BS) which has high potassium, K concentration and relatively low magnetic anomaly (indicating alteration zone) should be considered for further exploration.

Attempt should be made to model the various lithological units in the study area using the magnetic data. This data can also be supplemented with 3D electrical resistivity over the area to map the jasper deposit since it is known to be highly resistive (Jones, 1990).

References

Afenya, P. (1982). Ghana’s mineral resources for small-scale mining industries. (J. Neilson, Ed.) *Strategies for small-scale mining and mineral industries, 8*, 24-28.

Affaton, P., Sougy, J., & Trompette, R. (1980). The tectono-stratigraphic relationships between the Upper Precambrian and Lower Paleozoic Volta basin and the Pan-African Dahomeyide orogenic belt (West Africa). *American Journal of Science, 280*, 224-248.

Airo, M. (2005). Regional interpretation of aerogeophysical data: extracting compositional and structural features. *Geological Survey of Finland, Special Paper, 39*, 176–197.

Airo, M. L. (2002). Aeromagnetic and aeroradiometric response to hydrothermal alteration. *Surveys in Geophysics, 23*, 273–302.

Airo, M., & Loukola-Ruskeeniemi, K. (2003). Characterization of sulfide deposits by airborne magnetic and gamma-ray responses in eastern Finland. *Ore Geology Reviews, 24*, 67–84.

Amoako, P. Y., Amedofu, S. K., & Akamaluk, T. (l998). *Processing and Interpretation of Data from Airborne Geophysical Survey, Ghana Final Report.* Geological Survey Department of Ghana. Accra: Geological Survey Department of Ghana.

Asadi, H., & Hale, M. (1999). Integrated analysis of aeromagnetic, landsat TM and mineral occurrence data for epithermal gold exploration in northwest iran. *13th International Conference on Applied Geologic Remote Sensing, Vancouver.* British Columbia.

Atchuta Rao,, D., & Ram Badu, H. (1981). Nomograms for rapid evaluation of magnetic anomalies over long tabular bodies. *Pure and Applied Geophysics, 119*, 1037-1050.

Bell, S. V. (1962). *Ghana Geological Survey Annual Report.* Accra: Ghana Geological Survey.

Bell, S., & Crook, J. (2003). *The Geology of 1/4 Feild Sheets 182, Hohoe S. E with a contribution on the structural Relationship to Kpandu-Ho Area.* Accra: Ghana Geological Survey Department.

Beltrão, J., Silver, J., & Costa, J. (1991). Robust polynomial fitting method for regional gravity estimation. *Geophysics, 56*, 80–9.

Billings, S. (1998). Geophysical aspects of soil mapping using airborne gamma-ray spectrometry.

Blay, P. (2003). *The Geology of 1/4 Feild Sheets Nos. 184, 185 and 187, Hohoe N. E., Baglo S.W. and N.W.* Accra: Ghana Geological Survey Department .

Briggs, I. (1974). Machine contouring using minimum curvature. *Geophysics, 39*(1), 39-48.

Chandler , V. (1990). Geological interpretation of gravity and magnetic data over the central part of the Duluth Complex northeastern Minnesota. *Economic Geology, 85*, 861-829.

Clark, D. (1997). Magnetic properties of rocks and minerals. *AGSO Journal of Australian Geology and Geophysics, 17*(2), 83-103.

Cooper, G., & Cowan, D. (2006). Enhancing potential field data using filters based on the local phase. *Computers & Geosciences, 32*, 1585–1591.

Dapaah-Siakwan, S., & Gyau-Boakye, P. (2000). Hydrogeologic framework and borehole yields in Ghana. *Hydrogeology Journal, 8*, 405–416.

Delor, C., Fullgraff, T., Urien, P., Le Berre, P., Thomas, E., Roig, J., et al. (2009). *Geological Map Explanation – Map Sheets 0700A/2, 0700B/1, 0800D/1, 0800D/3, 0800C/2 & 0800C/4.* Accra: Geological Survey Department of Ghana (GSD).

Dickson, B., & Scott, K. (1997). Interpretation of aerial gamma-ray surveys adding the geochemical factors. *AGSO Journal of Australian Geology & Grophysics., 17*(2), 187-200.

Dickson, K., & Benneh, G. (1985). *A New Geography of Ghana.* England: Longman House, Burnt Mill, Harlou, Essex.

Direen, N. G., Lyons, P., Korsch, & Glen, R. (2001). Integrated geophysical appraisal of crustal architecture in the eastern Lachlan Orogen. *Exploration Geophysics, 109*, 136-142.

Dobrin, M., & Savit, C. (1988). *Introduction To Geophysical Prospecting* (Fourth Edition ed.). Singapore: McGraw-Hill.

Duffett, M. (1998). Gravity, magnetic and radiometric evidence for the geological setting of the Lady Loretta Pb-Zn-Ag deposit - a qualitative appraisal. *Economic Geology, 93*, 1295-1306.

Eisenlohr, B., & Hirdes, W. (1992). The structural development of the early Proterozoic Birimian and Tarkwaian rocks of southwest Ghana. *West Africa. Journal of African Earth Sciences, 14*(3), 313-325.

El-awady, M., El-etr, H., & Bakrah, A. (1984). Aeromagnetic geophysical investigation in El-Faiyum district, western desert, Egypt. *Qatar Univ. Sci. Bull, 5*, 335-357.

Fertl, W. (1983). Gamma-ray spectral logging: a new evaluation frontier. *World Oil*, 79-91.

Foss, C. (2011). Magnetic data Enhancement and Depth Estimation. (H. Gupta, Ed.) *Encyclopedia of Earth Sciences Series*, 736-746.

Galbraith, J. H., & Saunders, D. F. (1983). Rock classification by characteristics of aerial gamma-ray measurements. *Journal of Geochemical Exploration, 18*(1), 49-73.

Geotech Airborne Limited. (2009). *Integrated Interpretation Report on a Versatile Time Domain Electromagnetic (VTEM) Survey on the Hohoe Project Area.* Geological Survey Department, Accra, Ghana.

Ghana Statistical Service. (2012). *2010 Population and Housing Census (PHC).* Ghana Statistical Service, Accra.

Grant, F., & Martin, L. (1966). *Interpretation theory in applied Geophysics.* New York: McGraw-Hill Book Co.

Gregory, A., & Horwood, J. (1961). *A laboratory study of gamma-ray spectra at the surface of rocks.* Ottowa: Department of Energy, Mines and nnnResources.

Griffis, R. J., Barning, K., Agezo, F. L., & Akosah, F. K. (2002). *Gold Deposits of Ghana.* Accra, Ghana: Minerals Commission.

GSD. (1988). *Geological Map of Ghana (1:1 000 000) with mineral deposits.* Geological Survey Department of Ghana, Accra.

Guillemot, D. (1987). Airborne magnetometer and spectrometer survey over Gabon. *First Break, 5*(7).

Gunn, P. (1997). Regional magnetic and gravity responses of extensional sedimentary Basins. *AGSO Journal of Australian Geology & Geophysics, 17*(2), 115-131.

Gunn, P., Maidment, D., & Milligan, P. (1997a). Interpreting aeromagnetic data in areas of limited outcrop. *AGSO Journal of Australian Geology & Geophysics, 17*(2), 175–185.

Gunn, P., Minty, B., & Milligan, P. (1997b). The Airborne Gamma-Ray Spectrometric Response Over Arid Australian Terranes. In A. Gubins (Ed.), *Proceedings of Exploration 97: Fourth Decennial International Conference on Mineral Exploration*, (pp. 733-740). Australia.

Hardy, S. (2004). The Application and Analysis of Airborne Gamma Spectrometry (Radiometrics) for Mapping Soils in Central Queensland. *ISCO 2004 - 13th International Soil Conservation Organisation Conference.* Brisbane, Australia.

Hasting, D. (1982). On the tectonics and metallogenesis of West Africa: A model incorporating new geophysical data. *Geoexploration, 20*, 295-327.

Hirdes, W., Davis, D., & Eisenlohr, B. (1992). Reassessment of Proterozoic granitoid ages in Ghana on the basis of U/Pb zircon and monazite dating. *Precambrian Research, 56*, 89-96.

Hirst, T. (1946). *Reports on the Bibiani goldfield, Part I: The geology of the field.* Accra: Gold Coast Geological Survey Department.

Hoffman, P. (1999). The break-up of Rodinia, birth of Gondwana, true polar wander and the snowball Earth. *Journal of African Earth Sciences, 28*, 17-33.

Holm, R. (1974). Petrology of alkalic gneiss in the Dahomeyan of Ghana. *Geological Society of America Bulletin, 85*, 1441-1448.

Jones, W. (1990). The Buem volcanic and associated sedimentary rocks, Ghana: a field and geochemical investigation. *Journal of African Earth Sciences, 11*(3–4), 373-383.

Junner. (1940). The Geology of the Gold Coast and western Togoland. *Gold Coast Geological Survey Bulletin, 11*, 1-40.

Junner, N. (1935). *Gold in gold coast.* Accra, Ghana: Geological Survey Department.

Kennedy, W. (1964). *The structural differentiation of Africa in the Pan-African (±500 m.y.) tectonic episode.* UK: Leeds University Institute for African Geology.

Kesse, G. (1985). *The mineral and rock resources of Ghana.* United States: A.A. Balkema Publishers,Accord, MA.

Koulomzine, T., Lamontagne, Y., & Nadeau, A. (1970). New methods for the direct interpretation of magnetic anomalies caused by inclined dykes of infinite length. *Geophysics, 35*, 812-830.

Ku, C., & Sharp, J. (1983). Werner deconvolution for automated magnetic interpretation and its refinement using Marquart's inverse modeling. *Geophysics, 48*(6), 754-774.

Leube, A., Hirdes, W., Mauer, R., & Kesse, G. (1990). The early proterozoic Birimian supergroup of Ghana and some aspects of its associated gold mineralisation. *Precambrian Research, 46*, 139-165.

Li, X. (2008). *Magnetic reduction-to-the-pole at low latitudes.* Fugro Gravity and Magnetic Services. Houston, USA.: Fugro .

LUO, Y., XUE, D.-J., & WANG, M. (2010). Reduction to the Pole at the Geomagnetic Equator. *Chinese Journal of Geophysics, 53*(6), 1082-1089.

Mani, R. (1978). *The geology of the Dahomeyan of Ghana; Geology of Ghana Project.* Accra: Ghana Geological Survey Department.

Miller, H., & Singh, V. (1994). Potential field tilt—a new concept for location of potential field sources. *Journal of Applied Geophysics, 32*, 213–217.

Milligan, P., & Gunn, P. (1997). Enhancement and presentation of airborne geophysical data. *AGSO Journal of Australian Geology & Geophysics, 17*(2), 63-75.

Milsom, J. (2003). *Field Geophysics.* (Third, Ed.) London: Wiley.

Minty, B. (1997). Fundamentals of airborne gamma-ray spectrometry. *AGSO Journal of Australian Geology & Geophysics., 17*(2), 39-50.

Misener, D. (1987). *Interpretation of airborne geophysical survey results.* Toronto, Canada: Paterson, Grant & Watson Ltd.

Murphy, B. (2007). Airborne geophysics and the indian scenario. *Journal of Indian Geophysics, 11*(1), 1–28.

Murray, R. (1960). *The geology of the "Zuarungu" 1/2° Field Sheet.* Accra: Ghana Geological Survey Department Bulletin No.25.

Mushayandebvu, M., van Drielz, P., Reid, A., & Fairhead, J. (2001). Magnetic source parameters of two-dimensional structures using extended Euler deconvolution. *Geophysics, 66*(3), 814–823.

Oruc, B., & Selim, H. (2011). Interpretation of magnetic data in the Sinop area of Mid Black Sea, Turkey, using tilt derivative, Euler deconvolution, and discrete wavelet transform. *Journal of Applied Geophysics, 74*, 194–204.

Osae, S., Asiedu, D., Banoeng-Yakubo, B., Koeberl, C., & Dampare, S. (2006). Provenance and tectonic setting of Late Proterozoic Buem sandstones of southeastern Ghana: Evidence from geochemistry and detrital modes. *Journal of African Earth Sciences, 44*, 85–96.

Ostrovskiy, E. (1975). Antagonism of radioactive elements in wallrock alteration fields and its use in aerogamma spectrometric prospecting. *International Geology Review, 17*(4), 461-468.

Pesonen, L. J., Koeberl, C., & Hautaniemi, H. (2003). Airborne Geophysical Survey of the Lake Bosumtwi Meteorite Impact Structure. *Jahrbuch Der Geologischen Bundesanstalt, 143*(4), 581–604.

PGEO, E. K. (2012). *Technical Report on Sheini Hills Iron Project.* Canada: Cardero Resource Corporation.

Philips, J. (1997). *Potential-Field Geophysical Software for the PC,.* U.S.G.S. Open-File Report 97-725.

Reeves, C., Reford, S., & Millingan, P. (1997). Airborne geophysics:old methods, new images. In A. Gubins (Ed.), *Proceedings of the Fourth Decennial International Conference on Mineral Exploration,* (pp. 13-30). Australia.

Roest, W., Verhoef, J., & Pilkington, M. (1992). Magnetic interpretaion using 3-D analytical signal. *Geophysics, 57*, 116-125.

Roy, A. (1966). The method of continuation in mining geophysics. *Geoexploration, 4*, 65-83.

Salem, A., Williams, S., Fairhead, J., Ravat, D., & Smith, R. (2007). Tilt-depth method: a simple depth estimation method using first-order magnetic derivatives. *The Leading Edge , 26*, 1502-1505.

Shi, Z., & Butt, G. (2004). New enhancement filters for geological mapping. *17th Geophysical Conference and Exhibition.* USA: ASEG.

Silva, A., Pires, A., Mccafferty, A., De Moraes , R., & Xia, H. (2003). Application of Airborne Geophysical Data to Mineral Exploration in the Uneven Exposed Terrains of the Rio Das Velhas Greenstone Belt. *Revista Brasileira de Geociências, 33*, 17-28.

Smith, R., & O'Connell, M. (2007). An Improved Method for Trending of Features on Aeromagnetic Maps. In B. Milkereit, (Ed.), *Proceedings of Exploration 07: Fifth*

Decennial International Conference on Mineral Exploration, (pp. 853-861). Toronto, Canada.

Taylor, P., Moorbath, S., Leube, A., & Hirdes, W. (1988). Geochronology and crustal evolution of Early Proterozoic granite-greenstone terrains in Ghana. *West Africa: in International Conference and Workshop on the Geology of Ghana with Special Emphasis on Gold*, (pp. 43-45). Accra.

Telford, W., Gelbert, I., & Sheritt, R. (1990). *Applied Geophysics* (Second ed.). London: Cambridge University Press.

Verduzco, B., Fairhead, J., Green, C., & Mackenzie, C. (2004). New insights into magnetic derivatives for structural mapping. *The Leading Edge, 23*, 116-119.

Vernon, R., & Flood, R. (1988). Contrasting deformation of S- and I-type granitoids in the Lachlan Fold Belt, eastern Australia. *Tectonophysics, 147*, 127-143.

Villeneuve, M., & Cornée, J. (1994). Structure, evolution and palaeogeography of the West African Craton and bordering belts during the Neoproterozoic. *Precambrian Research, 69*, 307-326.

Wemegah, D., Menyeh, B., & Danuor, S. (2009). Magnetic Susceptibility Characterization of mineralized and non mineralized rocks of the Subenso Concession of Newmont Ghana Gold Limited. *Ghana Science Association Biennial Conference.* Accra.

Wilford, J., Bierwirth, P., & Craig, M. (1997). Application of airborne gamma-ray spectrometry in soil or regolith mapping and applied geomorphology. *Journal of Australian Geology & Geophysics, 17*(2), 201-216.

Wright. (1985). *Geology and Mineral Resources of West Africa.* Springer.

Wright, J., Hastings, D., Jones, W., & Williams, H. (1985). *Geology and Mineral Resources of West Africa.* London: George Allen and Unwin publishers Ltd.

Appendix

Appendix A 1 Generation of *Werner deconvolution* solutions

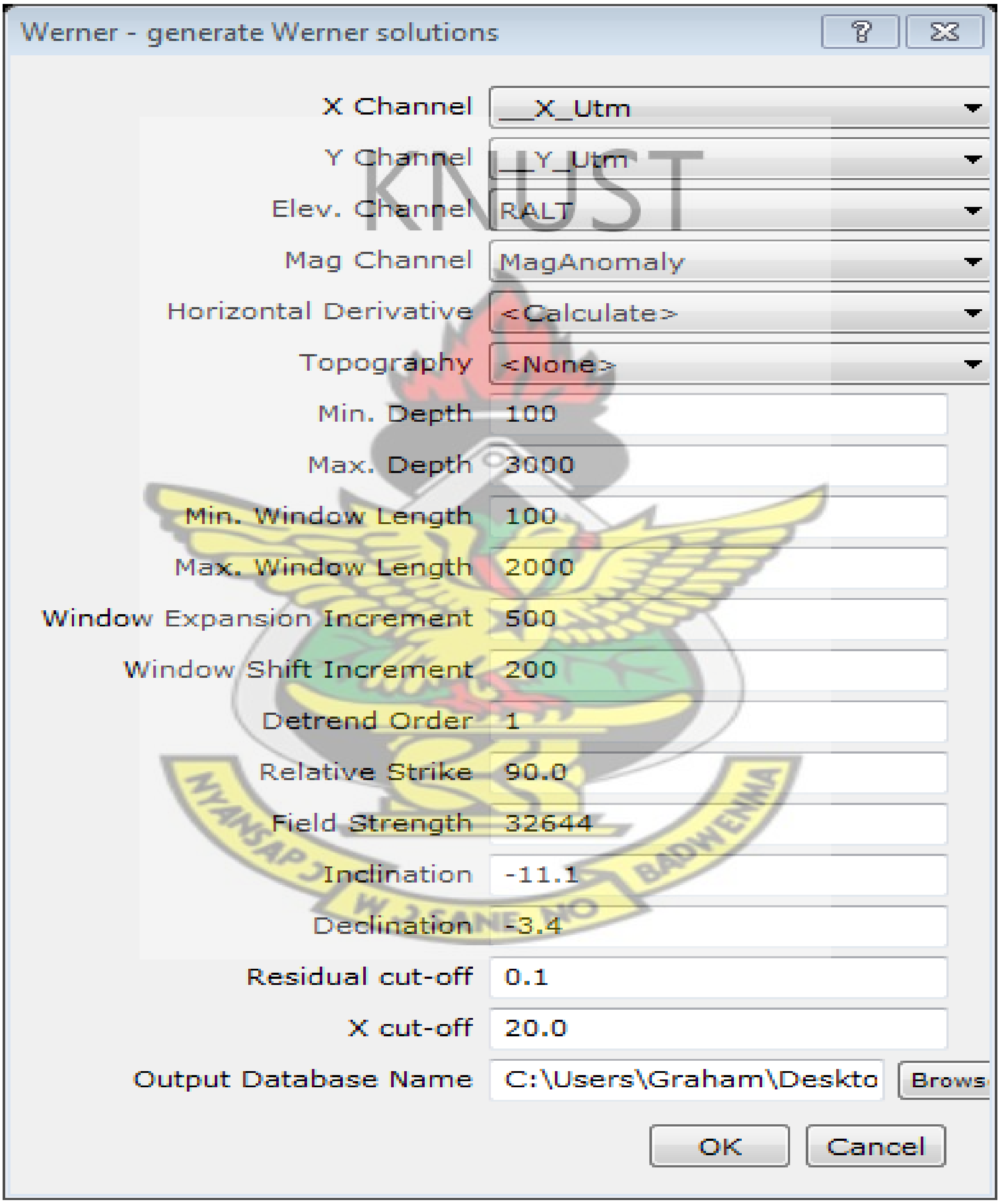

Figure A 1 Parameters dialog box for generating Werner solutions

Appendix A.2 *Werner deconvolution* solutions

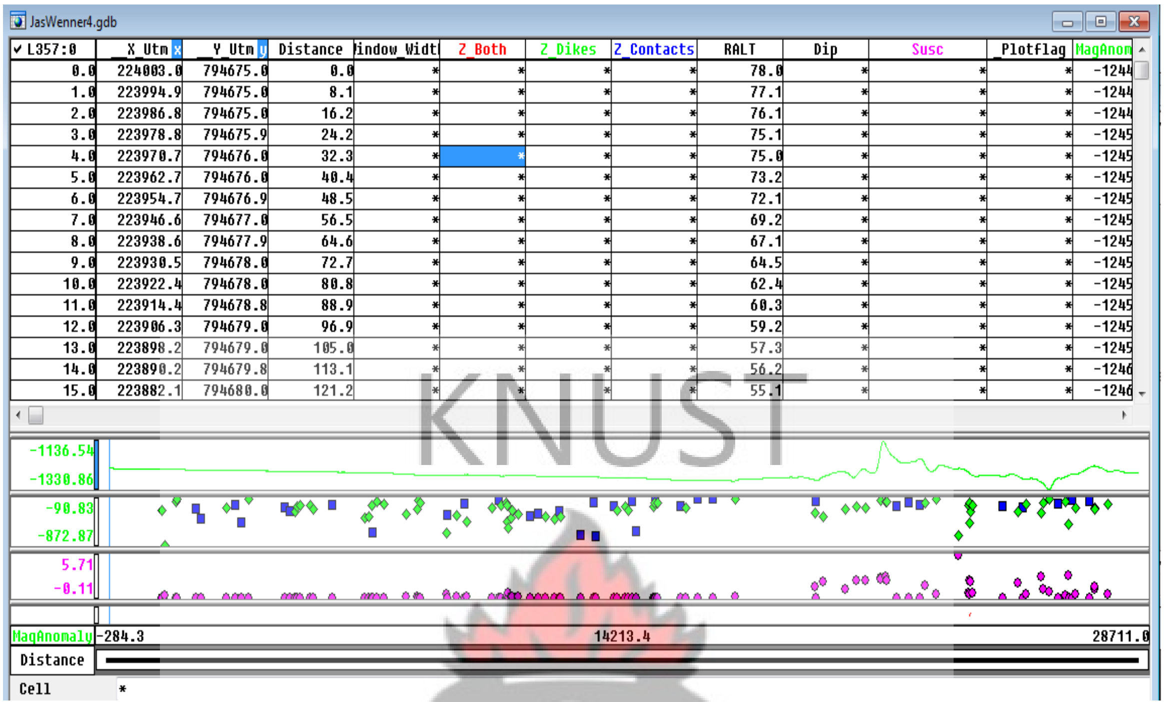
JasWenner4.gdb

L357:0	X_Utm	Y_Utm	Distance	Window_Widt	Z_Both	Z_Dikes	Z_Contacts	RALT	Dip	Susc	Plotflag	MagAnom
0.0	224003.0	794675.0	0.0	*	*	*	*	78.0	*	*	*	-1244
1.0	223994.9	794675.0	8.1	*	*	*	*	77.1	*	*	*	-1244
2.0	223986.8	794675.0	16.2	*	*	*	*	76.1	*	*	*	-1244
3.0	223978.8	794675.9	24.2	*	*	*	*	75.1	*	*	*	-1245
4.0	223970.7	794676.0	32.3	*	*	*	*	75.0	*	*	*	-1245
5.0	223962.7	794676.0	40.4	*	*	*	*	73.2	*	*	*	-1245
6.0	223954.7	794676.9	48.5	*	*	*	*	72.1	*	*	*	-1245
7.0	223946.6	794677.0	56.5	*	*	*	*	69.2	*	*	*	-1245
8.0	223938.6	794677.9	64.6	*	*	*	*	67.1	*	*	*	-1245
9.0	223930.5	794678.0	72.7	*	*	*	*	64.5	*	*	*	-1245
10.0	223922.4	794678.0	80.8	*	*	*	*	62.4	*	*	*	-1245
11.0	223914.4	794678.8	88.9	*	*	*	*	60.3	*	*	*	-1245
12.0	223906.3	794679.0	96.9	*	*	*	*	59.2	*	*	*	-1245
13.0	223898.2	794679.0	105.0	*	*	*	*	57.3	*	*	*	-1245
14.0	223890.2	794679.8	113.1	*	*	*	*	56.2	*	*	*	-1246
15.0	223882.1	794680.0	121.2	*	*	*	*	55.1	*	*	*	-1246

Figure A 2 Geosoft Oasis montaj database (GDB) displaying the Werner generated solutions

Appendix A.3 Script for extracting azimuth of lineaments

```
import math
def GetAzimuthPolyline(shape):
 radian = math.atan((shape.lastpoint.x - shape.firstpoint.x)/(shape.lastpoint.y - shape.firstpoint.y))
 degrees = radian * 180 / math.pi
 return degrees
__esri_field_calculator_splitter__
GetAzimuthPolyline( !Shape!)
```

Equation A 1 expression for extracting azimuth direction delineated lineament in ArcGIS 10.